Structural basis for the chaperone activity of alpha-B crystallin by solid-state NMR

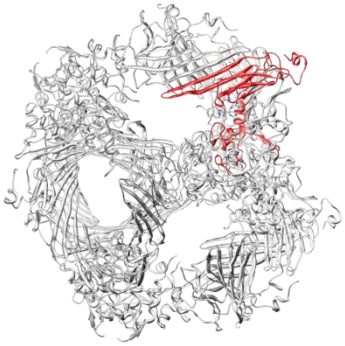

Dissertation zur Erlangung des akademischen Grades des Doktors der Naturwissenschaften (Dr. rer. nat.)
eingereicht im Fachbereich Biologie, Chemie, Pharmazie der Freien Universität Berlin
vorgelegt von **Stefan Marković** aus Waldshut
Berlin, Oktober 2012

1. Gutachter: Prof. Dr. Hartmut Oschkinat
2. Gutachter: Prof. Dr. Bernd Reif

Disputation am: 12.04.2013

Contents

Abbreviations

αB	alpha-B crystallin
αB-R120G	alpha-B crystallin mutant R120G
αB-10.1	truncated alpha-B crystallin residues 64-154
α-syn	alpha-synuclein
B_o	static magnetic field
B_1	radiofrequency pulse
CP	cross polarization
CSA	chemical shift anisotropy
DARR	dipolar-assisted rotational resonance
DPC	dodecylphosphocholine
EM	electron microscopy
FSLG	frequency switched Lee-Goldburg
γS	gamma-S crystallin
γS-G18V	gamma-S crystallin mutant G18V
HETCOR	heteronuclear correlation
HSP	heat shock protein
HSQC	heteronuclear single quantum coherence
INEPT	insensitive nucleus enhanced by polarization transfer
MAS	magic angle spinning
MS	mass spectrometry
NAC	non-amyloid component
NMR	nuclear magnetic resonance (spectroscopy)
OmpG	outer membrane protein G
PAR	proton-assisted recoupling
PAIN	proton-assisted recoupling of insensitive nuclei
PDB	protein data bank
PDSD	proton-driven spin diffusion
PEG	polyethylglycol (8000)
PMLG	phase-modulated Lee-Goldburg
PRE	paramagnetic relaxation enhancement
RF	radiofrequency
SAXS	small-angle X-ray scattering

sHSP	small heat shock protein
TEDOR	transferred echo double resonance
wt	wild-type

X-ray crystallography and Nuclear Magnetic Resonance spectroscopy (NMR) are well-established techniques for high resolution structural studies of biomolecules. In the recent years, solid-state NMR has become a popular tool for the investigation of systems that are heterogeneous or insoluble and therefore difficult to study with other techniques. A structure of (the core domain of) alpha-B crystallin, a polydisperse and oligomeric chaperone, that is involved in the protection system against cellular stress, has been solved by solid-state NMR previously [Jehle 08]. In the thesis presented here, functional studies on alpha-B crystallin have been performed, mainly by solid-state NMR, in order to be able to describe a structural mechanism of chaperone activity.

1. Introduction

Nuclear Magnetic Resonance spectroscopy (NMR) is a technique that enables the study of conformation and dynamics of molecules in solution or in the solid-state [Levitt 01; Cavanagh 08]. It relies on the interaction of the magnetic moment μ of nuclei with an external magnetic field B_0. Nuclear magnetic moments align with respect to this field (Fig.1.1).

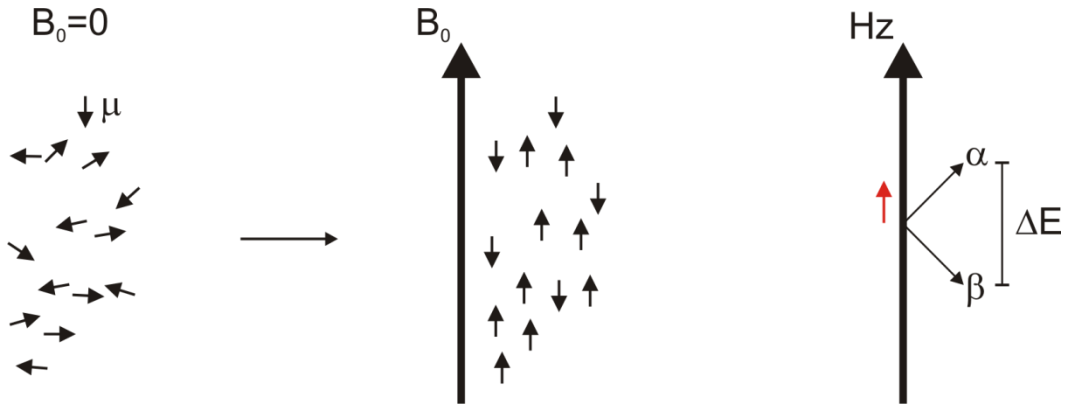

Fig.1.1: Nuclear spins μ align to an applied magnetic field B_0. This scheme is simplified. In reality only a small fraction of spins is completely polarized. Alignment of the spins leads to non-degenerate energy levels (α and β). Population differences lead to a net magnetization vector in z-direction (indicated in red).

This alignment makes the spins adapt non-degenerate energy levels, known as Zeeman splitting. A single dipole moment μ is defined as

$$\mu = \gamma J$$

where J is the spin angular momentum. J can only take discrete values according to

$$J = m\frac{h}{2\pi}$$

where m is the magnetic quantum number. It can adopt values ranging from –I, -I+1, …, 0, …, I-1,I where I is the so-called spin quantum number. For a given nucleus of I= ½ two energy levels are possible with

$$J = \pm\frac{h}{4\pi}$$

(called α (+) and β (-) states in the following) giving rise to a single transition (Fig.1.1, right). Spins with a spin quantum number of ½ behave beneficial in terms of resolution, as there is only one possible transition between α and β states giving rise to a single signal (peak) and – most importantly – no quadrupolar moment.

The initial net alignment is oriented along the z-the axis of the external field. Spins presses around z with their Larmor frequency (which can only be observed in the transverse plane). It is defined by

$$\omega = \gamma Bo$$

where γ is the gyromagnetic ratio of a spin. For an ensemble of identical spins the sum of all dipole moments is defined as magnetization M.

$$M = \sum_{J} \mu_i$$

In their equilibrium state, spins are randomly distributed in the x,y plane and therefore no net transverse magnetization can be detected (Fig.1.2). This random distribution is referred to as lack of phase coherence. A radiofrequency (RF) pulse (the B_1 field) orthogonal to the B_0 magnetic field is applied to rotate the spins and therefore giving

a net magnetization vector in the x,y plane, the so-called transverse magnetization. Transverse magnetization precesses with the Larmor frequency and can be detected by induction of a current in the receiver coil.

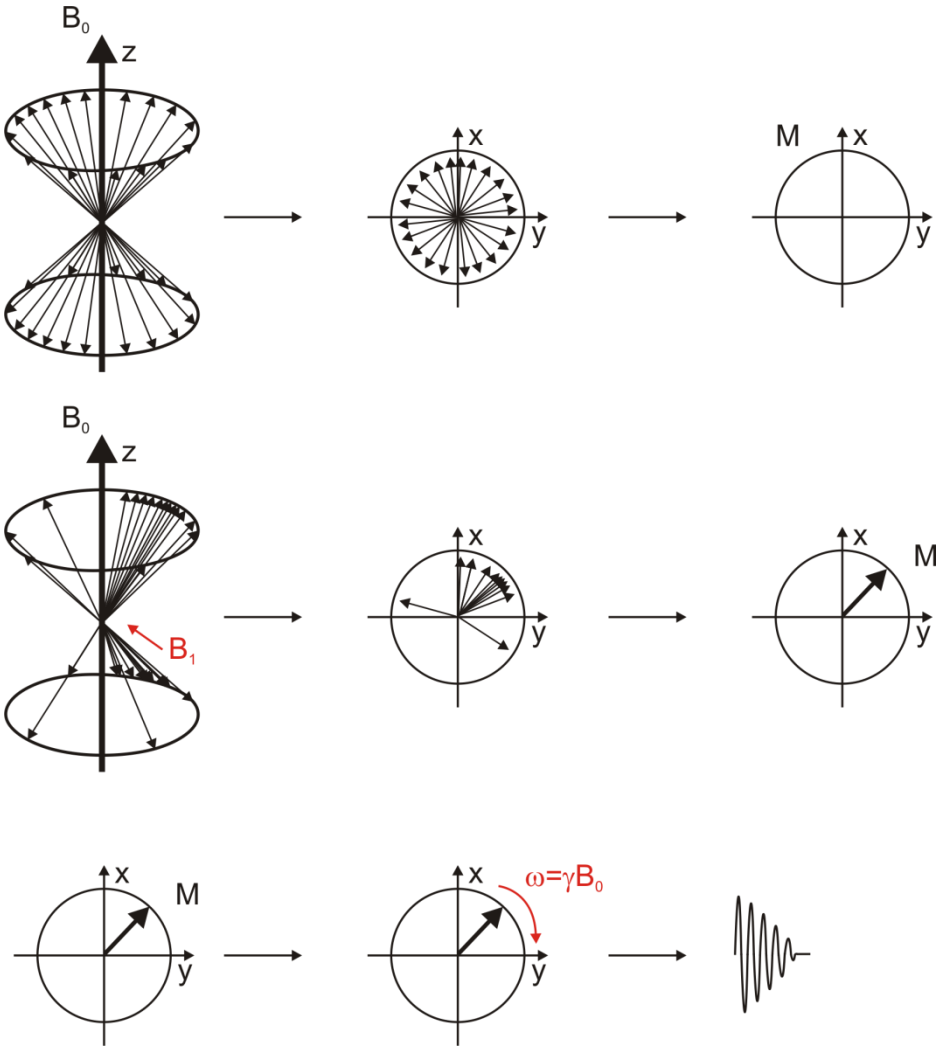

Fig.1.2: Vector model of an ensemble of spins. Top trace: Spins in their ground state without phase coherence. Middle trace: Application of a B_1 field creates phase coherence and therefore a net magnetization vector in the transverse plane. Bottom trace: The net magnetization vector precesses with the Larmor frequency and is detected in an NMR experiment.

1.1 Solid-state NMR spectroscopy

The benefit of solid-state NMR spectroscopy is that i) insoluble, heterogeneous systems can be studied and ii) transverse relaxation rates are barely dependent on the size of the molecule and therefore very big (e.g. oligomeric) systems can be studied [Duer 02].

As molecular tumbling is absent, dipolar couplings and chemical shift anisotropy (CSA) are not averaged, which affects the signal linewidth. The dipolar coupling

depends on the position of the vector connecting two nuclei with respect to the static magnetic field, their gyromagnetic ratios (γ) and distance r (Fig.1.3).

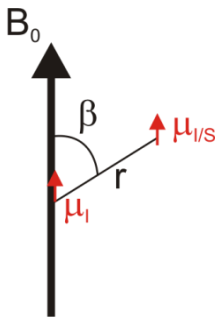

Fig.1.3: The strength of the dipolar coupling between two spins is dependent on their position in respect to the magnetic field, their distance and their gyromagnetic ratios.

The homonuclear dipolar coupling Hamiltonian is defined as

$$H_{\mathrm{II}} = -\frac{1}{2} d(3cos^2\beta - 1)\ 3I_{1z}I_{2z} - I_1I_2$$

with

$$d = \frac{\left(\frac{\mu_o}{4\pi}\right)\hbar{\gamma_{\mathrm{I}}}^2}{{r_{\mathrm{II}}}^3}$$

whereas the heteronuclear dipolar coupling Hamiltonian is defined as

$$H_{\mathrm{IS}} = -d(3cos^2\beta - 1)I_zS_z$$

with

$$d = \frac{\left(\frac{\mu_o}{4\pi}\right)\hbar\gamma_{\mathrm{I}}\gamma_{\mathrm{S}}}{{r_{\mathrm{IS}}}^3}$$

Chemical shift anisotropy is the dependence of the nuclear spin chemical shift on the orientation of its (non-spherical) electron cloud with respect to the B_0 magnetic field. Dipolar couplings and CSA can be removed or weakened by spinning the sample in an angle of 54.74° with respect to B_0, also known as the magic-angle (Fig.1.4).

Spinning around this angle leads to effective averaging of CSA and the dipolar coupling Hamiltonian to zero or at least small values and therefore tremendous line-narrowing.

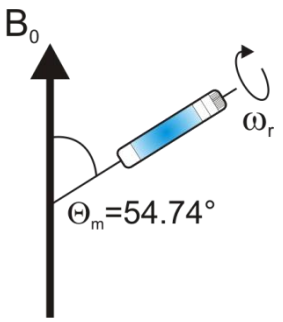

Fig.1.4: Magic-angle spinning (MAS) of the sample leads to tremendous line-narrowing as dipolar couplings and CSAs are (largely) averaged out.

In addition (high-power) dipolar decoupling pulse sequences further lead to an increase in resolution.

Dipolar couplings are also used to transfer polarization from sensitive to insensitive nuclei or recoupling between homonuclear or heteronuclear spins. Cross polarization (CP) [Pines 73] enables high-sensitivity detection of heteronuclei accompanied with short scan repetition rates (Fig.1.5). Two perpendicular B_1 spin-lock fields are applied on both nuclei (e.g. I and S) according to

$$\gamma_I B_I = \gamma_S B_S \pm n w_r$$

known as the Hartmann-Hahn condition, where n is an integer number and w_r the MAS frequency. Under that condition polarization transfer from the sensitive to the insensitive nucleus is achieved.

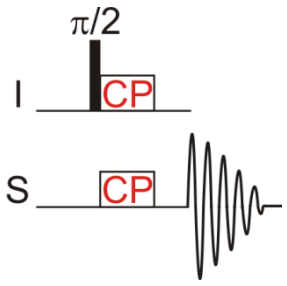

Fig.1.5: Cross polarization from I spins to S spins raises their sensitivity and shortens the scanning delay.

This enables high sensitivity detection of heteronuclei, which behave beneficial in terms of linewidth. In addition, the repetition delay between the scans depends on the I spin longitudinal relaxation time which may be much shorter than the S spin longitudinal relaxation time.

Most pulse sequences that were used in this thesis are designed to have an initial cross polarization step, often followed by magnetization transfer by spin diffusion or other recoupling techniques. Correlation spectra are obtained by either (proton-driven) spin diffusion (PDSD) [Szeverneyi 82] or recoupling sequences such as TEDOR [Hing 92] or PAIN [Lewandowski 07]. Details on these pulse sequences are given in the supplementary information.

1.2 Proton-detected solid-state NMR

In the past, solution NMR-like pulse sequences for biological solid-state NMR studies have not been used extensively as the proton homonuclear dipolar coupling Hamiltonian was not sufficiently averaged by slow magic angle spinning (MAS) rates. Therefore carbon detection in solid-state NMR has turned out to be useful for plenty of applications including structure determination of proteins [Castellani 02; Franks 12; McDermott 12]. Heteronuclear correlations (HETCOR) of fully protonated systems have been extensively recorded with use of FSLG or PMLG homonuclear proton decoupling under detection of the heteronucleus [van Rossum 02]. Proton-detected ^{15}N-^{1}H heteronuclear single quantum coherence (HSQC) spectra in the solid-state have only recently been performed routinely due to novel technical developments. Nowadays, fast MAS rates (up to 60 kHz) are feasible to weaken strong dipolar couplings. This can be combined with high levels of deuteration with low concentration proton back-exchange on labile sites [Chevelkov 06; Zhou 07]. Implementation of this methodology for solid-state NMR has enabled a broad range of solution NMR-like experiments for protein assignment and even fold calculation [Knight 11]. Fig.1.6 shows a solid-state NMR ^{15}N-^{1}H INEPT-HSQC spectrum of ^{2}H,^{13}C,^{15}N OmpG with 10% ^{1}H back-exchange on labile sites, crystallized in deuterated lipids [Linser 11]. Analysis of ^{15}N-^{1}H HSQC spectra of e.g. titration experiments is straightforward compared to other types of spectra, as only one cross peak per non-proline amino-acid is displayed.

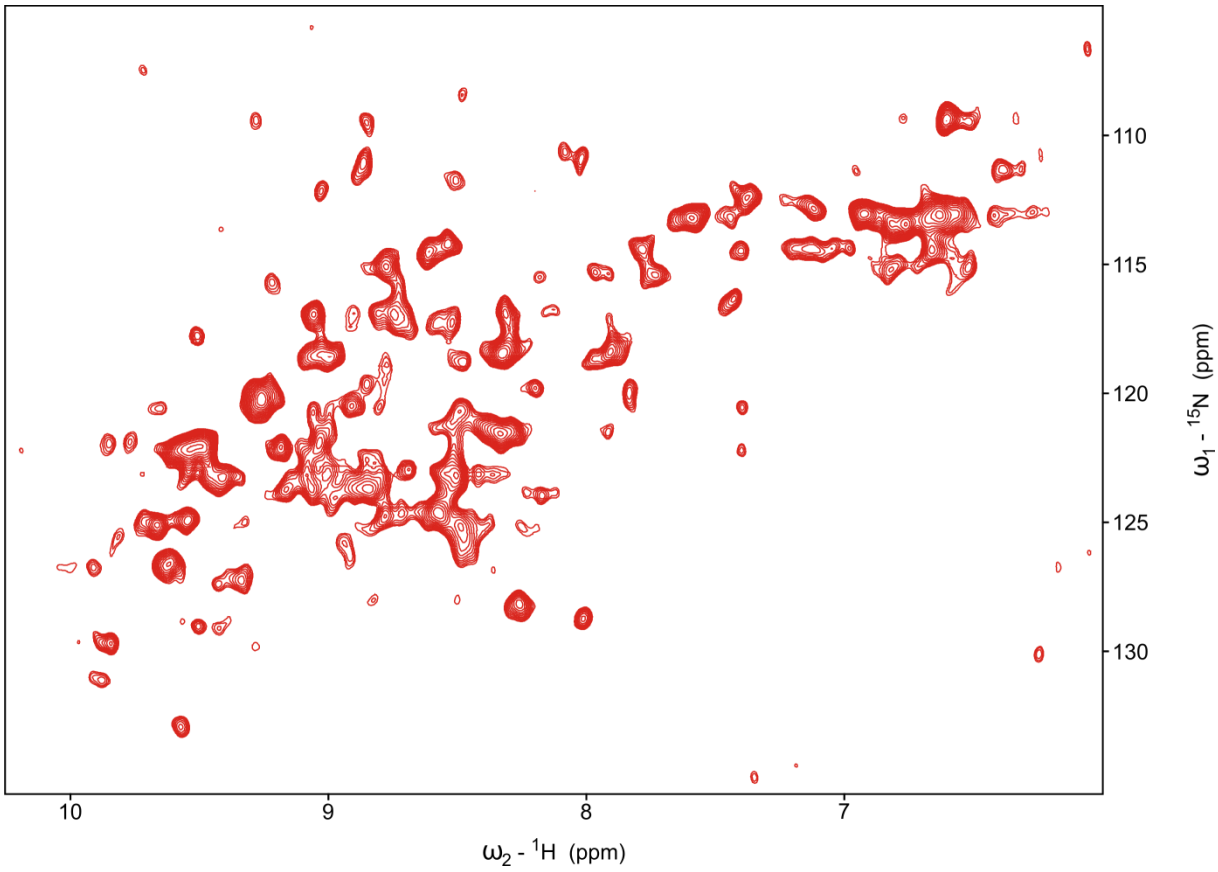

Fig.1.6: Solid-state NMR ^{15}N-^{1}H INEPT-HSQC of ^{2}H,^{13}C,^{15}N OmpG with 10% ^{1}H back-exchange on labile sites crystallized in deuterated lipids at 24 kHz MAS and 16.4T.

1.3 Interaction studies by NMR

In solution NMR spectroscopy, protein-protein interaction studies are performed routinely, by using ^{15}N-^{1}H HSQC spectra. In a system where unbound [U] and bound [B] conformations interconvert the equilibrium is defined as

$$U \leftrightarrows B$$

k_{on} is the kinetic rate-constant for complex formation whereas k_{off} is the kinetic rate-constant for complex dissociation. The exchange rate is defined by

$$k_{ex} = k_{on} + k_{off}$$

The population of spins in the bound state is defined by

$$P_{\mathrm{b}} = \frac{k_{\mathrm{on}}}{k_{\mathrm{on}} + k_{\mathrm{off}}}$$

and for spins in the unbound state

$$P_{\mathrm{u}} = \frac{k_{\mathrm{off}}}{k_{\mathrm{on}} + k_{\mathrm{off}}}$$

In NMR spectra, different situations may be observed, depending on the chemical shift difference of bound and unbound states and the accompanied k_{ex}. In the case of slow-exchange, the exchange rate is much smaller than the difference in chemical shift from both states. Bound and unbound conformations appear as distinct situations and cross peaks are weighted by their respective populations. In a fast-exchange situation, a single cross peak at the average of chemical shifts weighted by the respective populations appears. At intermediate-exchange the cross peak becomes too broad to be detected (Fig.1.7).

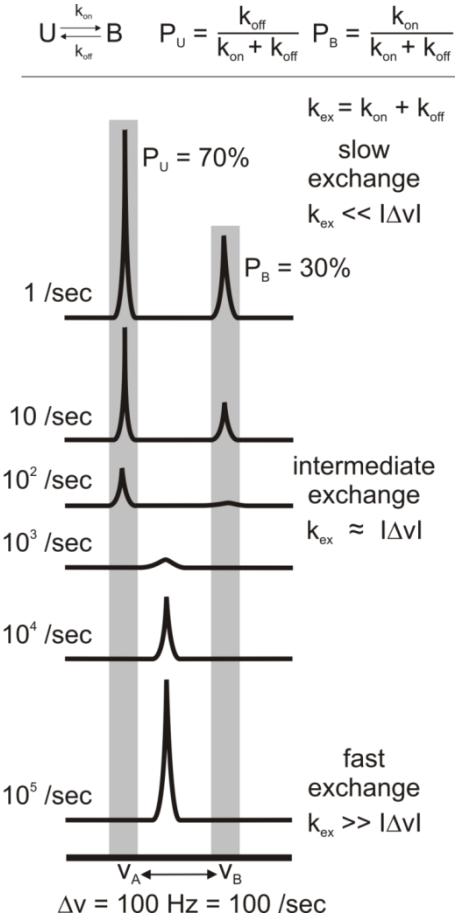

Fig.1.7: Kinetics determine whether exchange leads to separate peak populations, broadening or a shift in frequency for a signal.

Fig.1.8 depicts an example of a titration of ^{15}N labelled synaptobrevin-2 in aqueous solution or bound to dodecylphosphocholine (DPC) with unlabelled ligand CALM-ANTH [Koo 11]. In aqueous solution, the spectrum of the complex shows intermediate exchange broadening for a large set of residues. In contrast, the complex bound to DPC is in the fast-exchange regime leading to shifts for cross peaks of amide backbone and side-chain NH pairs involved in binding. The changes in intensity or chemical shift can then be plotted against the sequence or onto the structure.

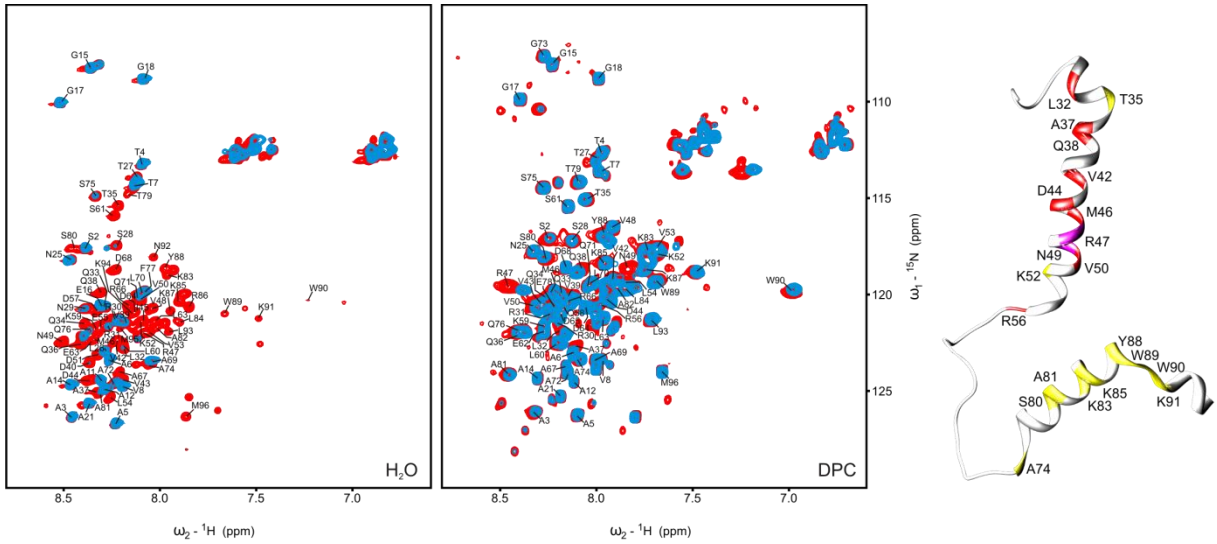

Fig.1.8: Solution NMR interaction experiment. ^{15}N-labelled synaptobrevin-2 is titrated with unlabelled CALM-ANTH ligand in double stoichiometric excess. Left: ^{15}N-^{1}H HSQC spectra of uncomplexed synaptobrevin-2 (red) and in complex with CALM-ANTH (blue) in aqueous buffer. A set of cross peaks in the blue spectrum is (intermediate) exchange broadened. Middle: ^{15}N-^{1}H HSQC spectra of uncomplexed synaptobrevin-2 (red) and in complex with CALM-ANTH (blue) in DPC containing buffer. A set of cross peaks in the blue spectrum experiences changes in chemical shift due to fast-exchange. Right: Chemical shift changes from the experiment in DPC containing buffer plotted onto the structure of DPC-bound synaptobrevin-2 (PDB ID 2KOG). Yellow: weak changes in chemical shift, red: intermediate changes in chemical shift, purple: strong changes in chemical shift upon binding of CALM-ANTH.

Protein-protein interaction studies by solid-state NMR are published rarely [Lange 06; Sun 09]. Problems may arise from sample preparation, e.g. insufficient complex precipitation or crystallization, or from complications with regards to analysis of carbon-detected spectra. Furthermore, carbon as a nucleus seems to barely experience significant chemical shift changes if binding is not accompanied with a structural rearrangement [Schütz 11]. Therefore intermolecular filtering approaches have been developed, that transfer magnetization between differentially isotopically

labelled interaction partners [Schütz 11; Zapke 11]. A complex of native porcine microtubules in complex with a $^{2}H,^{13}C,^{15}N$ Kar3 motordomain construct has been studied recently by solid-state NMR using intermolecular filtering (Fig.1.9) [Zapke 11]. Polarization from microtubule protons was transferred to motordomain carbons and then further to other carbons. The solid-state NMR carbon spectrum therefore shows only those cross peaks from amino acids of Kar3, which are in vicinity to microtubule protons. However, this approach is very sensitive to isotopic "impurities" and requires long measurement times.

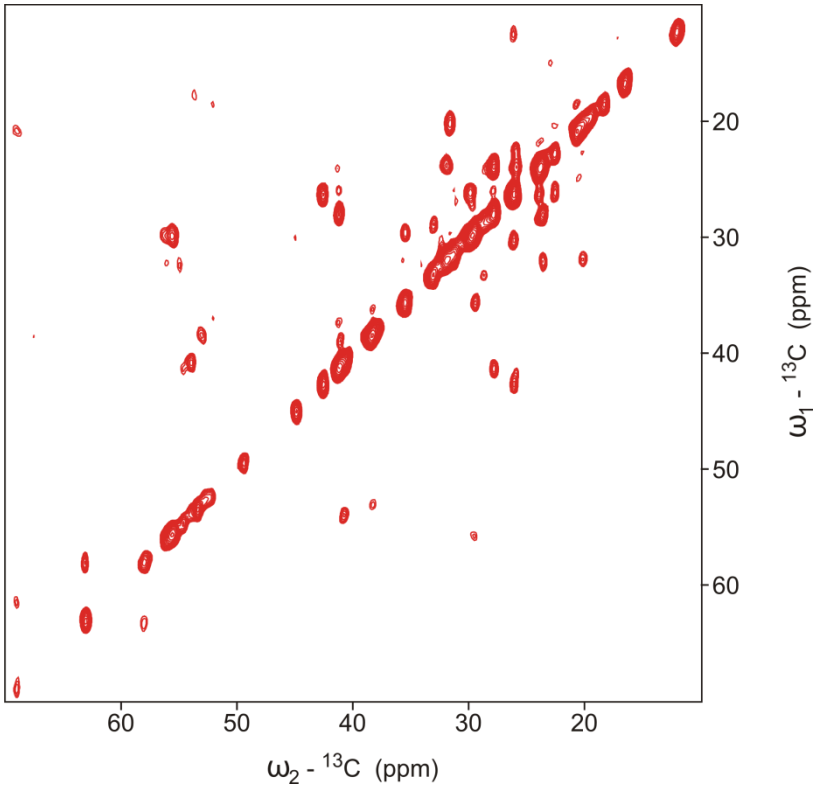

Fig.1.9: Interaction interface filtered solid-state NMR ^{13}C-^{13}C RFDR spectrum of $^{2}H,^{13}C,^{15}N$ Kar3 motordomain bound to porcine microtubules. ^{13}C-^{13}C cross peaks from Kar3 motordomain residues that are in vicinity to microtubule protons are detected.

To my knowledge, the benefit of HSQC-type experiments for protein-protein interaction studies has not been exploited in solid-state NMR so far. In this thesis, immobile-behaving protein complexes are studied as concentrated solutions by ("solid-state") MAS-NMR (known as FROSTY) also using HSQC methodology [Mainz 09; Gardinnet 12; Bertini 11].

1.4 Small-angle X-ray scattering

Small-angle X-ray scattering (SAXS) is a technique that can deliver low-resolution information about particle sizes and shapes [Mertens 10; Hura 09]. X-rays that are hitting on a particle are scattered by its electrons (Fig.1.10).

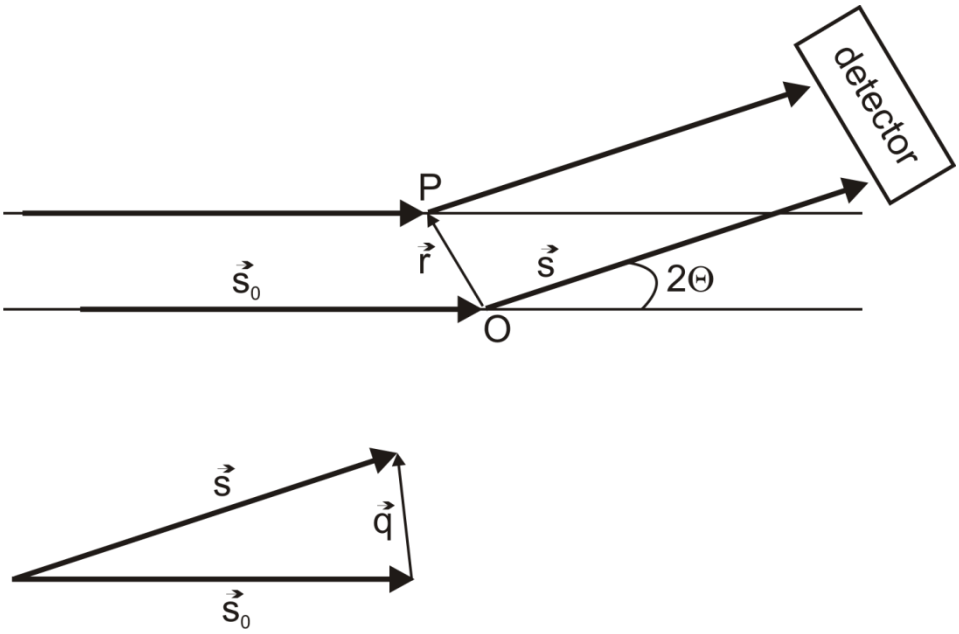

Fig.1.10: Principle of X-ray scattering, fundamental to SAXS measurements.

Elastic scattering occurs without loss of energy. Its intensity can be described by the Thomson formula:

$$I(2\Theta) = {r_0}^2 \frac{1 + \cos^2(2\Theta)}{2d^2} I_0$$

where d is the distance between the sample and the detector, r_0 the radius of the electron and Θ the scattering angle. Scattered waves are amplified in case of constructive interference, when other scattered waves have ideally the same phase or fulfill the Bragg condition. In case of a crystal, the order of the system allows collection of coherent scattering data at wider angles which is accompanied by an increase in data resolution. For a non-crystalline analyte, the scattering is incoherent. Constructive interference is then more likely achieved at small phase shifts i.e. small scattering angles (2Θ) and therefore limited to low-nm resolution. Therefore the detected signal can be seen as the contrast between the solvent and the low-resolution electron density of the system under study. The collected data is

represented as signal intensity plotted against the magnitude of the scattering vector q:

$$q = \frac{4\pi sin\Theta}{\lambda}$$

.

The distance distribution function can be obtained from Fourier transformation of the intensity profile by

$$p(r) = \frac{r^2}{2\pi^2}\int_0^\infty \frac{q^2 I(q)\sin(qr)}{qr}\,dq$$

It displays the distance between any pair of “scattering elements”. Therefore the radius of gyration R_g (which is defined as the average distance of all atoms to the centre of the molecule) and the maximum diameter are determined. In recent years, SAXS has become popular for *ab-initio* modelling of protein shapes, however this approach is not used in this thesis.

1.5 Alpha-B crystallin (αB)

Alpha-B crystallin (αB) belongs to the group of small heat shock proteins (sHsp) and is involved in the cellular stress protection system [Bloemendal 04; Horwitz 92]. It binds molten-globule states of its substrates to prevent protein misfolding and aggregation. Bound substrates are then further passed on to other heat shock proteins (Hsp) with refolding capabilities such as heat shock proteins 70, 90 [Haslbeck 05].

Structural studies of αB have been difficult, as the protein forms polydisperse oligomers of different size, which are too heterogenous to crystallize for X-ray diffraction studies and too large to yield resonable linewiths in conventional solution NMR spectra [Horwitz 92; Aquilina 03; Baldwin, Lioe, Hilton 11]. These oligomers have an average mass of 650 kDa with particles composed of 12 monomers up to more than 50. Oligomers may exchange dimers (after activation) and therefore grow and shrink in size. Dimer exchange is a proposed mode of chaperone action [Baldwin, Lioe, Robinson 11]. Exchanging dimers may bind unfolding substrates and

then be reintroduced into oligomers which then have the substrate bound [Haslbeck 05]. Thereby potential aggregation of the substrate is prevented (Fig.1.11).

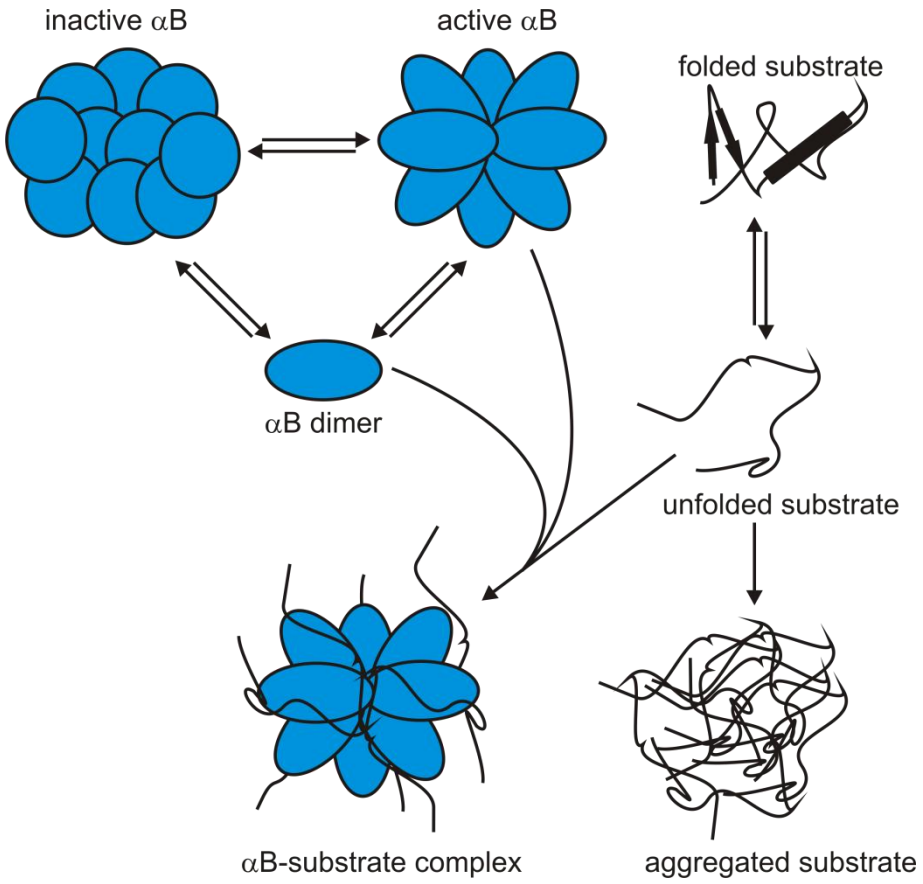

Fig.1.11: Model of protection of substrate aggregation by αB. The activated chaperone may loosen or dissociate, bind an unfolded substrate and reassemble to a chaperone-substrate oligomer complex.

The general domain organization can be divided into three distinct parts: a heterogenous N-terminal domain, a conserved α-crystallin core domain and a C-terminal tail (Fig.1.12).

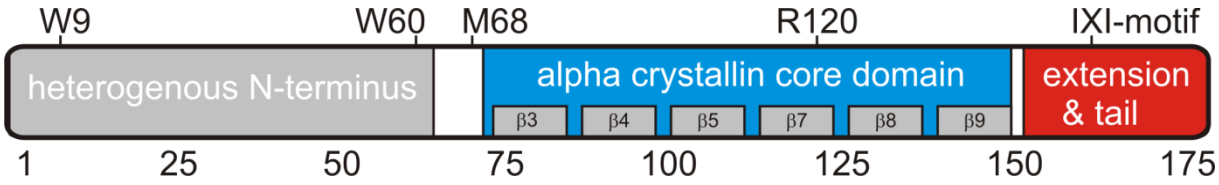

Fig.1.12: Domain organization of αB. W9, W60 and M68 are used in this thesis as monitors for the N-terminus. R120 is crucial for chaperone functionality. Also the IXI-motif is of functional importance as shown in the results section.

The N-terminal domain is partly helical and one factor contributing to oligomerization and polydispersity [Jehle 11]. The C-terminal extension is unstructured and involved in oligomerization [Jehle 10]. The α-crystallin core domain forms a β-sheet sandwich of two layers with three antiparallel β-strands each (Fig1.13) [Jehle 09].

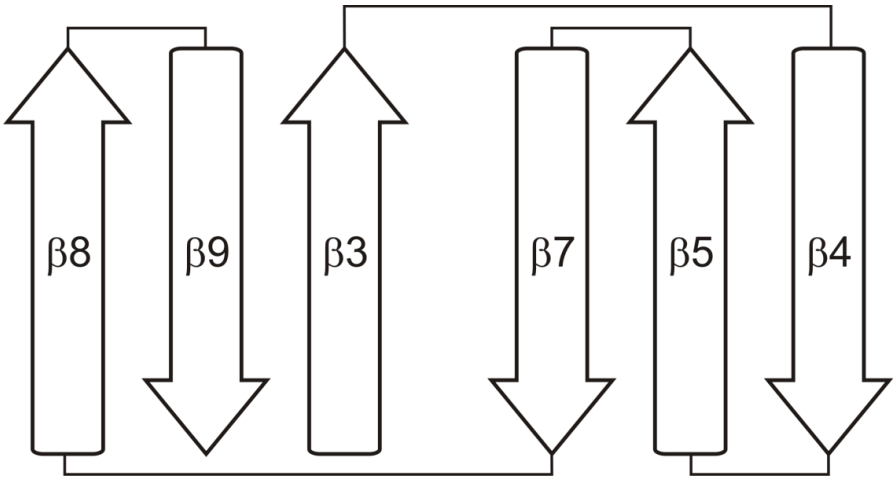

Fig.1.13: Secondary structure of the αB core domain.

Structures for dimers of the core domain exist from either solid-state NMR (in the context of full-length oligomers, PDB ID 2KLR, Fig.1.14) or from X-ray crystallography (truncated constructs without N/C-terminal domains) (PDB ID 3L1G, PDB ID 2WJ7) [Bagnéris 09; Laganowsky 10; Jehle 10].

Fig.1.14: Solid-state NMR structure of the αB core domain dimer in context of full-length αB oligomers.

The dimer interface is formed by an antiparallel β-sheet of β-strand 7 which (forms) hydrogen-bonds to β-strand 7 of another core domain, hence called αB dimer. This point-symmetric, dimeric building block shows a characteristic bent in the solid-sate NMR structure which is absent in the X-ray diffraction structures and may have functional importance [Jehle 10]. Other modes of oligomerization involve the N-terminal domain with itself and the C-terminal domain interacting with the core domain of another monomer, as presented in this thesis.

Oligomers of αB have been extensively studied by electron-microscopy (EM) (PDB ID 2YGD) [Haley 98; Peschek 09; Braun 11]. Oligomers of 24 monomers were chosen for reconstructions (Fig.1.15). The diameter of these particles was around 18 nm with a central cavity of 9 nm.

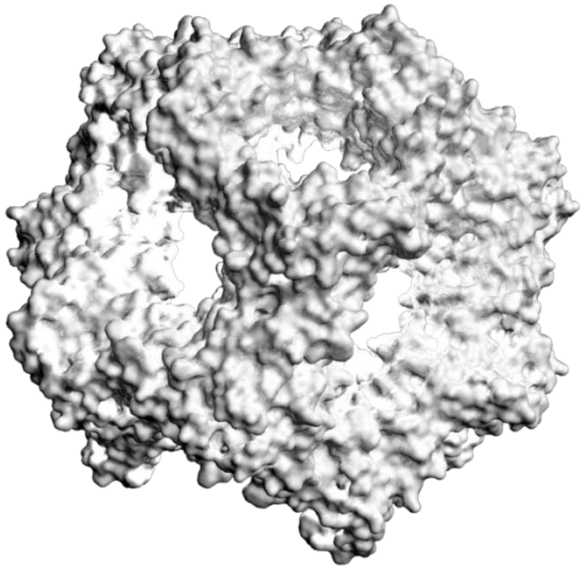

Fig.1.15: Model of an αB 24-mer on the basis of EM, solid-state NMR and crosslinking data (PDB ID 2YGD).

The αB mutant R120G is causing cataract and desmin-related myopathy [Vicart 98]. Its chaperone activity is altered and αB-R120G co-precipitation with e.g. desmin is observed [Bova 99; Wang 01; Der Perng 04]. The mutation site is located in the αB dimer interface. EM studies have shown that oligomeric size is doubled for αB-R120G [Bova 99]. It is not known if abolished chaperone activity originates from a local structural change in the binding site(s) or a different oligomer-dimer regulation. Therefore the heterogeneity of αB-R120G is investigated and discussed in this thesis.

1.6 Substrates of αB

A large set of substrates is reported for αB, such as Aβ, α-synuclein, β/γ-crystallins, desmin, microtubules and others [Sun, MacRae 05; Vicart 98; Augusteyn 04; Haslbeck 05; Shammas 11; Vicart 98; Ecroyd 08; Xi 06]. αB-related diseases involve cataract formation, desmin-related myopathy, Alzheimer's disease, Parkinson's disease and cancer [Sun, MacRae 05; Haslbeck 05]. Substrate interaction of αB is poorly understood in terms of structural biology, i.e. substrate binding sites of αB have not been mapped so far. Ideas about binding interfaces come from e.g. pin-point arrays, which study only isolated sequences but never the full-length protein [Ghosh 08; Ghosh 05].

α-synuclein (α-syn) is a 140 amino acid protein which is reported to be involved in Parkinson's disease [Trojanowsky 98; El-Agnaf 00]. Amyloid fibrils of α-syn make up a large part of aggregates that are named Lewy bodies and can be found in Parkinson's disease patients [Shults 06]. These deposits are suspected to either directly cause loss of dopaminergic neurons in the *substantia nigra* or be a consequence of its harmful species. It is assumed that the protein experiences a pathological gain of function prior to self-nucleation and deposition into Lewy bodies [Perry 99, Waxman 09]. No consent has been formed on the physiological function of the protein. It is assumed that pathology impairs membrane binding and rupture by α-syn [Reynolds 11].

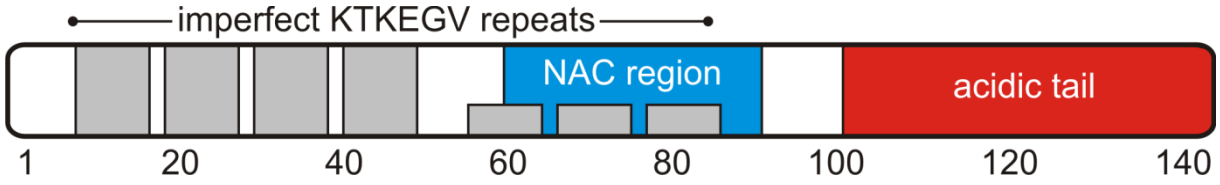

Fig.1.16: Sequence properties of α-syn. Seven imperfect KTKEGV repeats are indicated in grey. The NAC region (blue) is involved in intermolecular interactions in α-syn fibrils. The acidic C-terminal tail is indicated in red.

α-syn is highly charged with seven imperfect KTKEGV repeats in the N-terminus and a highly acidic C-terminal tail (Fig.1.16). It belongs to the group of intrinsically disordered proteins [Bernadó 05; Bertoncini 05]. Binding to micelles was reported previously, which induces α-helical structure in the N-terminal domain from residues 3

to 37 and residues 45 to 92 [Ulmer 05]. Both helices pack against each other when bound to small micelles, however not if planar lipid membranes are bound [Ferreon 09]. A recent fluorescence study reports membrane binding as the first step of α-syn aggregation on the lipid bilayer [Reynolds 11]. This aggregate expels lipids which causes membrane damage and subsequently disrupts the membrane.
α-syn fibrils have also been characterized by solid-state NMR [Heise 05; Vilar 08; Comellas 11; Gath 12]. Various polymporphs show intermolecular cross β-sheet structure for a stretch of residues named non-amyloid component (NAC) region. Recent studies also report secondary structure in the N-terminal domain [Comellas 11]. It is still under debate whether smaller oligomers or “mature” fibrils are the major cause of cell death, whilst the majority of publications suspect pre-fibrillar states as harmful species [Cookson 08; Reynolds 11]. αB has been reported to bind to α-syn and other fibril-forming proteins [Ecryod 08; Jellinger 00; Renkawek 99; Shammas 11; Waudby 10]. Furthermore it can be found co-aggregated with other proteins in Lewy bodies [Lowe 90]. In this thesis, the interaction of αB and α-syn is studied by NMR techniques in order to map the protein binding sites for one another.

Cataract formation is a protein misfolding disease caused by proteins that aggregate in the eye lens and thereby impair eye lens transparency [Michael 11; Bloemendal 04; Huang 10]. About 90% of the eye lens protein content belongs to the superfamily of crystallins [Augusteyn 04; Bloemendal 04]. These can be divided into two subgroups that are structurally and functionally not related with each other. While α-crystallins (A and B) act as chaperones to prevent aggregation of substrates, the β (A1, A2, A3, A4, B1, B2, B3) and γ (A, B, C, D, S) crystallins are structural proteins that give the eye lens its refraction properties.
The β/γ crystallins are structurally related as all members contain domains that are folded as greek-key motifs. β-crystallins are oligomeric in contrast to γ crystallins. γS crystallin (γS) can be found in the human eye lens cortex to maintain structural plasticity and refraction properties [Bloemendal 04]. It is composed of four greek-key motifs that are divided in two domains (Fig.1.17).

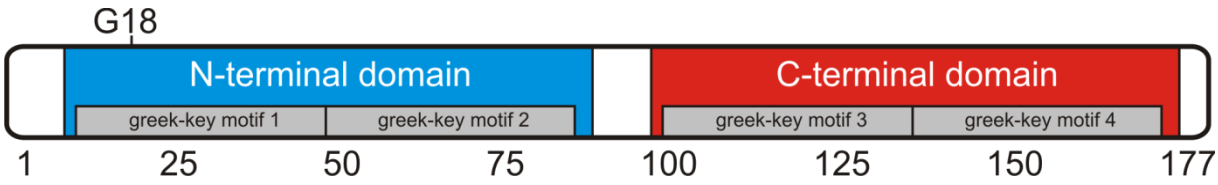

Fig.1.17: Domain organization of γS.

The solution-NMR structure of murine γS (PDB ID 1ZWM) shows that these two domains are structurally almost identical, whereas they are not similar in sequence (Fig.1.18) [Wu 05]. The G18V mutation in γS (γS-G18V) has been shown to cause cataract [Sun, Ma 05].

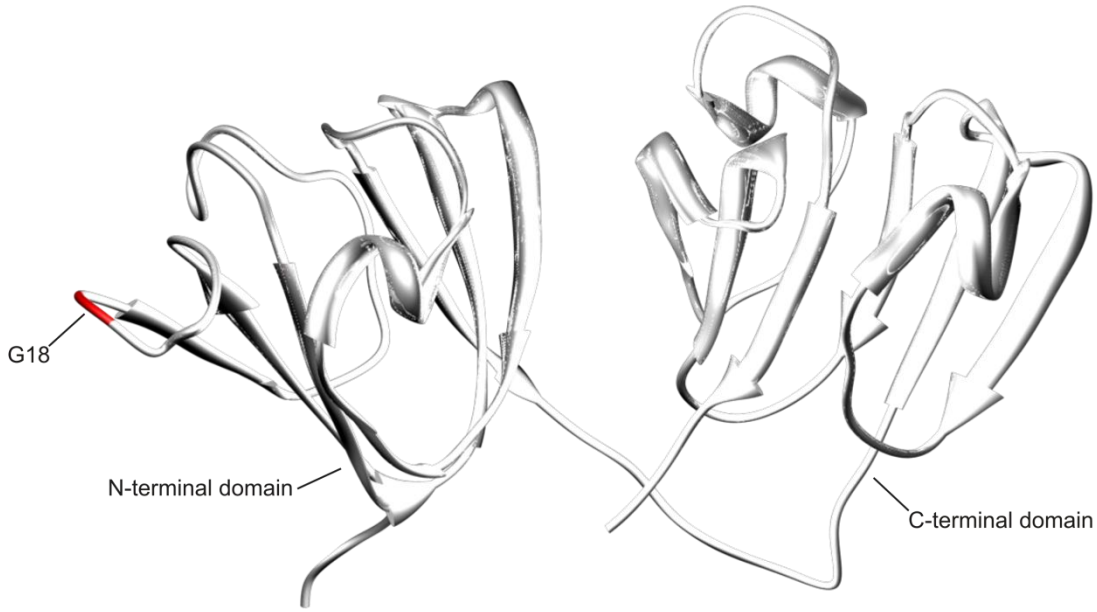

Fig.1.18: Solution-NMR structure of γS.

The interaction of wild-type (wt) and G18V γS with αB is studied in this thesis by NMR techniques.

1.7 Motivation

So far, the mechanism of the chaperone activity of alpha-B crystallin has not been described at atomic resolution. Its oligomeric size and polydisperse architecture have hampered structural studies by X-ray crystallography or solution NMR spectroscopy. This thesis attempts to answer questions regarding the structure-function relationships of alpha-B crystallin by solid-state NMR.

Substrate protein binding is preceded by activation of the chaperone, which indicates a potential exchange of chaperone dimers [Haslbeck 05]. This may facilitate an opening of substrate binding sites (Fig.1.11). Binding sites on the full-length chaperone have not been mapped at atomic resolution so far. It is proposed that alpha-B crystallin oligomerization, activation and substrate binding are connected by a structural trigger.

In this study, the structural basis for oligomerization, activation and substrate binding of alpha-B crystallin is investigated by solid-state NMR, solution NMR and SAXS. In particular, intermolecular contacts are measured in order to understand the mechanisms of oligomerization. Chaperone activation is studied by experiments at low pH, resembling a cellular stress situation, to locate residues that undergo a conformational change. Interaction studies with the Parkinson's disease related substrate alpha-synuclein and cataract related gamma-S crystallin are performed in order to locate the residues that are involved in substrate binding.

2. Results

The following chapter aims at understanding the structural basis for oligomerization of alpha-B crystallin and how it is connected to its mode of activation or activity.

In this context, the mechanisms for alpha-B crystallin oligomerization are studied by solid-state NMR with differentially labelled protomers. Three different pulse sequences that transfer magnetization between different protomers are used for collection of intermolecular restraints. These restraints are used for a structural analysis of oligomerization sites.

A drop in cellular pH is triggered under stress conditions [Haslbeck 05; Fulda 10]. Solid-state NMR PDSD experiments of alpha-B crystallin at high and low pH are recorded. Residues which are affected by pH are related to a pH-dependent activation mechanism. These pH sensitive residues may trigger structural effects on oligomer architecture. SAXS data of alpha-B crystallin oligomers at high and low pH are recorded and put into context with the NMR data. Thus a link between local and global pH-dependent structural changes upon activation can be described.

A mutation of arginine 120 to glycine in alpha-B crystallin causes cataract and desmin-related myopathy [Vicart 98]. Chaperone function of the mutant is reported to be abolished [Bova 99] however no structural explanation for its malfunction is reported. Solid-state NMR PDSD spectra of alpha-B crystallin R120G are analyzed to investigate its heterogeneity and fold. In addition, pH drop experiments are performed, in analogy to experiments with the wild-type protein. From this data, conclusions about a potential impaired activation are drawn.

Binding of alpha-B crystallin to the substrate proteins alpha-synuclein and gamma-S crystallin is investigated in order to locate the chaperone binding sites. Solid-state NMR spectra of chaperone-substrate complexes, in which only alpha-B crystallin is isotope labelled, are recorded. Signal perturbations due to binding are analyzed and plotted on the structure of alpha-B crystallin. In addition solution NMR experiments with isotpe labelled alpha-synuclein are performed to map the interaction site of (truncated) alpha-B crystallin on the substrate protein.

The data from oligomerization, pH activation and substrate binding are put together into a general context to draw conclusions about mechanistic features of the activity of alpha-B crystallin at atomic resolution.

2.1 Measurement of intermolecular contacts in αB oligomers

The oligomerization of αB was studied by measuring intermolecular correlation spectra by solid-state NMR. Mixed oligomers of αB were prepared, in which half of the monomers were isotopically labelled with ^{13}C, whilst being ^{15}N depleted and the other half labelled with ^{15}N with ^{13}C depletion. Thus, two-dimensional ^{15}N-^{13}C correlation spectroscopy generates cross peaks with $^{15}N/^{13}C$ frequencies originating from different monomers (Fig.2.1). For ^{13}C labelled protomers the glycerol labelling scheme [McIntosh 90; LeMaster 90; LeMaster 96] was applied (see supplementary for details).

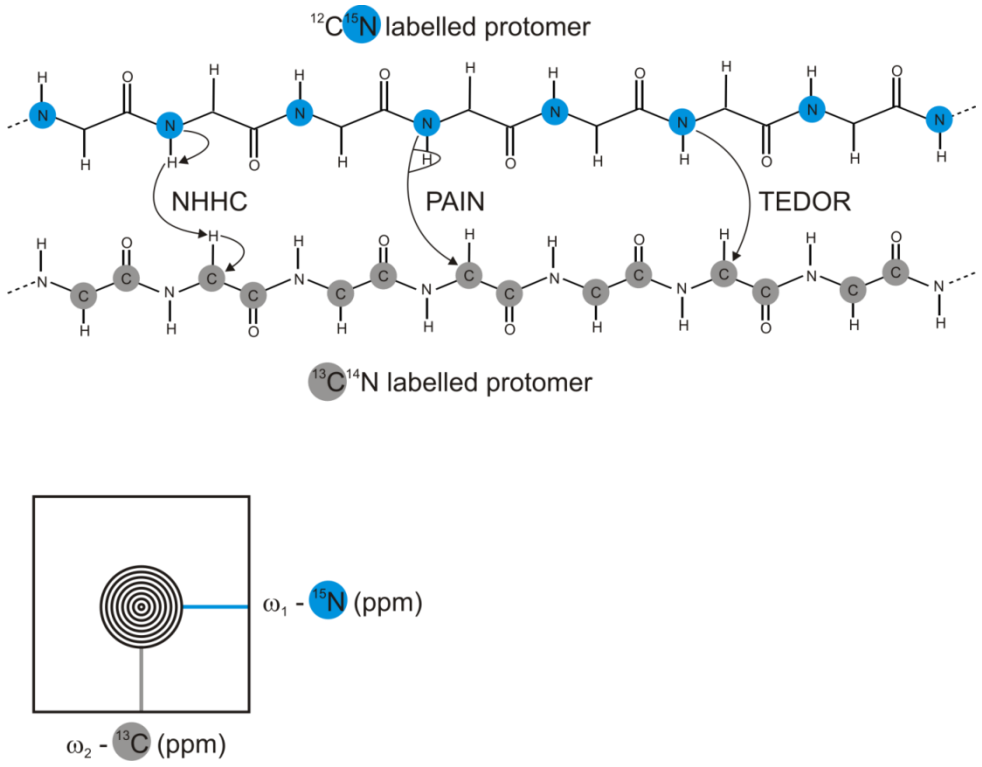

Fig.2.1: Top: Measurement of intermolecular contacts was achieved by mixing protomers of complementary isotopic labelling. Half of the protomers contained ^{15}N labelling only whereas the other half contained ^{13}C labelling only. ^{15}N-^{13}C recoupling techniques such as NHHC, PAIN and TEDOR were used to create cross peaks that correlate two spins from different protomers. Bottom: A crosspeak in such a ^{15}N-^{13}C correlation spectrum correlates a ^{15}N frequency from one protomer with a ^{13}C frequency from a different protomer.

TEDOR, PAIN and NHHC pulse sequences [Hing 92; Lewandowski 07; Etzkorn 04] were used for the measurement of intermolecular contacts (see supplement for experimental details). Fig.2.2 shows heteronuclear correlation spectra using samples

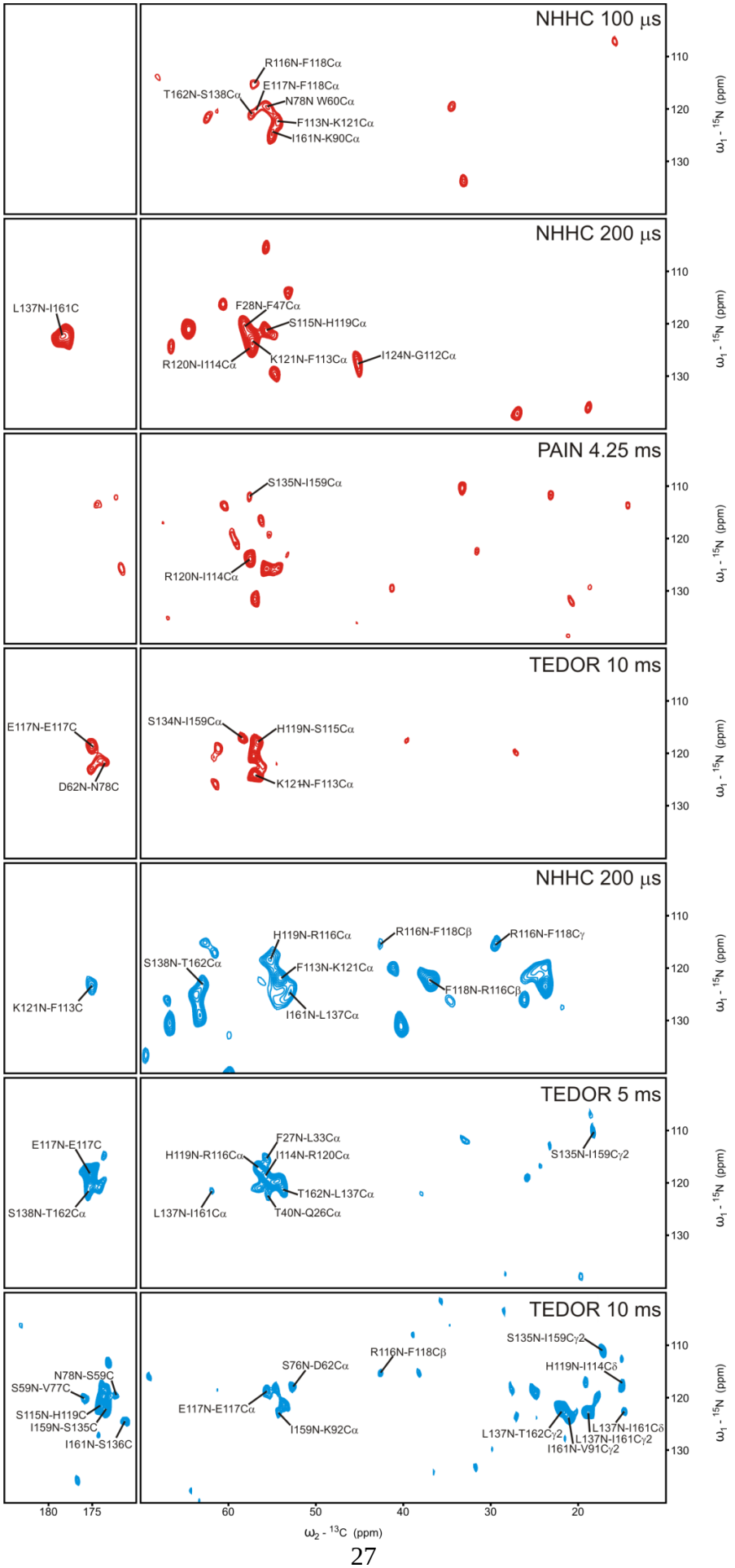
NHHC 100 μs
R116N-F118Cα
E117N-F118Cα
T162N-S138Cα
N78N W60Cα
F113N-K121Cα
I161N-K90Cα
NHHC 200 μs
L137N-I161C
F28N-F47Cα
S115N-H119Cα
R120N-I114Cα
K121N-F113Cα
I124N-G112Cα
PAIN 4.25 ms
S135N-I159Cα
R120N-I114Cα
TEDOR 10 ms
E117N-E117C
D62N-N78C
S134N-I159Cα
H119N-S115Cα
K121N-F113Cα
NHHC 200 μs
K121N-F113C
S138N-T162Cα
H119N-R116Cα
F113N-K121Cα
I161N-L137Cα
R116N-F118Cβ
R116N-F118Cγ
F118N-R116Cβ
TEDOR 5 ms
E117N-E117C
S138N-T162Cα
F27N-L33Cα
H119N-R116Cα
I114N-R120Cα
T162N-L137Cα
L137N-I161Cα
T40N-Q26Cα
S135N-I159Cγ2
TEDOR 10 ms
N78N-S59C
S59N-V77C
S115N-H119C
I159N-S135C
I161N-S136C
S76N-D62Cα
E117N-E117Cα
I159N-K92Cα
R116N-F118Cβ
S135N-I159Cγ2
H119N-I114Cδ
L137N-T162Cγ2
L137N-I161Cγ2
I161N-V91Cγ2
L137N-I161Cδ
110
120
130
ω1 - 15N (ppm)
180
175
60
50
40
30
20
ω2 - 13C (ppm)

Fig.2.2 (on page 27): Intermolecular correlation spectra measured on αB complexes of isotopically mixed protomers. Red spectra were measured on 2G^{13}C αB in complex with ^{15}N αB in a stoichiometry of 1:1. 1) 100 µs NHHC. 2) 200 µs NHHC. 3) 4.25 ms PAIN. 4) 10 ms TEDOR. Blue spectra were measured on 1,3G^{13}C αB in complex with ^{15}N αB in a stoichiometry of 1:1. 5) 200 µs NHHC. 6) 5 ms TEDOR. 7) 10 ms TEDOR.

of mixed oligomers. In general spectra from different pulse sequences provide a non-identical set of cross peaks. TEDOR spectroscopy turned out to be the most reliable of the three sequences used, due to better sensitivity and reduced assignment ambiguity. Recoupling in the PAIN sequence requires an additional third (proton) spin. During PAIN mixing, also homonuclear PAR mixing may occur, which can create correlations that are not necessarily the closest in reality [Nielsen 12]. To reduce this effect only short PAIN mixing times were used. NHHC correlates carbon and nitrogen signals by proton-proton mixing and turned out to be least sensitive.

Four interaction sites between protomers could be identified using correlations of mixed oligomers: the N-terminal domain interacting with itself, a tentative β-strand 2 with β-strand 3 of the core domain, β-strand 7 with itself forming the αB β7-β7 dimer interface and the C-terminal IXI-motif with a groove formed by β-strands 4 and 8 of the core domain. Further cross peaks could be identified but not assigned unambiguously due to the lack of resolution or multiple assignment options. In the following, the latter interaction is discussed further; the respective contacts measured from mixed samples are listed in Tab.2.1.

The information content from mixed 2G^{13}C samples turned out to be rather low, due to insufficient resolution in the Cα region. Side chain correlations are not detected that easily, because the majority of spins is not or only partially labelled.

In contrast, the spectra of the mixed 1,3G^{13}C sample deliver a rich amount of information. Especially TEDOR spectra with long mixing times give a set of nitrogen to methyl or methylene side chain contacts which define the interaction unambiguously. Most prominently I159, I161 and T162 are involved in interactions with the core domain. This so-called IXI-motif binds in a parallel fashion with respect to β-strand 8 and in an antiparallel fashion with respect to β-strand 4. In the following chapter, these contacts have been used to model this intermolecular interaction site.

spectrum	contact
2G PAIN 4.25 ms	S135N-I159Cα
2G NHHC 100 μs	I161N-K90Cα
2G NHHC 200 μs	L137N-I161C
2G TEDOR 10 ms	S135N-I159Cα
1,3G NHHC 200 μs	I161N-L137Cα
	S138N-T162Cα
1,3G TEDOR 5 ms	S135N-I159Cγ2
	T162N-L137Cα
	L137N-I161Cα
	S138N-T162C
1,3G TEDOR 10 ms	S135N-I159Cγ2
	L137N-I161Cδ
	L137N-I161Cγ2
	I161N-V91Cγ2
	L137N-T162Cγ2
	I159N-K92Cα
	S138N-T162Cα

Tab.2.1: Intermolecular contacts measured between the IXI-motif and the αB core domain from measurements of isotopically mixed protomers.

2.2 Modelling the IXI-motif interaction site

The peptide ^{157}PERTIPITREEK^{166}, resembling the αB IXI-motif was modelled *in silico* using the "build structure" application of UCSF Chimera [Pettersen 04]. The peptide has been docked onto the αB core domain dimer using HADDOCK [Dominguez 03]. Separate PDB files of core domain and peptide as well as all intermolecular contacts from Tab.2.1 with an upper bound limit of 7Å were used. Details on the modelling and docking procedure are given in the supplementary. The calculated model is presented in Fig.2.3. The αB core domain forms a groove with its β-strands 4 and 8; named β4/8-groove in the following. This groove presents a surface with two holes, predestined to be filled. The C-terminal IXI-motif residues I159 and I161 fill these holes with their side chains reminiscent of an intermolecular socket-plug relationship.

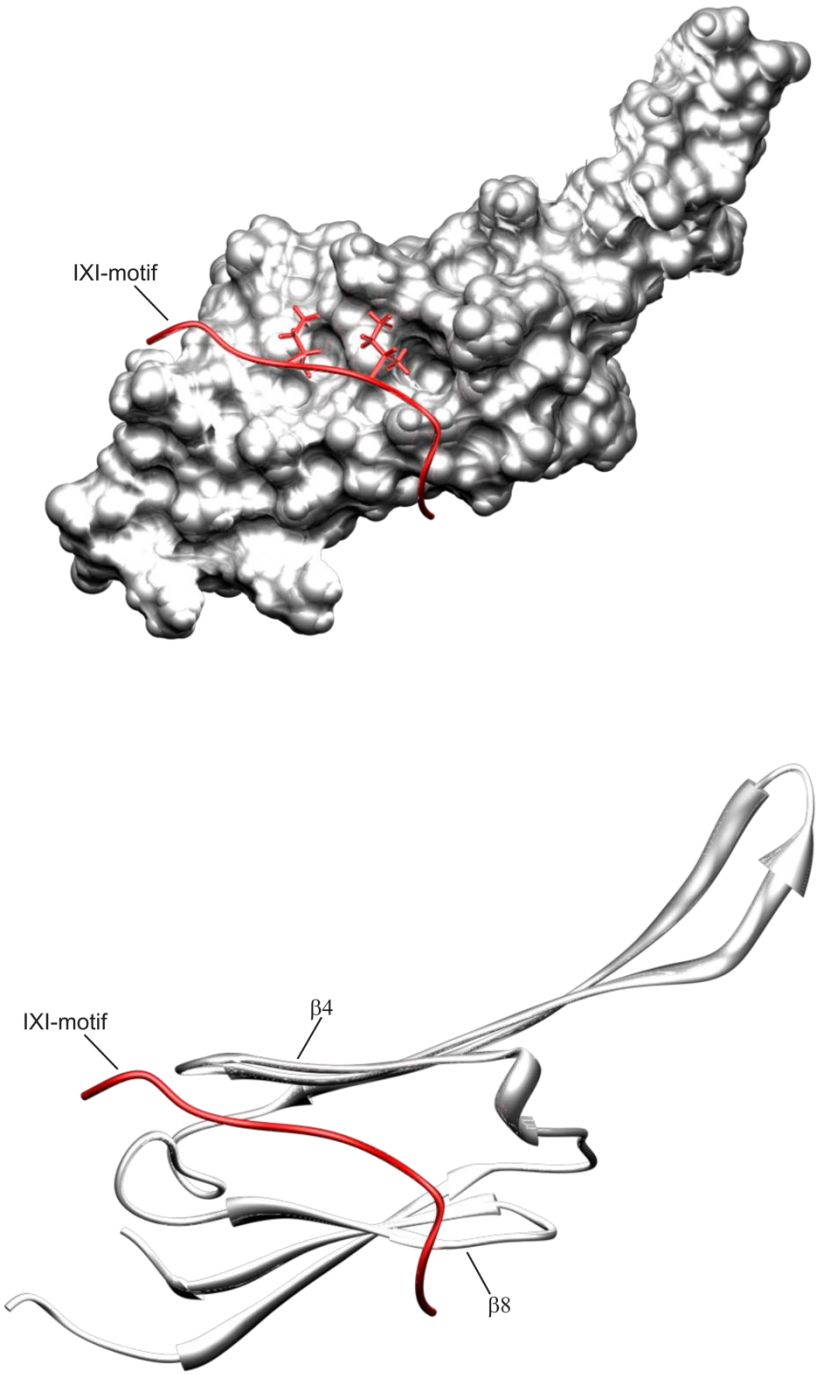

Fig.2.3: Top: Structure of an αB monomer with an IXI-motif peptide bound (in red) from another monomer. I159 and I161 side-chains are depicted. Bottom: Structure as ribbon representation.

After deposition of this model to the PDB, crystal structures of truncated αA/αB crystallin core domain dimers with their corresponding IXI-motifs have been published (PDB ID 3L1G) [Laganowsky 10]. Comparison of the docked solid-state NMR structure with the crystal structure shows a similar architecture and mode of binding (see discussion).

2.3 Activation of αB by pH drop (NMR)

Under cellular stress conditions, a drop in cellular pH is triggered [Haslbeck 05; Fulda 10]. This may lead to activation of αB [Stevens 93; Koteiche 03]. To demonstrate an activated state of αB, PDSD spectra of uniformly labelled protein were recorded at high (7.5) and low (6.5) pH. The majority of residues experience no change in chemical shift. In contrast, residues that are involved in the interaction between β4/8-groove and the IXI-motif show chemical shift perturbations (Fig.2.4). A smearing of resonances for cross peaks of I159, I161 and I133 suggest a structural change, potentially a detachment of the IXI-motif to liberate the β4/8-groove.

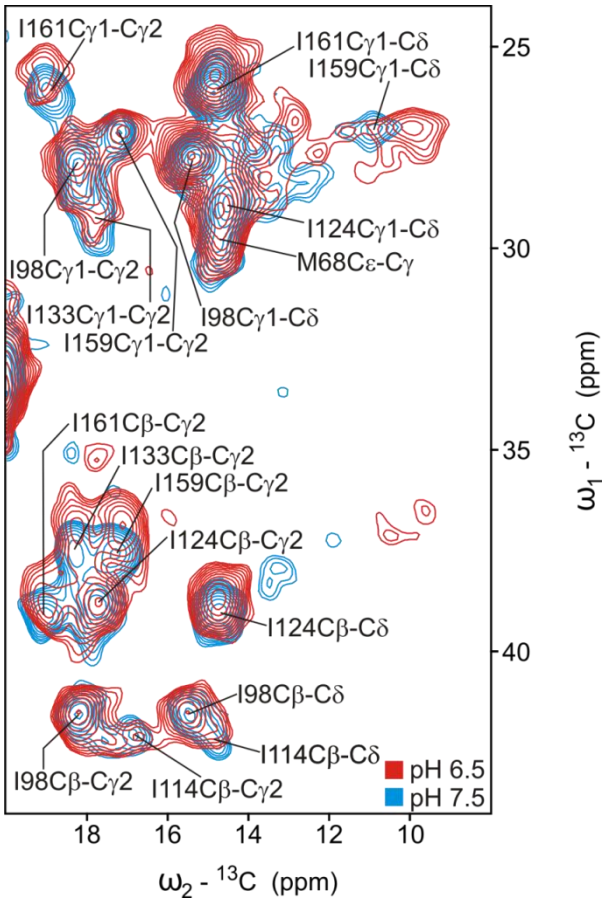

Fig.2.4: pH-drop experiment for ^{13}C,^{15}N labelled αB. Zoom into isoleucine region. Red: 15 ms PDSD of αB at pH 6.5. Blue: 15 ms PDSD of αB at pH 7.5.

To prove this hypothesis, solution NMR spectra of full-length αB oligomers were recorded. Spectra of large particles usually display just a restricted set of cross peaks resulting from mobile residues and thus display dynamics that is on a time scale faster than the overall particle correlation time (Fig.2.5).

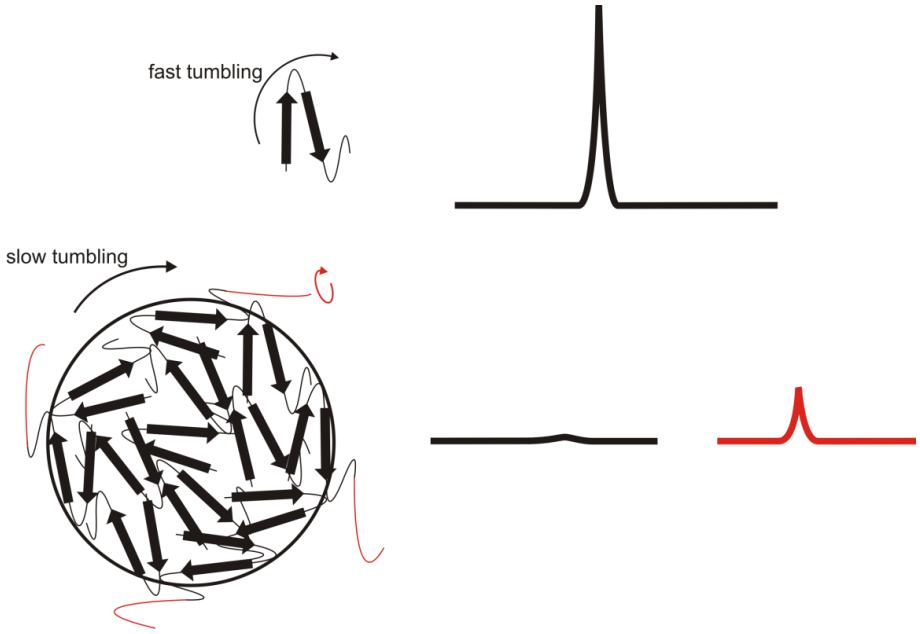

Fig.2.5: Correlation between linewidth and molecular tumbling in solution NMR. Top trace: Small molecules tumble quickly and therefore experience slow transverse relaxation. Detected signals are narrow. Bottom trace: Very slowly tumbling particles relax very quickly and consequently the signals may be broadened beyond detection. However, flexible segments (indicated in red) that exhibit dynamics which are independent of the overall particle motion may relax slower and therefore show up in the spectra.

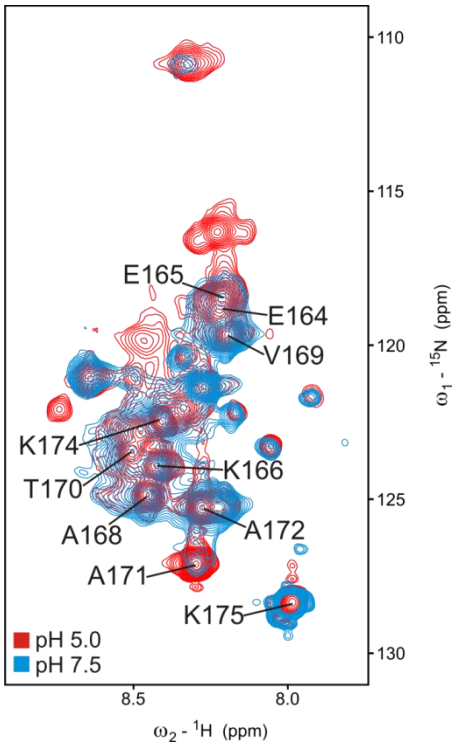

Fig.2.6: pH drop experiment for ^{13}C,^{15}N labelled αB by solution NMR. Blue: HSQC spectrum of αB at pH 7.5. Red: HSQC spectrum of αB at pH 5. Terminal residues, such as A171 become more dynamic upon pH drop, which is reflected in a gain in cross peak intensity. Assignments from [Treweek 10].

In these spectra only flexible residues from the N-/C-termini are visible. Upon pH drop, more cross peaks appear, which indicates that these dynamic regions in the protein become more extended, likely due to detachment of the IXI-motif (Fig.2.6).
Clearly an increase in intensity can be seen for e.g. A171 demonstrating that the C-terminus becomes more flexible. Other cross peaks that appear upon pH drop could not be assigned unambiguously and may also arise from an additional gain in flexibility from other regions (e.g. the N-terminus or loops) from the protein. It is important to mention that a similar effect can also arise from a slower amide proton exchange rate at low pH. To investigate the situation further, the liberation of the IXI-motif was analyzed by SAXS.

2.4 Activation of αB by pH drop (SAXS)

Small-angle X-ray scattering was used to obtain information about αB particle sizes (details on the measurement and data analysis are given in the supplementary). Measurements at pH 7.5 resulted in an averaged radius of gyration R_g of 5.2 nm with a maximum diameter D_{max} of 15.6 nm, which is in agreement with reported particle sizes from other methods (Fig.2.7 top, Fig.2.8 top) [Mainz 11].
Upon pH drop the particle grows to an R_g of 5.9 nm with a D_{max} of 18 nm, indicating an opened conformation (Fig.2.7 bottom, Fig.2.8 bottom). This finding is in agreement with the proposed model of IXI-motif liberation upon pH drop.
Due to its polydispersity, no attempts have been made to reconstruct the 3D electron density *ab-initio*. The pH activation of wild-type αB is compared to pH activation data of the disease-related mutant αB-R120G in chapters 2.6 & 2.7.

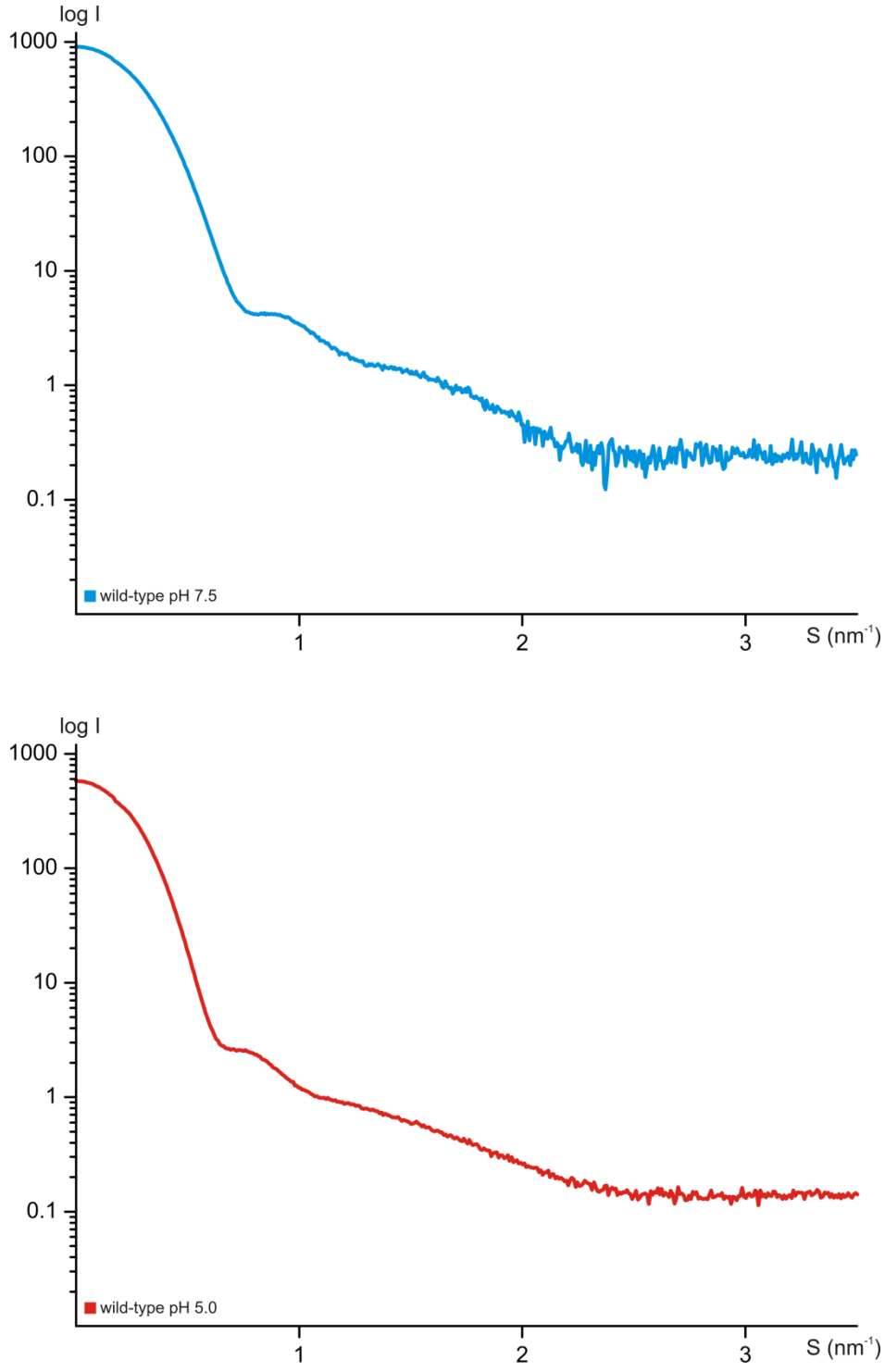

Fig.2.7: SAXS scattering profiles of αB at pH 7.5 (top) and pH 5 (bottom).

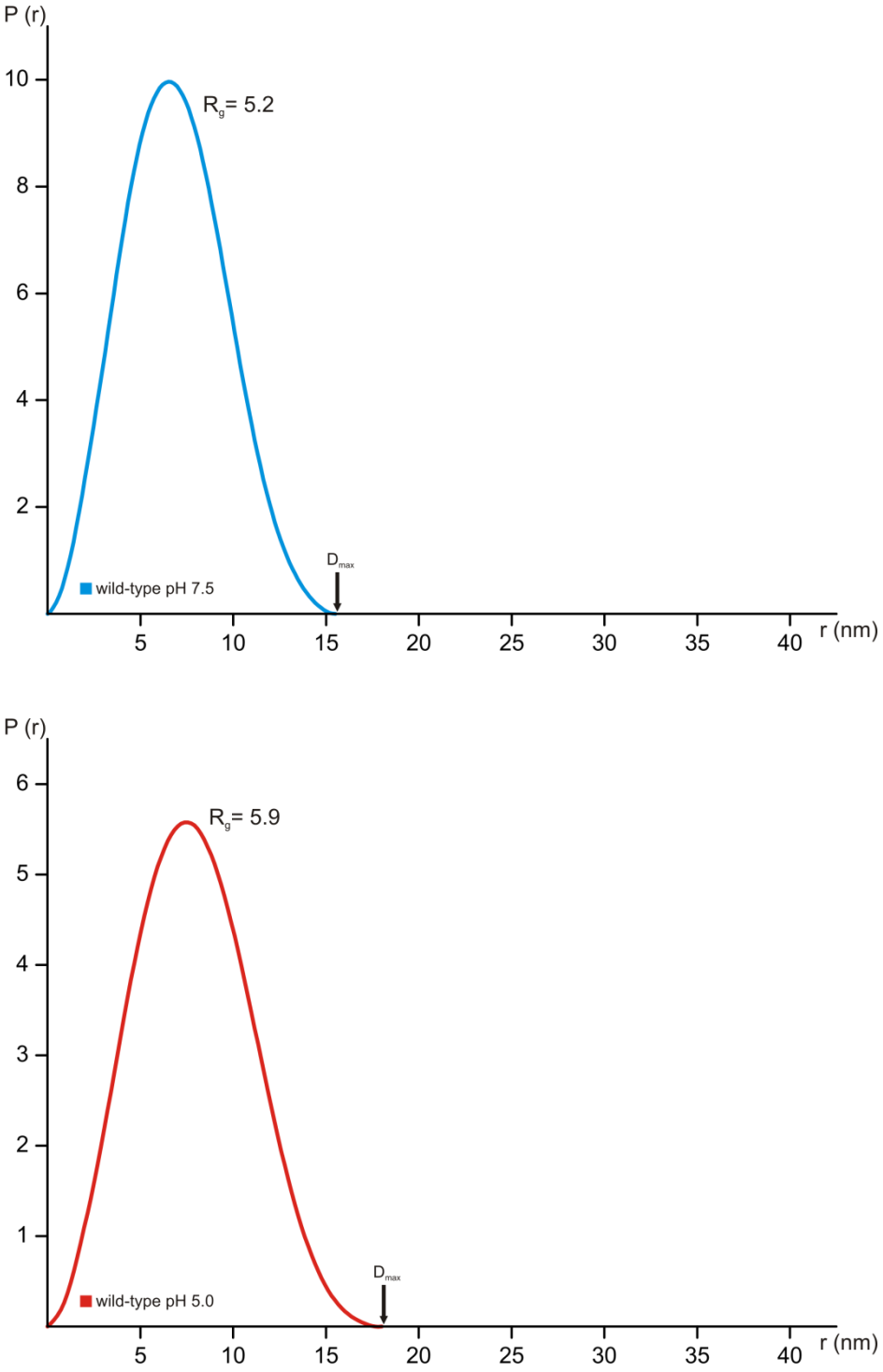

Fig.2.8: Distance distribution functions of αB at pH 7.5 (top) and pH 5 (bottom) from SAXS data.

2.5 The αB-R120G monomer in full-length oligomers is conformationally not more heterogenous than the wild-type

Mutation of arginine 120 to glycine in αB causes desmin-related myopathy and cataract [Vicart 98]. The following chapters present data on structural features of αB-R120G and its pH activation.

Comparison of solid-state NMR spectra from wild-type αB and αB-R120G show shift differences for cross peaks from residues that are close to the mutation site, as reported previously (Fig.2.9) [Jehle 08].

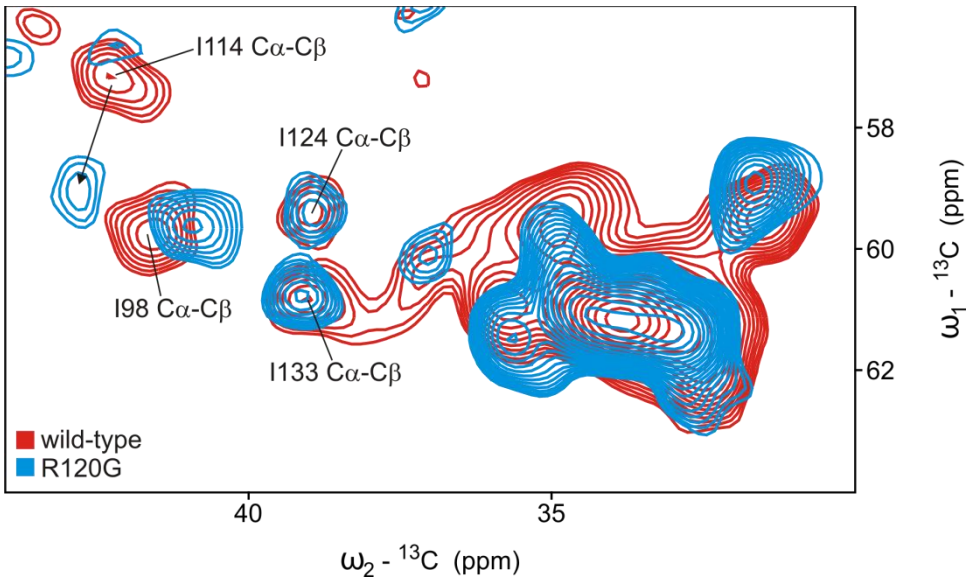

Fig.2.9: Comparison of isoleucine region from 50 ms PDSD spectra of 2G^{13}C^{15}N wild-type αB (red) and 2G^{13}C^{15}N αB-R120G (blue). No increase in local signal heterogeneity can be observed. Adapted from [Jehle 08].

The largest shift difference can be found for signals of I114 which is the intermolecular β-sheet hydrogen-bonding partner for R120 in the wild-type. The mutant protein has been reported to be less stable and more polydisperse than the wild-type [Bova 99]. However, no loss in resolution or cross peak doubling can be observed. Fig.2.9 shows solid-state NMR spectra for the isoleucine region which show no increase in heterogeneity of the core domain (I98, I114, I124, I133) in the mutant. For the N-terminus (I10), and the C-terminus (I159, I161) also no increase in heterogeneity can be observed, concluded from the Cβ-Cδ region of the same spectra (overlay not shown, see blue spectra in Fig.2.11 for comparison). Spectra of αB with specific amino-acid labelling using ^{13}C,^{15}N methionine and tryptophane were

recorded to study the heterogeneity in the N-terminal domain. Reporter resonances of W9, W60 and M68 of wild-type αB (with specific amino acid labelling PFMW) and αB-R120G (with specific amino acid labelling MW) were compared. No gross change in signal heterogeneity for these few residues can be observed (Fig.2.10).

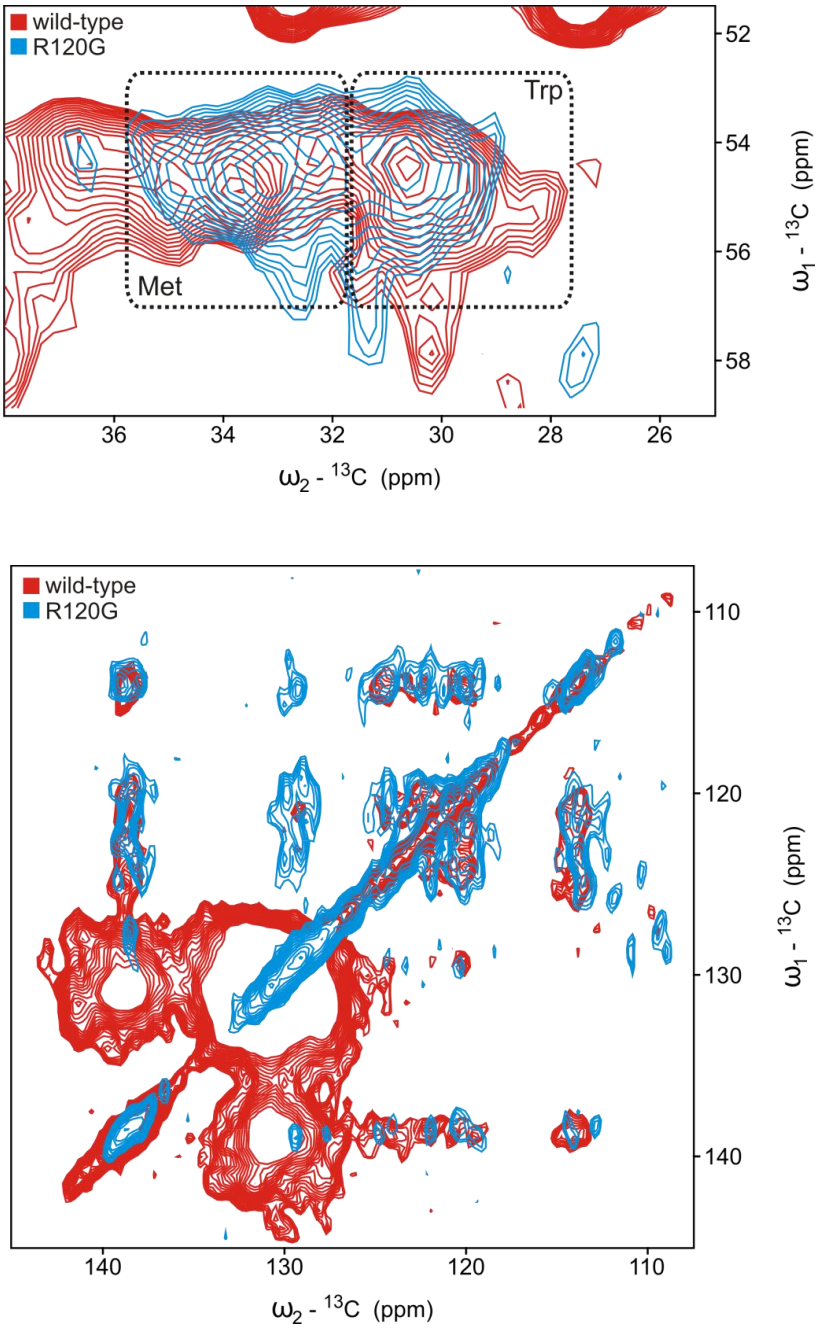

Fig.2.10: Comparison MW regions from 40 ms DARR spectra of PFMW-labelled wild-type αB (red) and MW-labelled αB-R120G (blue). Top: MW aliphatic region. Bottom: W aromatic region. No increase in local heterogeneity can be observed.

In conclusion, the larger polydispersity of αB-R120G is not caused by a change in protomer heterogeneity.

2.6 Activation of αB-R120G by pH drop (NMR)

Chaperoning malfunction of αB-R120G may potentially originate from irregular (pH) activation. In the following the pH activation of αB-R120G is studied by solid-state NMR.

The attempt to prepare a sample of αB-R120G at pH 6.5 resulted in precipitation. However, samples at pH 5 remained soluble and therefore all pH drop experiments on αB-R120G are carried out at either pH 7.5 or pH 5 and compared to wild-type data at pH 7.5 or pH 5 respectively. Upon pH drop, changes for the β4/8-groove and IXI-motif interaction are observed, similar as to the wild-type pH drop experiment. Additionally, cross peaks for I114, which is the hydrogen-bonding partner of R120 in the wild-type, show significant chemical shift changes (Fig.2.11). These changes are absent in the pH-drop experiment of wild-type αB. This gain in pH sensitivity for chemical shifts of residues in the αB-R120G β7-β7 dimer interface is further investigated by SAXS to link this local conformational change to global effects on oligomer size.

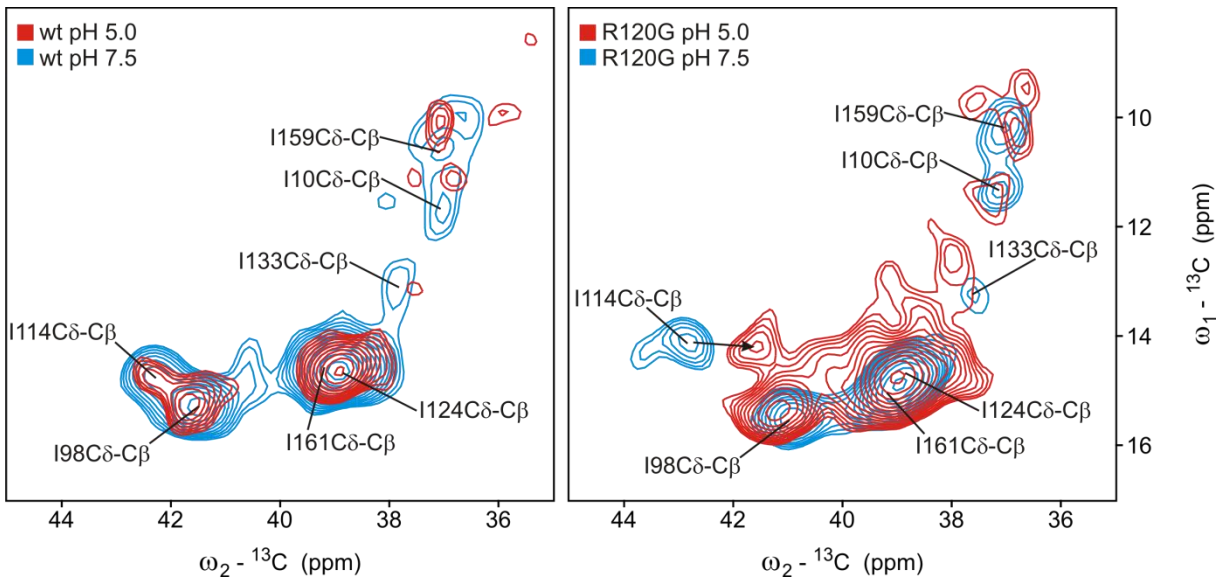

Fig.2.11: Comparison of isoleucine regions from 50 ms PDSD spectra of 2G^{13}C^{15}N wild-type αB and 2G^{13}C^{15}N αB-R120G upon pH drop. Left: wild-type αB pH drop. Right: αB-R120G pH drop. A shift upon pH drop for I114 resonances in αB-R120G can be seen (indicated by an arrow), which is absent in wild-type αB.

2.7 Activation of αB-R120G by pH drop (SAXS)

Measurements for αB-R120G at high pH resulted in a radius of gyration R_g of 7.9 nm with a D_{max} of 30 nm, which is in agreement with particle sizes determined from other methods (Fig.2.12 top, Fig 2.13. top) [Bova 99].

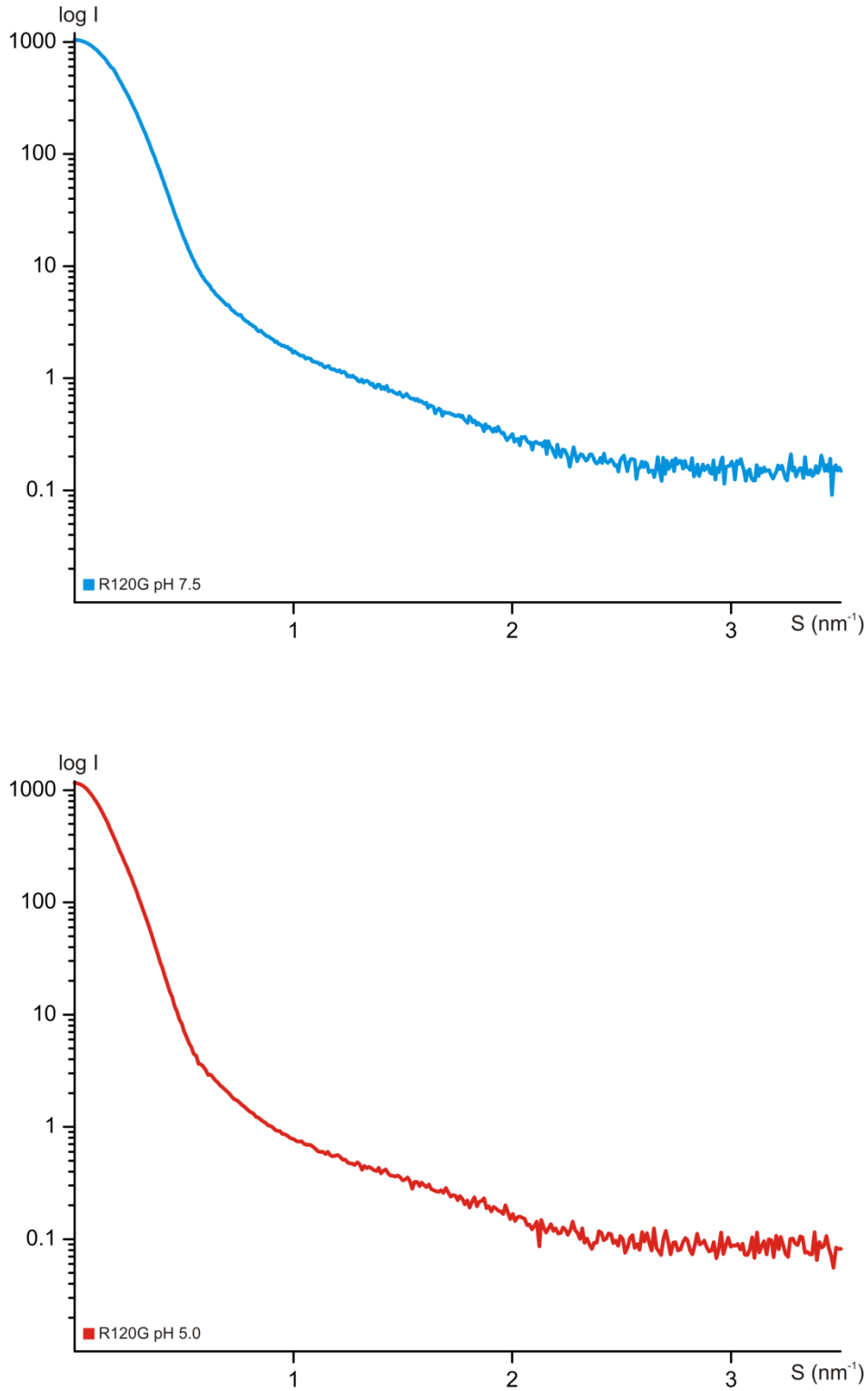

Fig.2.12: SAXS scattering profiles of αB-R120G at pH 7.5 (top) and pH 5 (bottom).

The effect of the point mutation therefore leads to an approximate doubling in oligomer size (the D_{max} of wild-type αB is 15.6 nm). Low-pH measurements resulted in a radius of gyration R_g of 11.1 nm with a D_{max} of 40 nm.

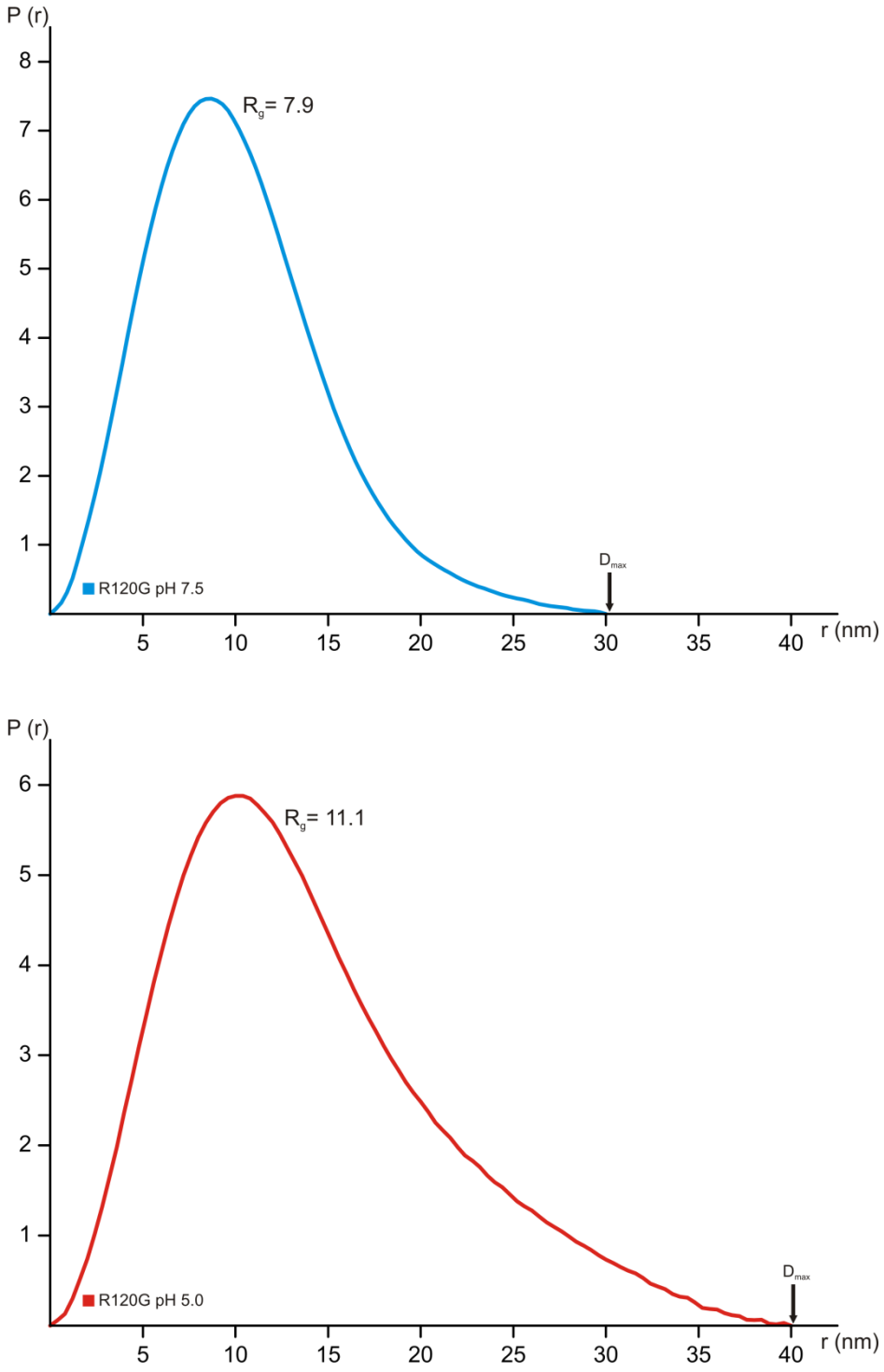

Fig.2.13: Distance distribution functions of αB-R120G at pH 7.5 (top) and pH 5 (bottom) from SAXS data.

This significant increase in particle size cannot be explained through a simple detachment of the IXI-motif from the oligomer body, as suggested for the wild-type situation. It is rather suggested that the oligomeric equilibrium is heavily distorted leading to uncontrolled growth.

2.8 The β4/8-groove of αB is a binding site for α-synuclein

A hallmark of Parkinson's disease is the formation of Lewy bodies [Shults 06] that, to a large extend, contain amyloid fibrils of the protein α-synuclein (α-syn) [Perry 99, Waxman 09]. Previous studies have reported inhibition of α-syn fibril formation by αB, however these studys do not explain a structural mechanism of binding [Ecryod 08; Jellinger 00; Renkawek 99; Shammas 11; Waudby 10]. In the following chapter the interaction of αB and α-syn is studied by NMR techniques to map binding sites for one another. Isotopically labelled αB was complexed with unlabelled α-syn and studied by solid-state NMR. Inversely, isotopically labelled α-syn was complexed with an unlabelled, truncated αB construct (explained below) and studied by solution NMR.

Complexes of unlabelled α-syn with 1,3G^{13}C αB in a stoichiometry of 4:1 were prepared and precipitated. The precipitation yield turned out to be low. Comparison of PDSD spectra of bound and unbound states reveal chemical shift changes and loss of intensity for cross peaks of residues in β-strands 4, 8, 9, their connecting loops and the IXI-motif (Fig.2.14, Fig.2.15). A list of observed changes is given in Tab.2.2.

Further chemical shift changes can be found, e.g. for unassigned/unstructured prolines which are predominant in the N-terminal domain (or P160). Therefore additional binding sites cannot be fully excluded. The interaction can be classified as weak, as the chemical shift changes upon binding are not exceptionally strong. Nevertheless the data analysis yields a coherent picture of the binding site. The residues that experience signal perturbations upon α-syn binding have been highlighted in the structure of the αB core domain with its bound IXI-motif in Fig.2.16.

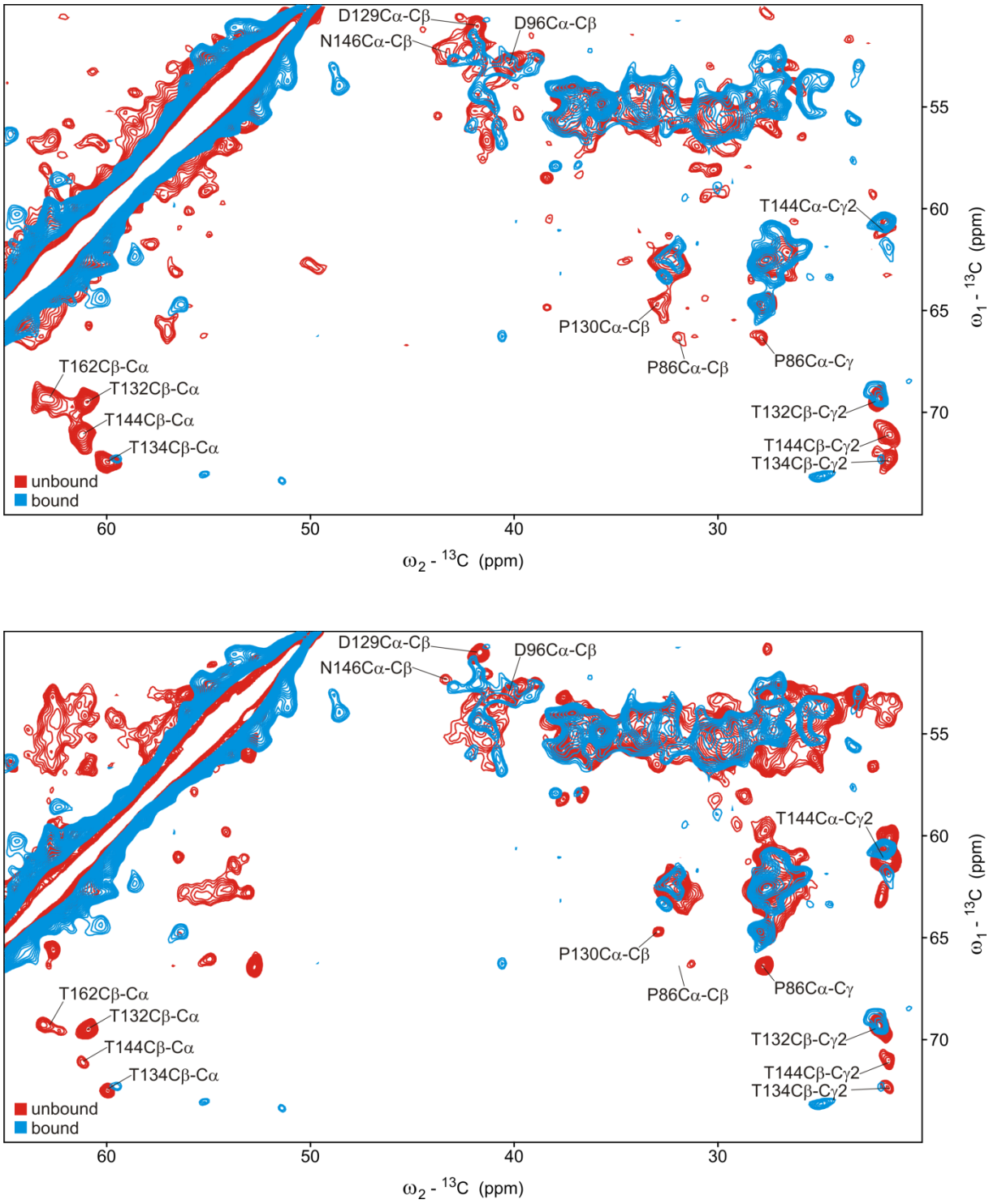

Fig.2.14: Signal pertubations for 1,3G^{13}C^{15}N labelled αB in complex with unlabelled α-syn. Top: Red: 50 ms PDSD of αB. Blue: 50 ms PDSD of αB in complex with α-syn in a stoichiometry of 1:4. Bottom: Red: 200 ms PDSD of αB. Blue: 50 ms PDSD of αB in complex with α-syn in a stoichiometry of 1:4. Assignments for cross peaks with strongest perturbations are indicated.

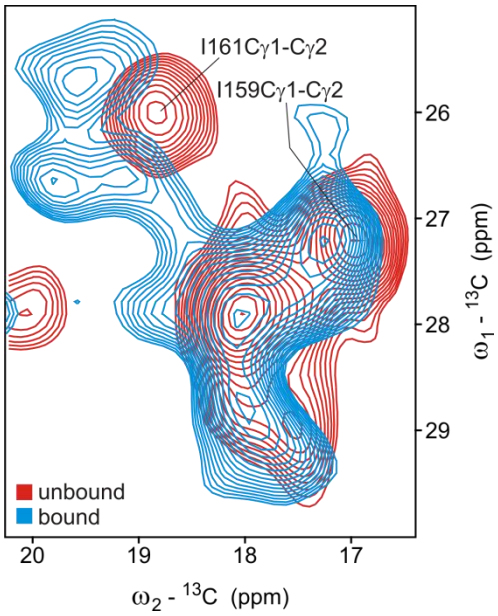

Fig.2.15: Signal pertubations for 1,3G^{13}C^{15}N labelled αB in complex with unlabelled α-syn. Zoom into the isoleucine region. Red: 50 ms PDSD of αB. Blue: 50 ms PDSD of αB in complex with α-syn in a stoichiometry of 1:4. Assignments for cross peaks with strongest perturbations are indicated.

residue	position in structure
P86	loop to β4
D129	loop to β8
P130	loop to β8
T132	β8
T134	β8
T144	β9
N146	β9
I159	IXI-motif
I161	IXI-motif
T162	IXI-motif

Tab.2.2: List of αB residues that experience perturbations in their signals upon complexation with α-syn.

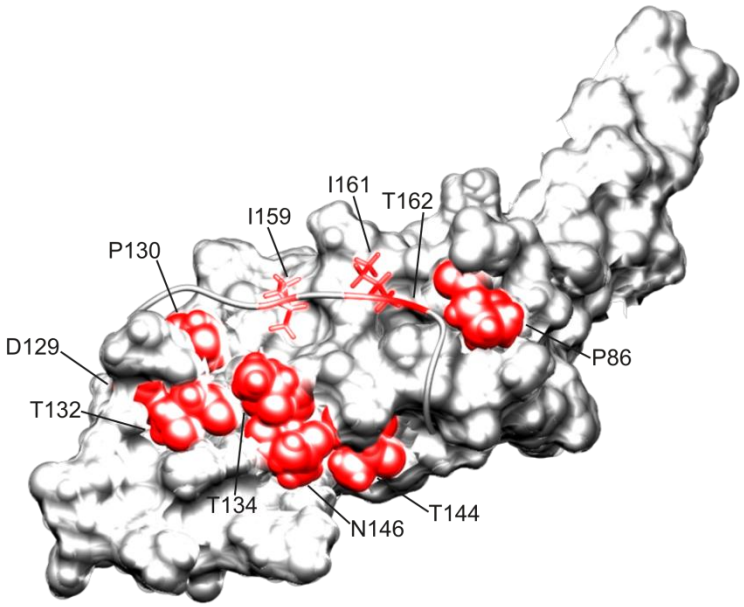

Fig.2.16: A binding site of α-syn on the αB surface. The β4/β8-groove with an IXI-motif strand from another monomer bound is depicted. αB residues that experience signal perturbation upon binding are highlighted in red.

To demonstrate the binding site on α-syn, solution NMR ^{15}N-^{1}H HSQC spectra employing ^{15}N labelled α-syn were measured. As αB oligomers exceed the size limit for conventional solution NMR methods, a truncated αB core domain construct (named αB-10.1 in the following), which forms exclusively dimers in solution was used (Fig.2.17).

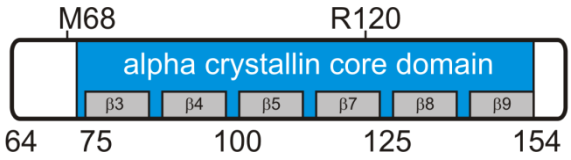

Fig.2.17: Truncated αB-10.1 forms dimers in solution and therefore has a suitable size for solution NMR interaction studies. In this case unlabelled αB-10.1 is complexed with ^{15}N-labelled α-syn.

^{15}N-^{1}H HSQC spectra of α-syn alone and in complex with unlabelled αB-10.1 in a stoichiometry of 1:6 were recorded (Fig.2.18).

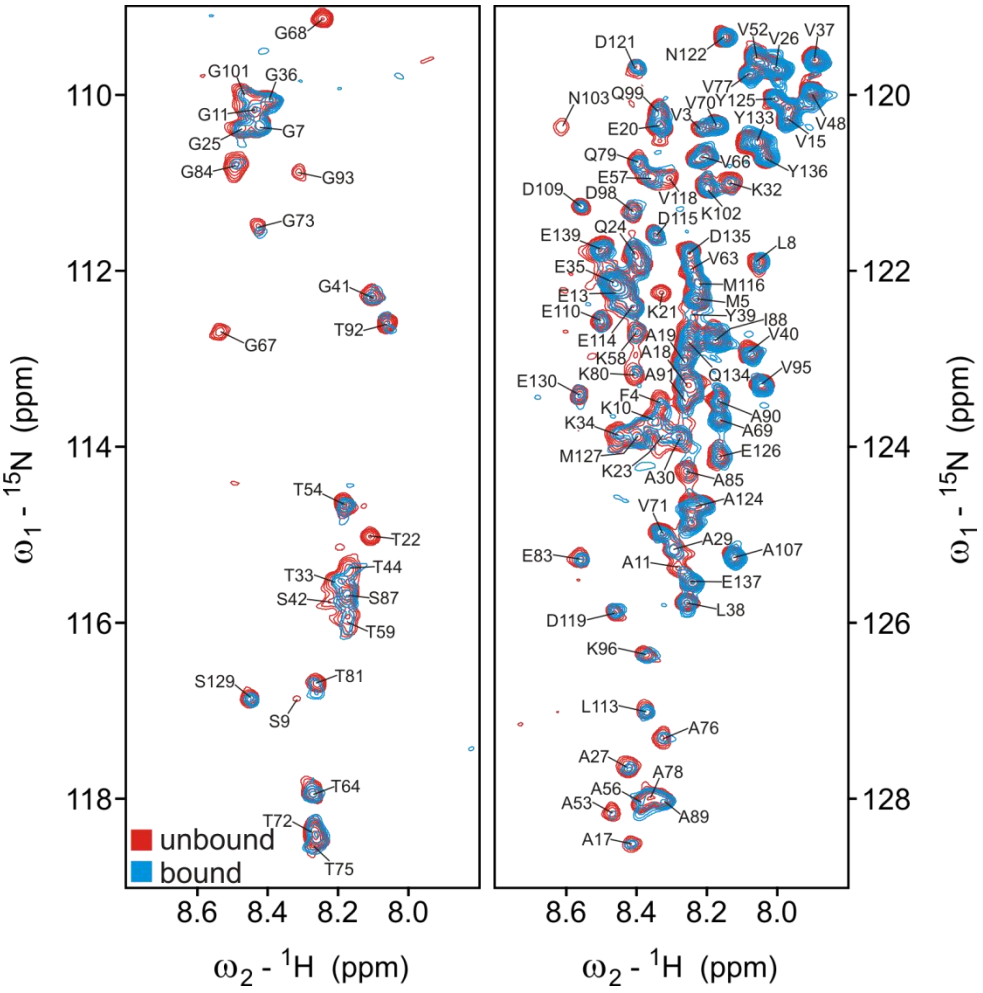

Fig.2.18: Solution NMR ^{15}N-^{1}H HSQC titration of ^{15}N-labelled α-syn with unlabelled αB-10.1. Two separate samples were prepared, a control sample with α-syn only (red) and in complex with six-fold molar excess of αB-10.1 (blue). A decrease in intensity can be observed upon binding. For presentational reasons the ^{15}N-^{1}H HSQC spectrum has been split into two parts for upfield (left) and downfield (right) regions in the nitrogen dimension.

Most cross peaks experience either significant exchange broadening due to an interaction or enhanced T2 relaxation through complex formation. However, the latter seems not very likely due to the comparably small molecular weight of the αB-10.1 dimers. A control sample of α-syn alone was treated in the same manner. In conclusion, loss of signal intensity did not originate from aggregation of sole α-syn and its subsequent enhanced T2 relaxation. Fig.2.19 shows peak intensity ratios of ^{15}N-^{1}H HSQC spectra of bound over unbound α-syn plotted against the amino acid sequence.

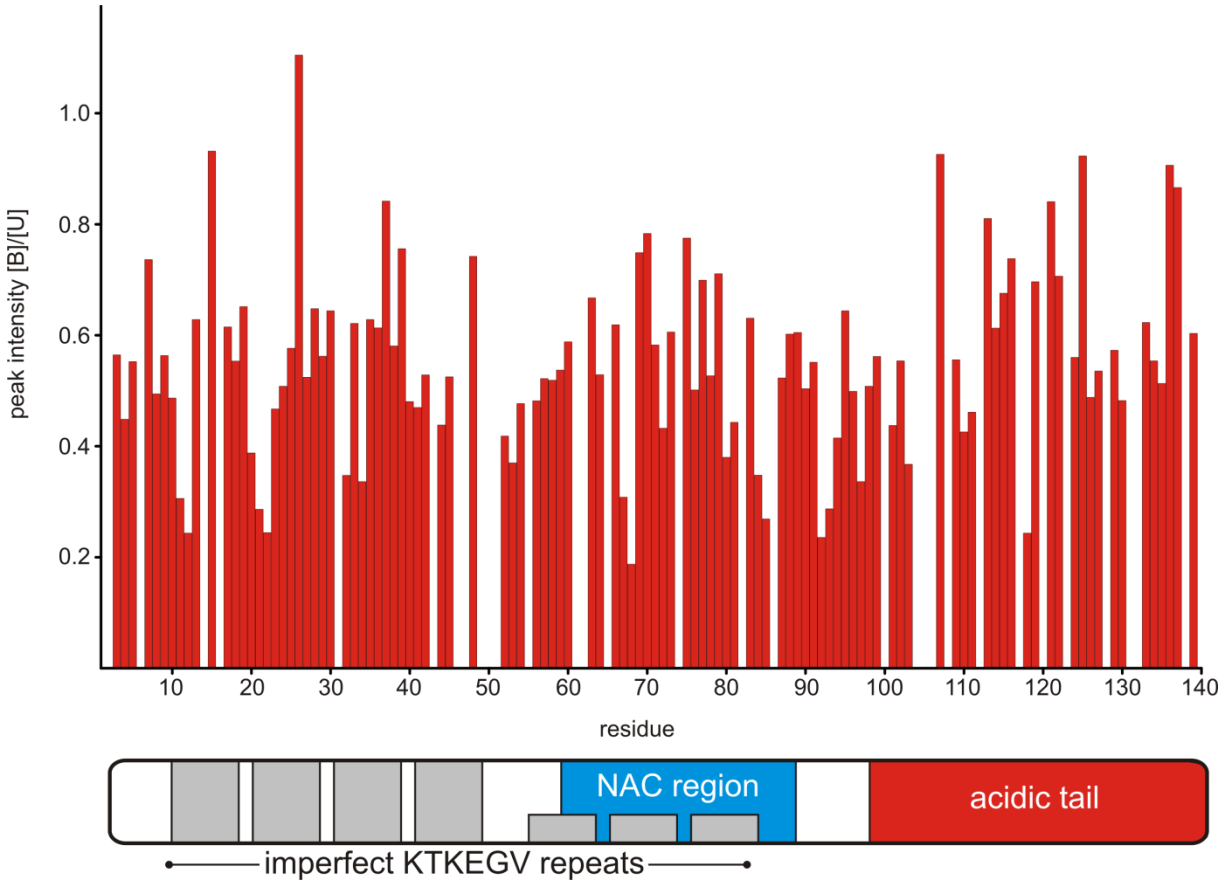

Fig.2.19: Peak intensity ratios for ^{15}N-labelled α-syn in complex with αB-10.1 over ^{15}N-labelled α-syn alone, plotted against the α-syn sequence. The lower the ratio, the more exchange broadening and therefore strong interaction with αB-10.1.

No single binding site can be identified, as the entire sequence of α-syn shows exchange broadening. Therefore the interaction between αB and α-syn turns out to have a specific binding site on the chaperone, but not on the substrate.

2.9 Binding site of αB for γS-crystallin and its mutant γS-crystallin G18V

Aggregation of the protein γS-crystallin (γS) and its mutant G18V leads to cataracts in the eye lens [Bloemendal 04; Sun, Ma 05]. αB has been shown to bind γS and prevent its aggregation [Acosta-Sampson 10; Horwitz 92; Raman 95; Boyle 94; Gopalakrishnan 94; Takemoto 94; Wang 94; Weinreb 00]. However, these studies lack a structural explanation for the interaction. In the following, the interaction between isotopically labelled αB and unlabelled γS is investigated by solid-state NMR, to map the chaperone binding site. Furthermore novel technical approaches

have been applied for the study of this interaction, such as amino acid specific isotope labelling, FROSTY solution-MAS spectroscopy [Mainz 09; Gardinnet 12; Bertini 11] and proton-detected ^{15}N-^{1}H HSQC spectroscopy [Chevelkov 06; Zhou 07].

Complexes of deuterated γS with ^{13}C,^{15}N αB in a stoichiometry of 1:1 were prepared and precipitated. Comparison of solid-state NMR PDSD spectra of bound and unbound αB showed broadening of cross peaks for I114 (Fig.2.20).

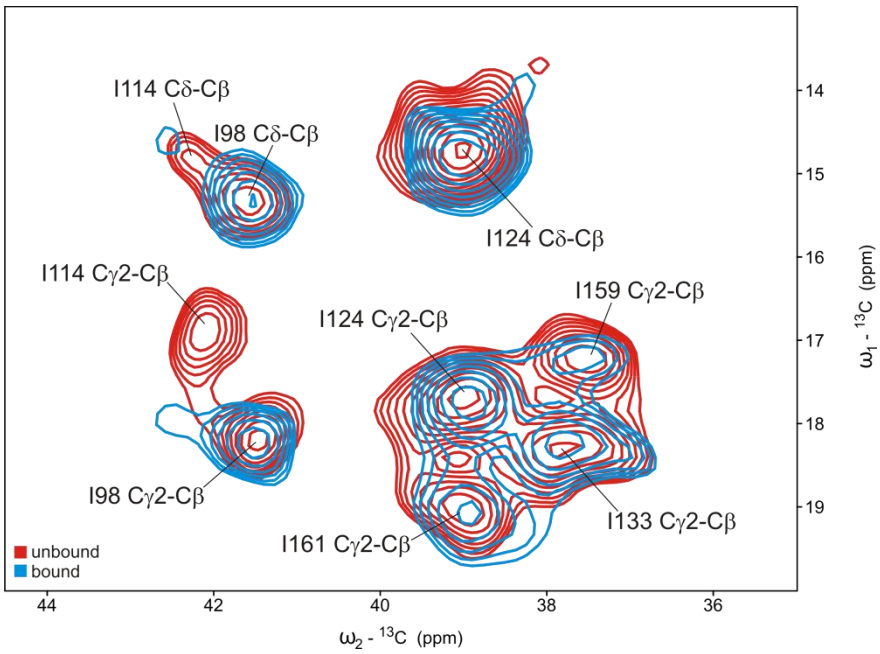

Fig.2.20: Complex of ^{13}C,^{15}N labelled αB in complex with unlabelled γS precipitated by PEG-8000. Zoom into the isoleucine region. Red: 50 ms PDSD of αB. Blue: 50 ms PDSD of ^{13}C,^{15}N labelled αB in complex with unlabelled γS in a stoichiometry of 1:1.

While mapping of the binding site was sufficiently achieved by this methodology for the case of α-syn, a clear picture of the binding site could not be demonstrated for γS. Therefore novel technical approaches have been used to improve the quality of the data. First, new samples with amino acid specific labelling were prepared (the labelling schemes are discussed in detail in the supplementary). Deuterated αB with ^{1}H,^{13}C,^{15}N-RIGAS was complexed with unlabelled γS in a stoichiometry of 1:1.8. The solution was concentrated for FROSTY solution MAS measurements [Mainz 09; Gardinnet 12; Bertini 11] and therefore not precipitated.

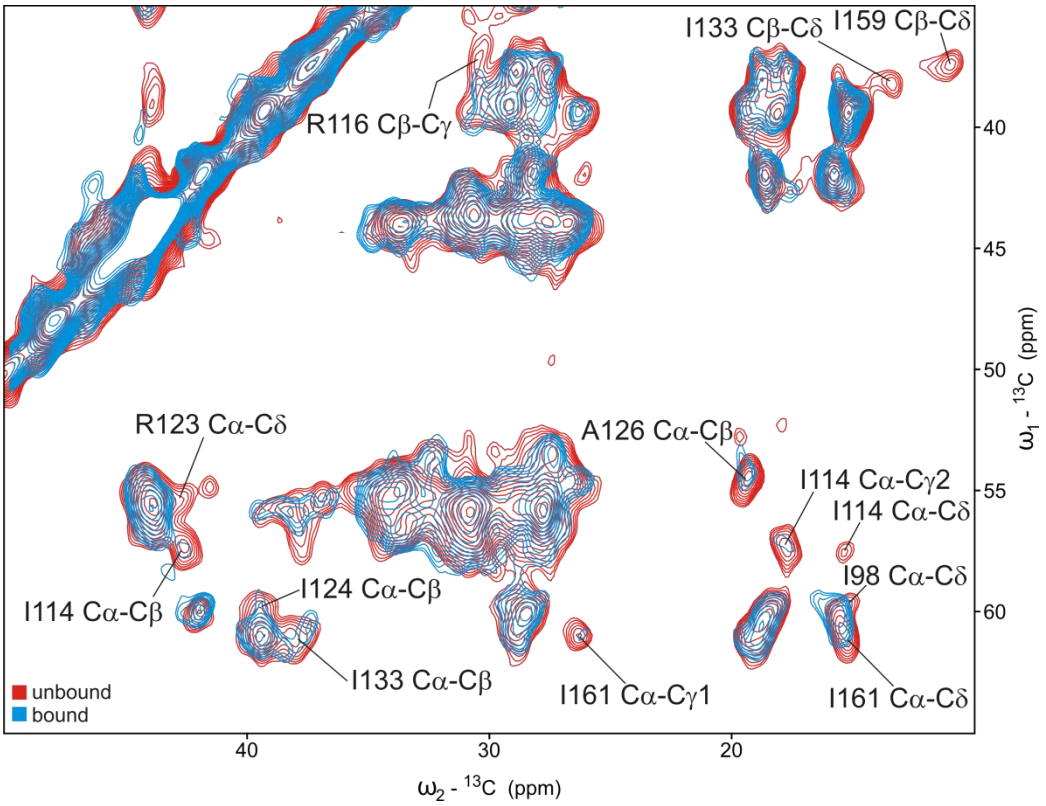

Fig.2.21: Spectra of $^{13}C,^{15}N$ RIGAS labelled αB in complex with unlabelled γS by FROSTY solution-MAS NMR. Red: 50 ms PDSD of $^{13}C,^{15}N$ RIGAS labelled αB. Blue: 50 ms PDSD of $^{13}C,^{15}N$ RIGAS labelled αB in complex with unlabelled γS in a stoichiometry of 1:1.8. Assignments for cross peaks with strongest perturbations are indicated.

Comparison of spectra of bound and unbound αB shows changes for signals of I114, as seen in the spectra of the precipitated sample. Additional changes could be mapped and are shown in Fig.2.21. Predominantly signals from amino acids from the β7-β7 dimer interface are perturbed, however changes are also observed for signals of I133, I159 and I161 which belong to the β4/8-groove and its bound IXI-motif. Affected residues are highlighted on the αB core domain structure in Fig.2.22. In contrast to complexes of αB with α-syn, which show weak binding, the changes in the spectra of complexes of γS with αB are not sufficient to confirm weak binding and hence are classified as indicators of transient binding.

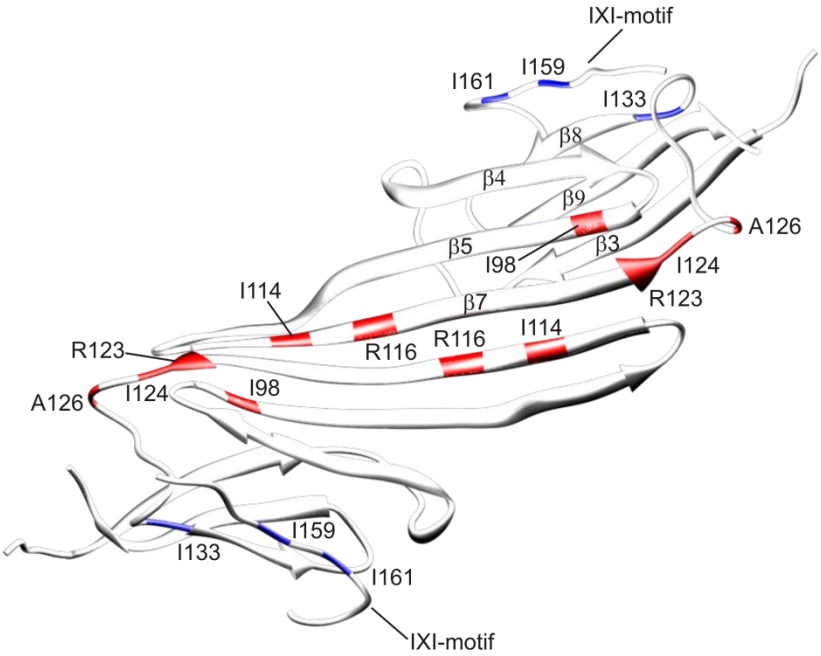

Fig.2.22: Indicators of transient binding of γS on the αB surface. αB residues that experience signal perturbations upon binding are highlighted. Two independent sites can be identified, the groove formed by the β7-β7 dimer interface (red) and the β4/8-groove with its bound IXI-motif (blue).

As mentioned in the introduction, γS-G18V aggregates even at low temperatures and causes cataract. A complex of deuterated αB with $^{1}H,^{13}C,^{15}N$-RIGAS and unlabelled γS-G18V was prepared analogously. In this case, similar signal changes from residues in the β7-β7 dimer interface the β4/8-groove and its bound IXI-motif can be observed (Fig.2.23). The corresponding residues have been highlighted in the structure of the αB core domain dimer (Fig.2.24). Also in this case the signal pertubations are classified as indicators of transient binding.

In summary, the combination of ^{13}C-detected solution MAS spectroscopy (and therefore avoiding precipitation) and amino acid specific labelling enabled a somewhat detailed identification of two transient binding sites.

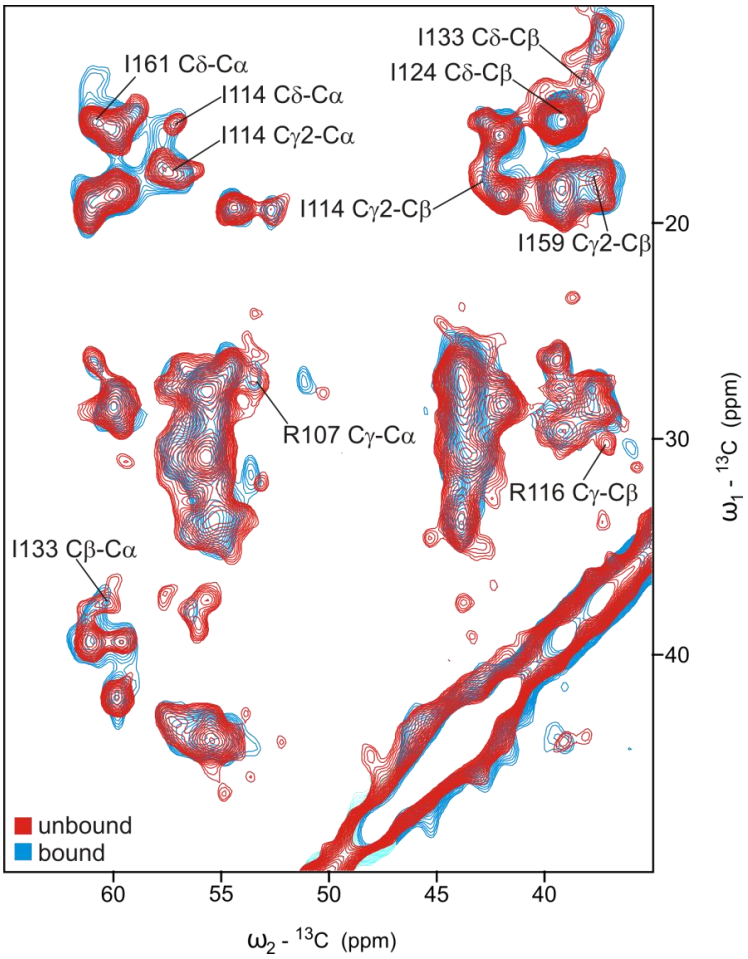

Fig.2.23: Spectra of $^{13}C,^{15}N$ RIGAS labelled αB in complex with unlabelled γS-G18V by FROSTY solution-MAS NMR. Red: 50 ms PDSD of $^{13}C,^{15}N$ RIGAS labelled αB. Blue: 50 ms PDSD of $^{13}C,^{15}N$ RIGAS labelled αB in complex with unlabelled γS-G18V in a stoichiometry of 1:1.8. Assignments for cross peaks with strongest perturbations are indicated.

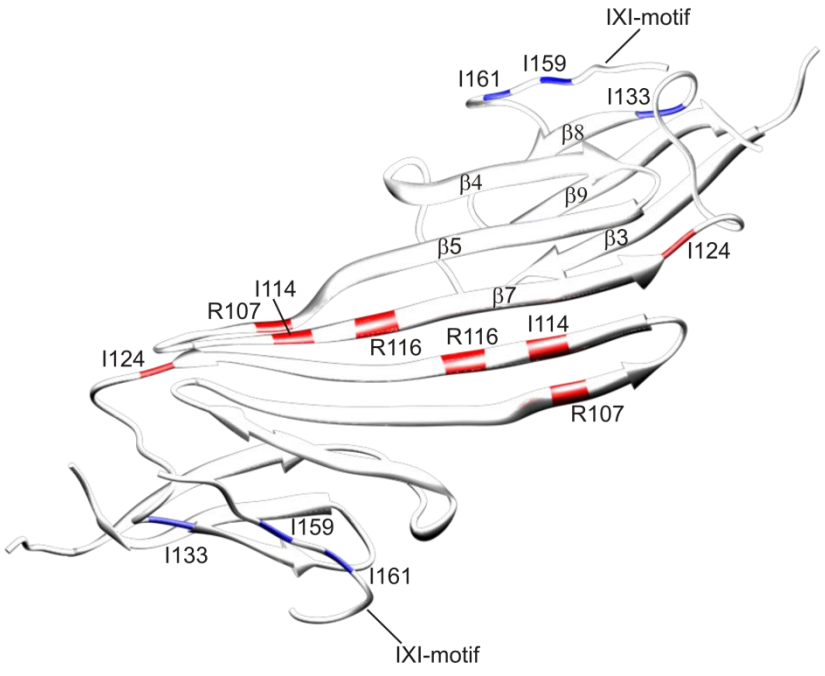

Fig.2.24 (on page 50): Indicators of transient binding of γS-G18V on the αB surface. αB residues that experience signal perturbations upon binding are highlighted. Two independent sites can be identified, the groove formed by the β7-β7 dimer interface (red) and the β4/8-groove with its bound IXI-motif (blue).

In recent years, fast MAS in combination with protein deuteration enabled acquisition of proton-detected solid-state NMR spectra as common in solution NMR [Chevelkov 06; Zhou 07]. The advantage of proton-detected 2D ^{15}N-^{1}H HSQC spectra is that a single signal for every non-proline amino acid is displayed, resulting fingerprint-like spectra for the entire protein. In solution NMR, protein-protein interaction studies are routinely performed to map interaction sites using this methodology (see introduction). In the following, proton-detected FROSTY solution MAS spectroscopy is used in a similar manner to solution NMR methods in order to map interaction sites in a more convenient and sensitive way. This chapter therefore aims at testing the applicability of novel technologies for binding studies of transient binding partners, with only a tentative interpretation with regards to a biological result. Proton-detected FROSTY solution MAS NMR was applied to record ^{15}N-^{1}H HSQC-type experiments of uncomplexed αB and its complex with γS. Fig.2.25 displays the CP-based ^{15}N-^{1}H HSQC spectra of PFLS-depleted (top) and IVWY-labelled (bottom) ^{2}H,^{13}C,^{15}N αB with 20% ^{1}H back-exchange, both shown in red. Solution NMR assignments of truncated αB-10.1 are plotted onto the ^{15}N-^{1}H HSQC spectra. Solution NMR assignments of truncated αB-10.1 have been provided by Andi Mainz (TU München). These assignments will be used in cases where a clear distinction of signals is possible. Complexes of ^{2}H,^{13}C,^{15}N αB with 20% ^{1}H back-exchange and unlabelled γS in a stoichiometry of 1:1.8 were formed. CP-based ^{15}N-^{1}H HSQC spectra of unbound and bound αB are depicted in Fig.2.25 in blue. A good set of reporter resonances can be found and their changes in chemical shift or peak intensity traced. The ^{15}N-^{1}H HSQC spectra are more sensitive to binding compared to carbon-detected spectra, however in this case significant shift changes are mainly seen for signals of residues that have no assignment overlap with αB-10.1.

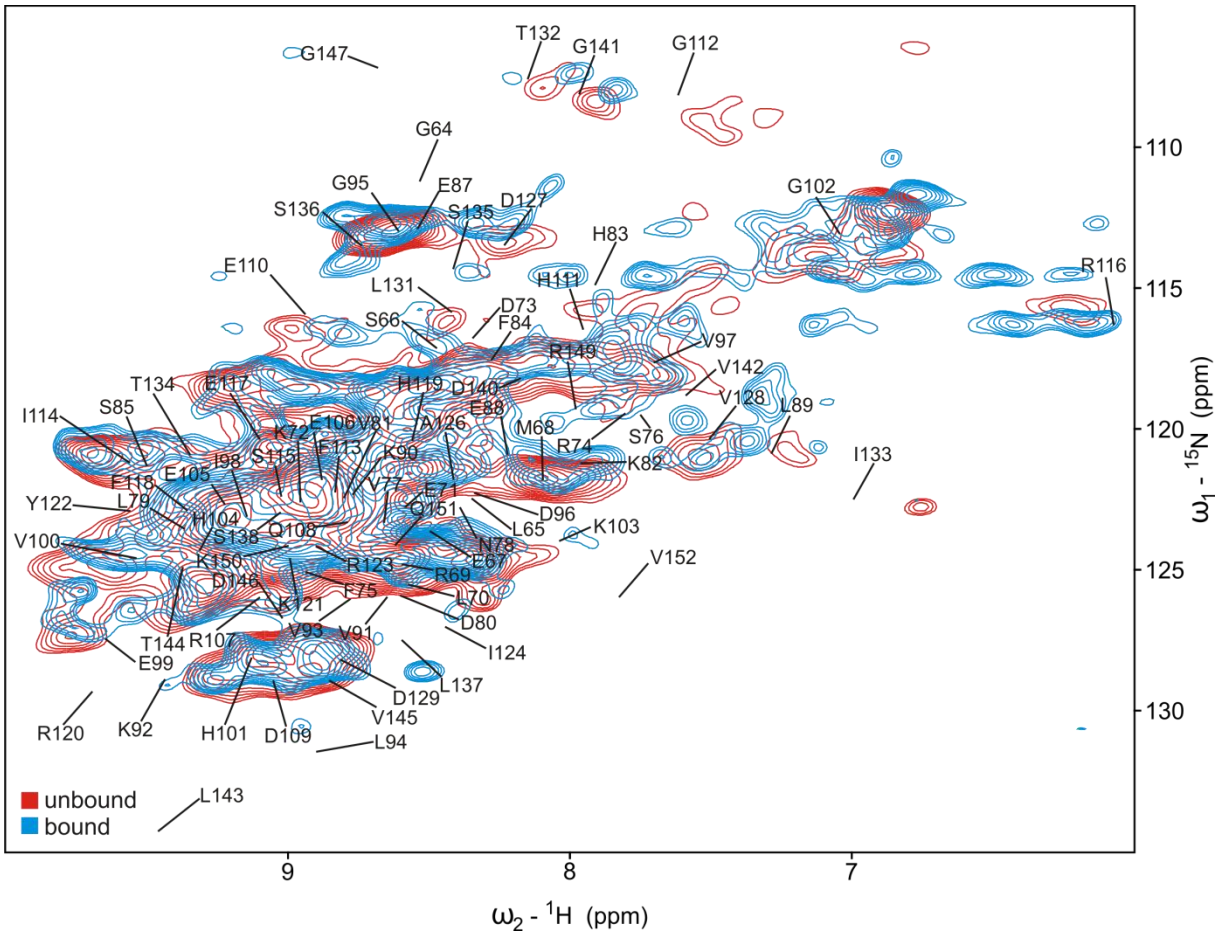
T132
G141
G112
G147
G64
G95
E87
D127
S136
S135
G102
H83
E110
H111
R116
L131
D73
S66
F84
R149
V97
V142
T134
V128
L89
S85
M68
S76
I114
R74
I133
K82
Y122
L79
Q151
D96
V100
L65
K103
S138
Q108
N78
K150
R123
E67
V152
R69
D146
F75
L70
K121
D80
T144
R107
V93
V91
I124
E99
L137
D129
V145
R120
K92
H101
D109
L94
L143
unbound
bound
110
115
120
125
130
9
8
7
ω2 - 1H (ppm)
ω1 - 15N (ppm)

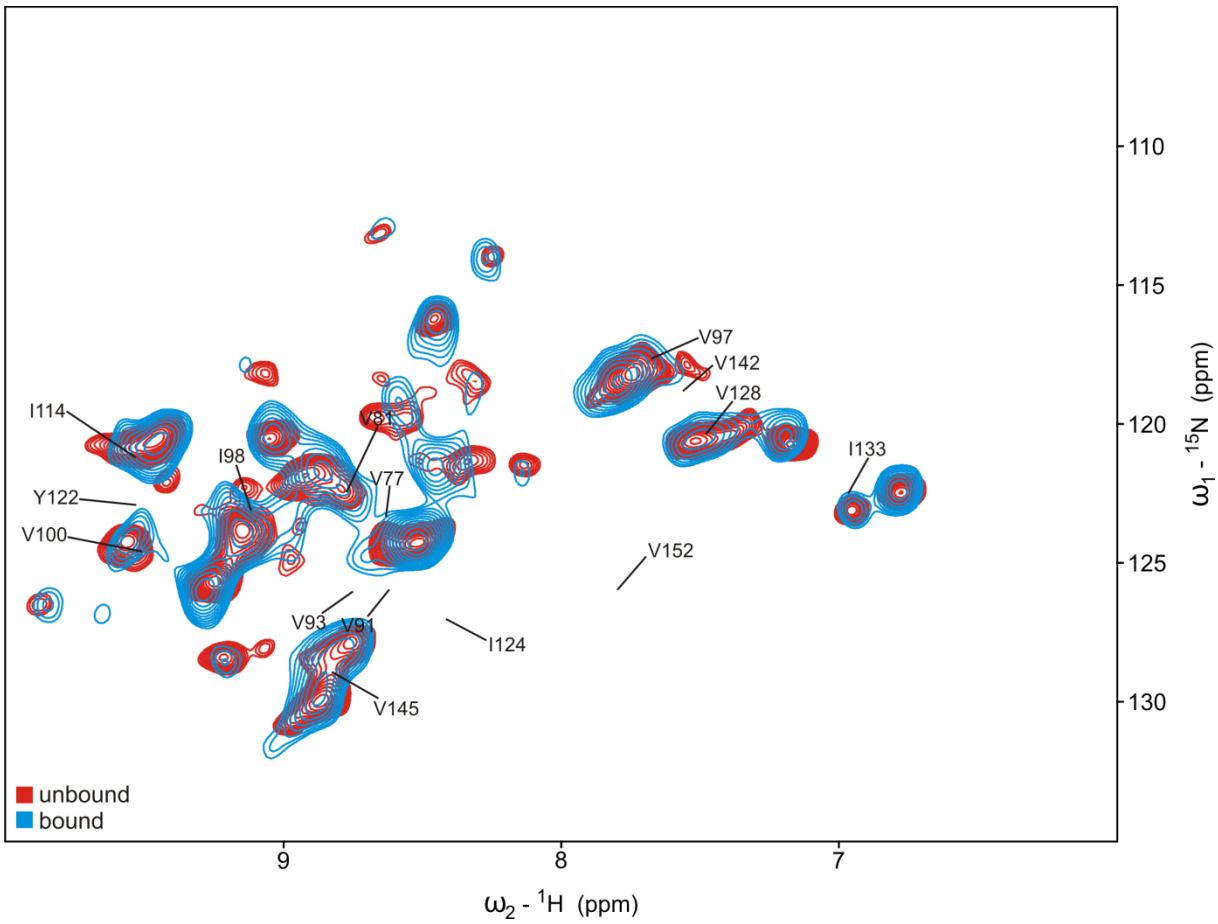
V97
V142
V128
I114
V81
I133
I98
V77
Y122
V100
V152
V93
V91
I124
V145
unbound
bound
110
115
120
125
130
9
8
7
ω2 - 1H (ppm)
ω1 - 15N (ppm)

Fig.2.25 (on page 52): Spectra of isotopically labelled αB in complex with unlabelled γS by FROSTY solution MAS NMR. Top: Red: ^{15}N-^{1}H CP-HSQC of PFLS-depleted ^{2}H,^{13}C,^{15}N αB with 20% ^{1}H back-exchange. Blue: ^{15}N-^{1}H CP-HSQC of PFLS-depleted ^{2}H,^{13}C,^{15}N αB with 20% ^{1}H back-exchange in complex with unlabelled γS in a stoichiometry of 1:1.8. Bottom: Red: ^{15}N-^{1}H CP-HSQC of IVWY-labelled ^{2}H,^{13}C,^{15}N αB with 20% ^{1}H back-exchange. Blue: ^{15}N-^{1}H CP-HSQC of IVWY-labelled ^{2}H,^{13}C,^{15}N αB with 20% ^{1}H back-exchange in complex with unlabelled γS in a stoichiometry of 1:1.8. Assignments were taken from solution NMR assignments of αB-10.1.

INEPT-based ^{15}N-^{1}H HSQC spectra of uncomplexed αB (^{2}H,^{13}C,^{15}N IVWY labelled with 20% ^{1}H back-exchange) and in complex with unlabelled γS are depicted in Fig.2.26. Spins of residues that are flexible typically exhibit long coherence lifetimes, which is beneficial for polarization transfer by INEPT. Therefore INEPT-based ^{15}N-^{1}H HSQC spectra additionally may show a set of residues which are likely in the N-/C-termini or in some loop regions.

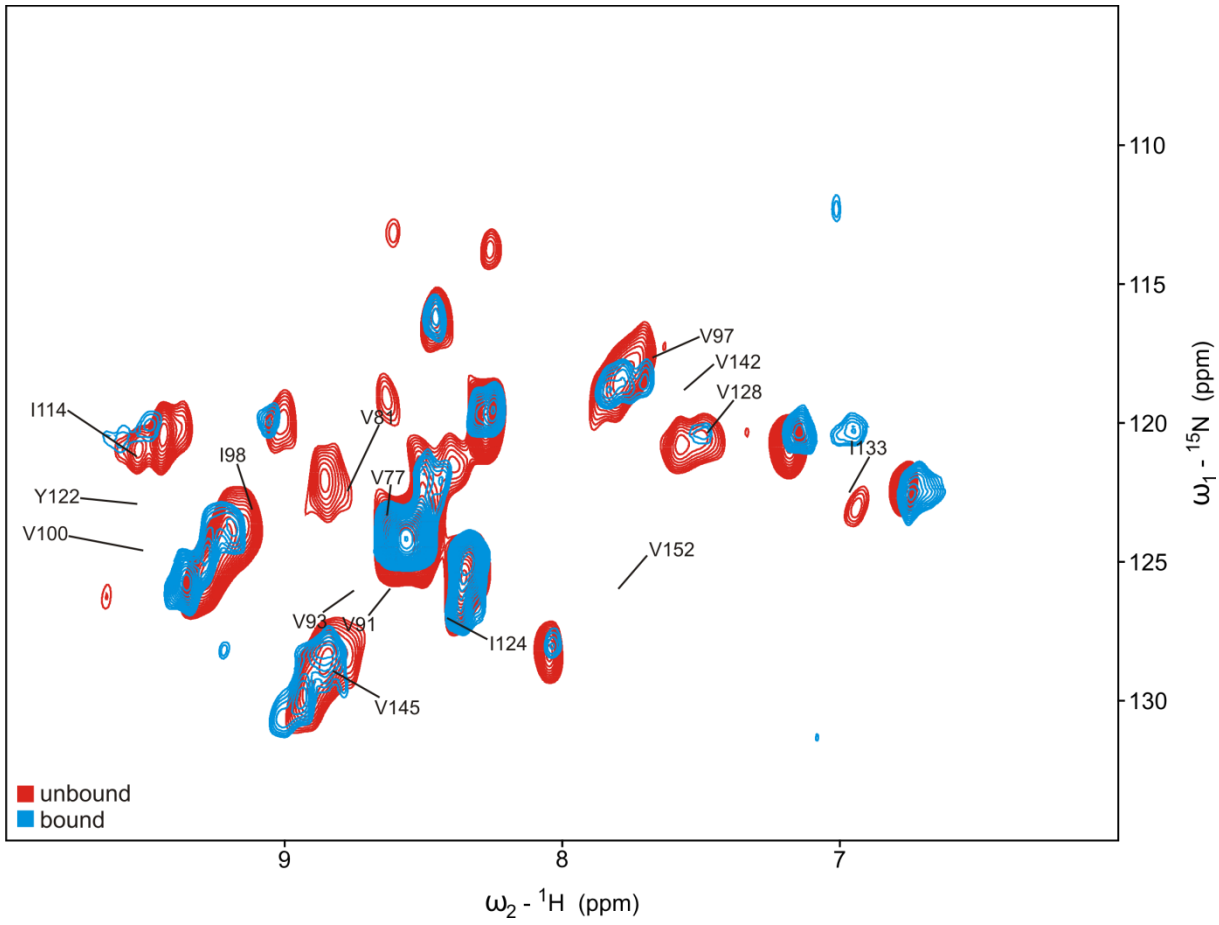

Fig.2.26: Spectra of isotopically labelled αB in complex with unlabelled γS by FROSTY solution MAS NMR. Red: ^{15}N-^{1}H INEPT-HSQC of IVWY-labelled ^{2}H,^{13}C,^{15}N αB with 20% ^{1}H back-exchange. Blue: ^{15}N-^{1}H INEPT-HSQC of IVWY-labelled ^{2}H,^{13}C,^{15}N αB with 20% ^{1}H back-exchange in complex with unlabelled γS in a stoichiometry of 1:1.8. Assignments were taken from solution NMR assignments of αB-10.1

The perturbations upon complexation as observed in INEPT-based ^{15}N-^{1}H HSQC spectra are stronger as compared to the CP-based ^{15}N-^{1}H HSQC spectra. Changes can be seen for signals from the β7-β7 dimer interface, β-strand 3 (which is in proximity to the β7-β7 dimer interface) and β-strand 8. It is tempting to state that INEPT-transfer may select for protomers with different dynamics, which may be involved in binding, whereas CP-transfer may select for weaker bound or unbound, protomers. However this interpretation is merely speculative and needs further investigation.

3. Discussion

During the progress of this thesis, several structural biology strategies for the study of the oligomerization behaviour of αB have been published. These papers are briefly discussed and put into context with the results from this thesis.

X-ray structures of truncated αB constructs that encompass the sequence of the core domain have been solved by the labs of Slingsby (PDB ID 2WJ7) at pH 9 and Eisenberg (PDB ID 3L1G) at pH 4.6 [Bagnéris 09; Laganowsky 10]. These constructs lack N-termini and the construct used in the Slingsby study additionally lacks the C-terminus, therefore the protein assembles and crystallizes mainly into dimers, trimers and tetramers. Comparison of the monomers from crystal structures with the solid-state NMR monomer structure (which was solved in the context of full-length oligomers at pH 7.5) shows barely differences in the overall protein fold (Fig.3.1).

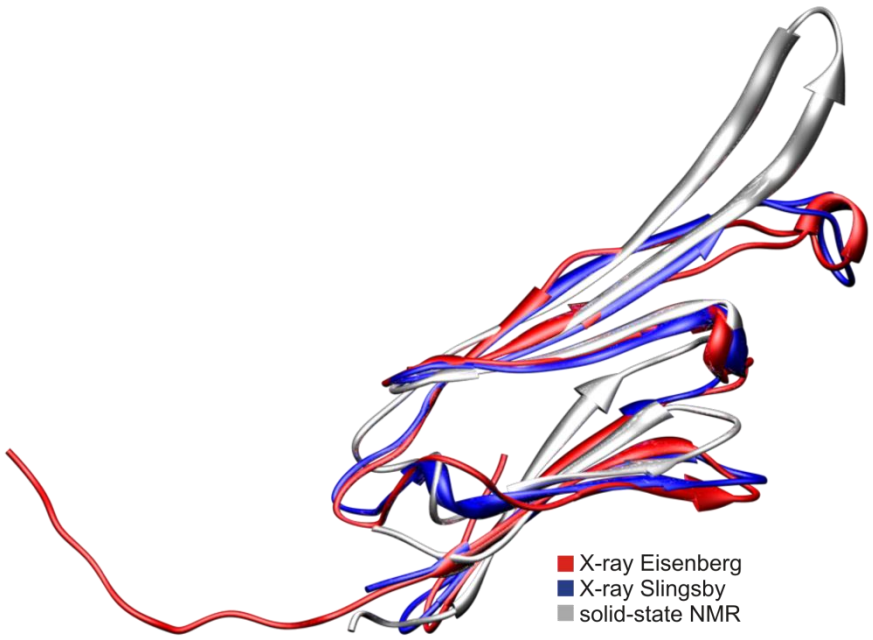

Fig.3.1: Comparison of αB core domain monomer structures. Solid-state NMR structure in white, crystal structure from the lab of Slingsby in blue, crystal structure from the lab of Eisenberg in red. Both crystal structures were solved on truncated constructs whereas the solid-state NMR structure was solved in the context of full-length oligomers.

However the solid-state NMR structure exhibits a bent β-sheet formed by β-strands 4, 5 and 7 from both dimers which is even in the crystal structures [Jehle 10]. This feature is likely to be pH dependent and may therefore have functional importance.

In addition the Eisenberg structure shows different β7-β7 dimer interface strand

registers which are not detected by solid-state NMR or in the crystal structure of Slingsby. All three structures show a β7-β7 dimer interface in which E117 hydrogen bonds to E117' to form a point-symmetric intermolecular β-sheet (in the following named E117 dimer interface). The Eisenberg structure additionally shows a dimer interface with a different register that is point-symmetric in F118 (in the following named F118 dimer interface). In the E117 dimer interface intermolecular cation-π interactions between R116 and F118' are prominent interactions that are absent in the F118 dimer interface. Notably, in the F118 dimer interface R116 and R120 from both monomers interact with a single $SO4^{2-}$, which is presumably part of the crystallization buffer. Therefore the F118 dimer interface seems to be stabilized by crystallization supplements and may not occur under native conditions. This register may potentially be detected by solid-state NMR, when spectra of mixed protomers are recorded with higher sensitivity. Furthermore, it cannot be excluded that the register shift is originating from preparation of crystals at pH 4.6 whereas the other structures were solved at pH 7.5 (solid-state NMR) and pH 9 (Slingsby structure). Overall, the β7-β7 dimer is reported to be the active chaperoning unit which may partially detach from the oligomer to "fish" for substrates [Haslbeck 05; Baldwin, Lioe, Robinson 11]. Recent reports also mention that monomeric HSP26, a homologue of αB, may be the sole chaperoning unit [Chen 10]. Interestingly, at neutral pH, oligomers that are built of even numbers of monomers are more populated than oligomers that are built of odd numbers of monomers, as detected by mass-spectrometry [Baldwin, Lioe, Hilton 11]. The data indicate that dimers are the exchanging species. This trend is further discussed later in the context of oligomer buildup and pH activation.

Intermolecular restraints from solid-state NMR have been used to model an important oligomerization site. The conserved C-terminal IXI-motif binds intermolecularly to a groove formed by β-strands 4 and 8. This interaction serves as a basis for higher-order oligomerization. The Eisenberg construct of truncated αB includes the IXI-motif. The crystal structure clearly shows a similar binding mode of the IXI-motif to the β4/8-groove as compared to the docked solid-state NMR structure. Both structures show particularly isoleucines 159 and 161 buried in the core domain of another monomer.

In contrast, recent solution NMR (relaxation dispersion) measurements from the group of Lewis Kay show exchange dynamics of the IXI-motif on the millisecond timescale, contradicting a tight interaction with the β4/8-groove [Baldwin, Hilton, Lioe

11]. The data suggest an involvement of the C-terminus in oligomerization, however an interaction with residues upstream of the IXI-motif is proposed. This tethering point could not be specified further due to a very restricted (isoleucine) labelling scheme that was applied to enable solution NMR of particles of that size. Recently, populations of oligomers with the IXI-motif bound to the core domain have been detected under lower temperature conditions from the same group [Baldwin 12]. Cross-linking studies in combination with MS and EM had also confirmed an IXI-motif bound to the β4/8-groove [Braun 11]. Comparing the solid-state NMR structure of the bound IXI-motif to the crystal structure of truncated αA with its bound IXI-motif (PDB ID 3L1F), one finds that binding is inverted. This feature may arise from either different surfaces of the core domain or/and different IXI-motif sequences of αA. While the αB IXI-motif sequence is palindromic (RT**IPI**TR) the αA sequence is not (RA**IPV**SR). The orientation for the IXI-motif in hetero-oligomers of αA/αB is currently unknown.

N-terminal truncation constructs of αB with retained IXI-motif form hexamers in solution [Braun 11]. These hexamers have been modelled as trimer of dimers in several studies (Fig.3.2) and resemble a similar barrel-like organization compared to monodisperse homologues such as HSP16.5 from *M.jannashii* and HSP16.9 from *T.aestivum* [Kim 98; van Montfort 01].

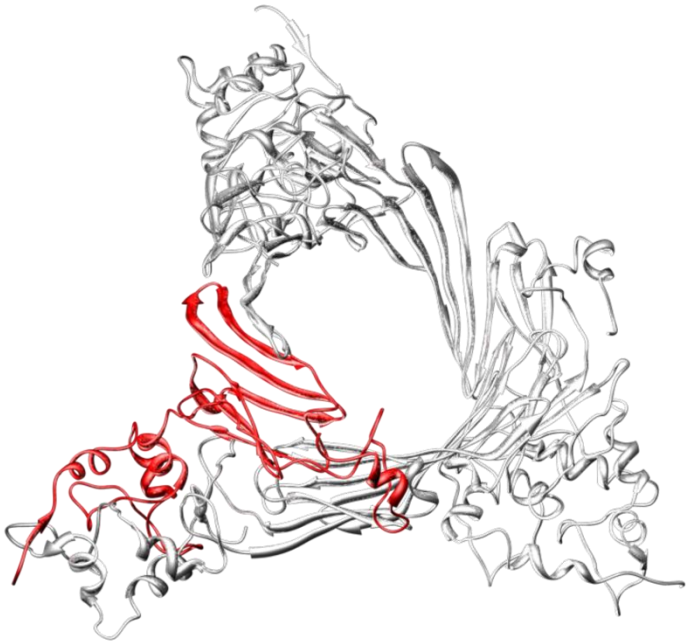

Fig.3.2: A trimer of dimers of αB as a building-block for higher oligomers, also driven by binding of the IXI-motif to the β4/8-groove. A monomer is highlighted in red. Model from solid-state NMR, EM and crosslinking data.

Three different 24-mer models of αB were previously modelled from solid-state NMR and SAXS data [Jehle 11], from EM and cross-linking data (Fig.3.3) [Braun 11] and from a combination of solution NMR, MS and EM [Baldwin, Lioe, Hilton 11].

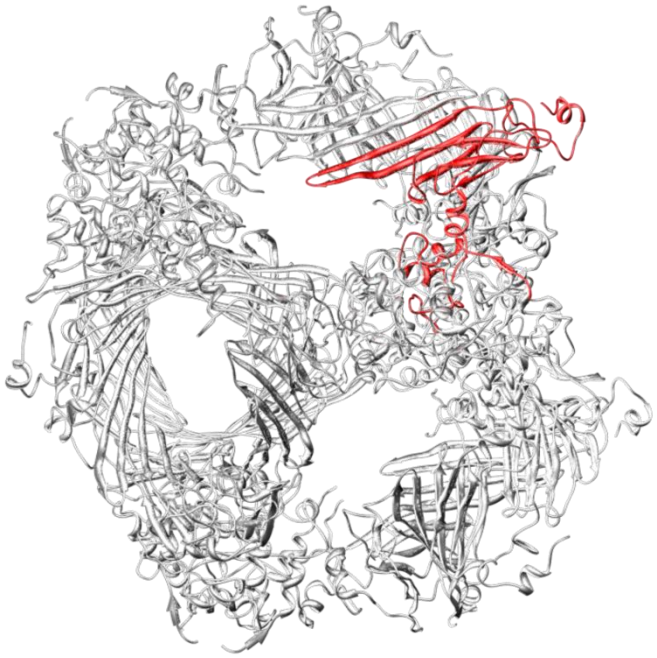

Fig.3.3: A 24-mer model of αB from solid-state NMR, EM and cross-linking data. Four trimer of dimer barrels from Fig.3.2 oligomerize in a tetrahedral arrangement. A monomer is highlighted in red.

In these models, the overall architecture can be described as tetrahedral. A ring-like trimer of dimers that is held together by intermolecular an IXI-motif binding is positioned in each corner. These rings are held together by oligomerization of the N-terminal domains that associate with each other. This particle was taken as a basis for modelling of higher/lower numbered oligomers. While all studies deliver a similar result in modelling a 24-mer particle, explanations for higher numbered oligomers vary in each study. It seems that despite reliable modelling efforts that revealed the structure of monomers, dimers, and selected oligomers, the structural basis for polydispersity is still not fully understood.

A drop in pH leads to chemical shift changes of I159 and I161 in the IXI-motif and I133 from its binding groove on β-strand 8. This suggests a loosening or dislocation of the IXI-motif to liberate the core domain for potential substrates. Solution NMR of full-length αB shows a restricted set of cross peaks for residues which exhibit motion faster than the overall particle correlation time. These residues are located in

dynamic loops as well as in N- and C-termini that likely radiate out of the oligomer sphere. The signals detected show an increase in signal intensity upon pH drop (e.g. A171) which suggests an increase in dynamics by loosening of its upstream constriction point – the IXI-motif. This is supported by SAXS data showing an increase in oligomer size. Reconstructions of SAXS data had shown additional density radiating out of the oligomer at low pH only [Jehle 10]. This leads to an increase in average oligomer size from 15.6 nm to 18 nm. It has been shown that the affinity of αB towards desmin is significantly increased upon pH drop [Bennardini 92]. Interestingly, populations of oligomers with an odd number of monomers are significantly increasing at low pH [Baldwin, Lioe, Hilton 11]. Previously, the β4/8-groove has been suggested to act as a chaperone binding site, which is in agreement with data from this thesis (discussed below) [Bhattacharyya 06; Ghosh 05]. Therefore the IXI-motif may not just be an oligomerization site but rather a regulator of chaperone activity by autoinhibition. Upon stress conditions, it may dislocate and expose a chaperone binding site.

The αB point mutation R120G causes cataract and desmin-related myopathy [Vicart 98]. Several studies report loss or gain in substrate affinity, promotion of unfolding of substrates, higher polydispersity and inherent instability [Bova 99; Treweek 05]. In the wild-type structure(s), R120 is a hydrogen-bonding partner of I114 at the β7-β7 dimer interface. Further, the R120 side chain forms an intermolecular electrostatic interaction with D109 across the β7-β7 dimer interface. Solid-state NMR spectra of the full-length αB-R120G mutant show chemical shift changes for residues that are structurally close to the mutation site. In these spectra, no increase in signal heterogeneity can be observed when compared to wild-type data, suggesting that the αB monomer overall fold is similar. A crystal structure of an N-/C-terminal truncated αB-R120G construct has been solved in the lab of Christine Slingsby (PDB ID 2Y1Z) [Clark 11]. In this construct the overall structure of the monomer appears not to be distorted (Fig.3.4). Removal of the R120 positive charge leads to a distortion of a network of charges. D80 and H83’ (from another monomer) form electrostatic interactions, which cover up a groove, that is formed by the β7-β7 dimer interface (hence called β7-β7 groove), which is accessible in the wild-type (Fig.3.5).

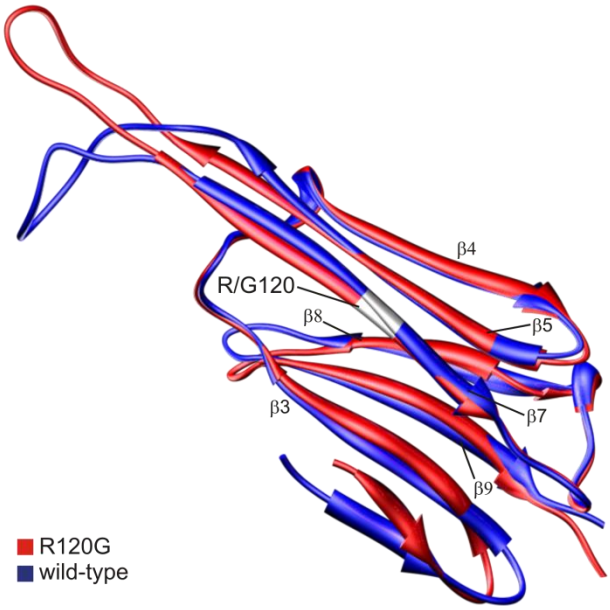

Fig.3.4: Comparison of crystal structures of truncated αB constructs for wild-type (blue) and R120G (red) from the lab of Slingsby. The mutation site at position 120 is highlighted in grey. The overall fold of both monomers is similar.

Also the αB-R120G dimer interface is strengthened compared to the wild-type [Clark 11]. Therefore the data hint at a strengthening of intermolecular interactions. SAXS data confirm that αB-R120G oligomer size is doubled compared to the wild-type protein and that its polydispersity is significantly increased [Bova 99]. As heterogeneity for the mutant monomer is not significantly altered, this increase in polydispersity is likely due to irregular intermolecular interactions. The D80-H83' interaction strengthens the αB-R120G dimer in a dimeric construct, but may also cause higher-order oligomerization in the full-length protein. pH drop experiments for αB-R120G show in pH effects on the chemical shifts of residues around mutation site, which are absent in the wild-type. This may arise from histidine protonation leading to stronger interactions, such as D80-H83' or additional intermolecular binding, that is pH-dependent. SAXS data show that the αB-R120G oligomer size is significantly increased from 30 nm to 40 nm upon pH drop (Fig.3.6).

Future solid-state NMR studies of complexes of αB-R120G with substrates may reveal whether, and under which conditions, the β7-β7 groove is able to interact with its clients.

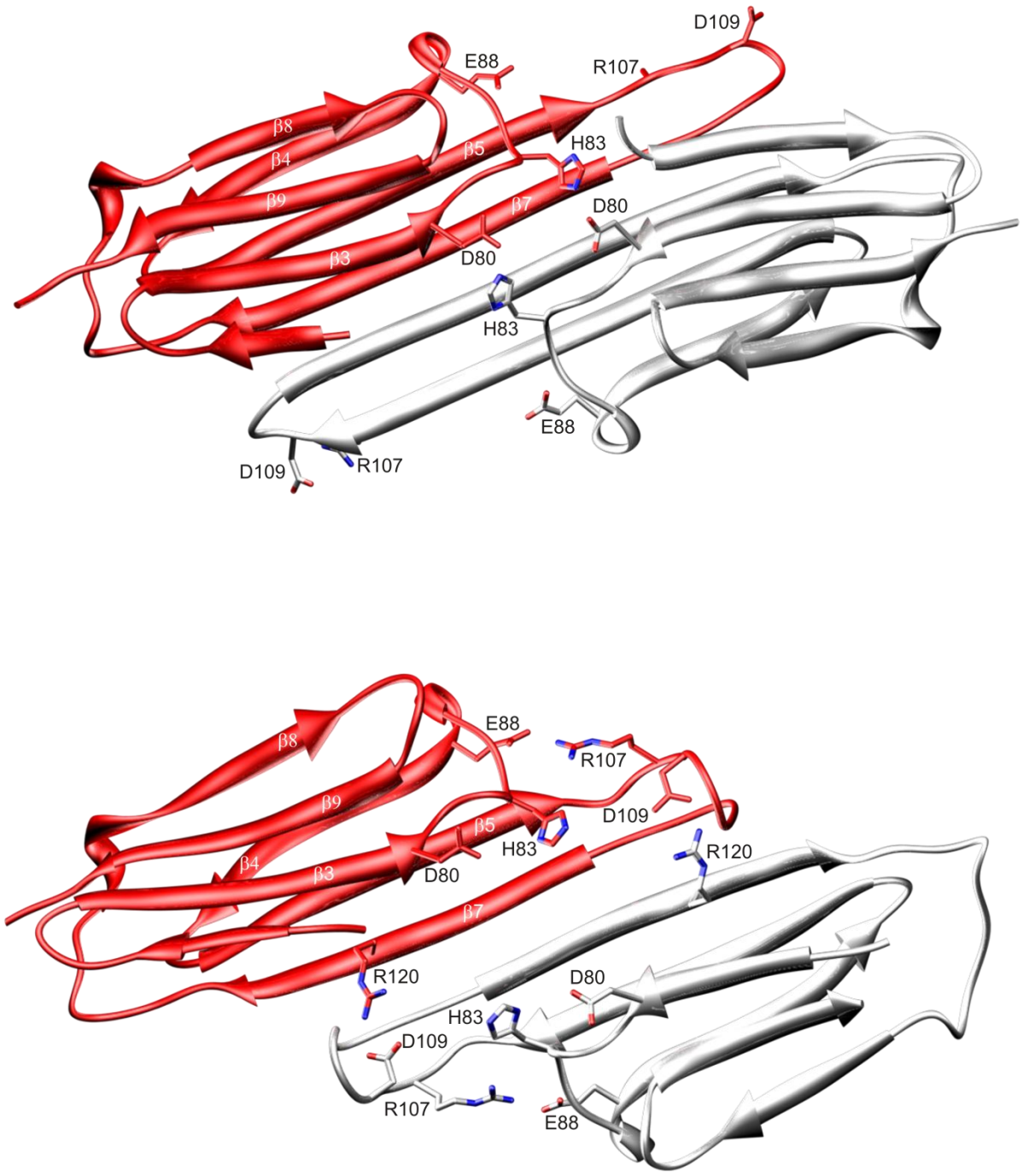

Fig.3.5: Comparison of crystal structures of truncated αB constructs for wild-type (bottom) and αB-R120G (top) from the lab of Slingsby. Both structures show a network of charged interactions. Bottom: The wild-type structure shows intermolecular electrostatic interactions between R120 and D109' and intramolecular interactions between D80 and H83. Top: The αB-R120G structure shows a different network of electrostatic interactions with an intermolecular D80-H83' interaction that leads to closure of the groove formed by the β7-β7 dimer interface.

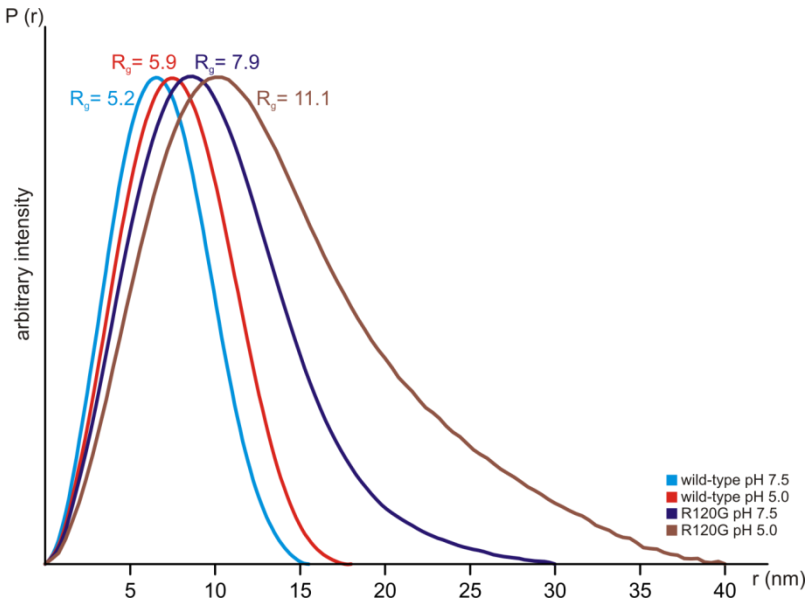

Fig.3.6: Distance distribution functions from of αB at pH 7.5 (blue) and pH 5 (red) and αB-R120G at pH 7.5 (purple) and pH 5 (brown) from SAXS data.

So far, the interaction of αB with substrate proteins has been studied extensively without any closer reference to structural information [Bruinsma 11; Ecroyd 08]. Several fluorescence studies measured thioflavin-T fluorescence of α-syn fibrils and report a decrease in fibril formation up to 70% in the presence of αB. Interestingly, sub-stoichiometric amounts of αB sufficed to exhibit full protection which suggests multiple interaction sites or protection by constant substrate binding and release [Rekas 04]. Another study reported lack of α-syn fibril formation and formation of amorphous aggregates in the presence of αB [Rekas 04]. Furthermore, binding of αB to already formed fibrils of α-syn prevented further fibril elongation [Waudby 10]. α-syn toxicity has been reduced by 20% in the presence of αB, in a cell culture model system [Outeiro 06]. α-syn A53T transgenic mice exhibited upregulation of αB (by 100%) in pathological regions, whereas levels of heat shock proteins 90/70/60/40 remained constant [Wang 08]. An upregulation of αB in Parkinson's disease has also been reported previously [Sun 05].

Solution NMR showed no specific binding site for αB-10.1 on α-syn. Rather all signals experience a decrease in intensity which may arise from conformational exchange or formation of a large complex that promotes peak broadening by T2 relaxation enhancement. This broadening did not occur in the control sample which was ^{15}N-labelled α-syn alone, otherwise equally treated. Mapping of the interaction

site of αB has been performed at atomic resolution on the full-length protein. Isotopically labelled αB was complexed with unlabelled α-syn to be studied by solid-state NMR. Changes in chemical shift or broadening can be observed mainly for resonances of residues from β-strand 8 and the IXI-motif, but also for resonances from β-strands 4 and 9. In this thesis, this binding site was shown to be an interaction site for αB homo-oligomerisation, which may be pH-modulated. Binding to α-syn occurs via the same binding site. IXI-motif pH drop chemical shift changes are all upfield in contrast to downfield shift changes for substrate binding. Therefore the magnetic environment of the chaperone-substrate complex must be different under these two conditions. The binding site may experience some IXI-motif dislocation before the substrate binds. As the IXI-motif side chain spins also experience strong chemical shift changes, it seems unlikely they stay “buried” in the core domain but rather dislocate and may also aid substrate binding. It is likely that αB possesses multiple binding sites that have different affinities depending on the substrate protein [Koteiche 03]. To my knowledge, this study presents for the first time a binding site of full-length αB mapped at atomic resolution.

Complexes of labelled αB with unlabelled wild-type γS-crystallin (γS) or γS-crystallin G18V (γS-G18V) showed weak signal perturbations, which in this thesis are called indicators of transient binding. In both cases the client protein affects different sites on the chaperone, either the groove formed by the β7-β7 dimer interface or, as shown for the substrate α-syn, the IXI-motif and β-strand 8. Proton-detected FROSTY solution-MAS experiments on these complexes enabled a more convenient analysis of binding effects.

The interaction of γ-crystallins (e.g. γS) with αB has been studied extensively by CD, SAXS, light scattering and fluorescence methods [Acosta-Sampson 10; Horwitz 92; Raman 95; Boyle 94; Gopalakrishnan 94; Takemoto 94; Wang 94; Weinreb 00]. These studies report significant reduction of aggregation of γS upon refolding from denaturant or thermal stress in the presence of αB. A comparison of binding affinities indicates that αB interacts more tightly with γ-crystallins than with β-crystallins [Putilina 03; Wang 94]. Especially γS was shown to be most effective in disturbing the αB subunit exchange, indicative of being the tightest binder. Takemoto et al. report that fetal γS binds to fetal αB, however no interaction between aged proteins can be observed [Takemoto 08]. They state that oxidation, deamidation and other modifications may have a strong effect on client recognition and chaperoning activity.

The perturbations in the solid-state NMR spectra of αB upon complexation of the chaperone with γS can be put into context with data from Carolyn Kingsley and Rachel Martin (UC Irvine, personal communication), who studied the interaction of unlabelled αB with labelled γS by solution NMR. Their data shows only transient, unspecific binding of γS to αB at a wide range of temperatures. However γS-G18V showed strong signal perturbations and a specific interaction to αB at temperatures that are below the T_m of γS-G18V. γS-G18V signals with strongest intensity perturbations upon binding are plotted onto the structure of wild-type γS (Fig.3.7 & Fig 3.8).

Clearly the chaperone binds residues around the mutation site. This specific effect was not seen for wild-type γS in the presence of αB. Inversely, this difference in affinity and specificity of αB to wild-type γS and γS-G18V could not be seen from carbon-detected solid-state NMR experiments, as shown in Fig.2.20 and Fig.2.22.

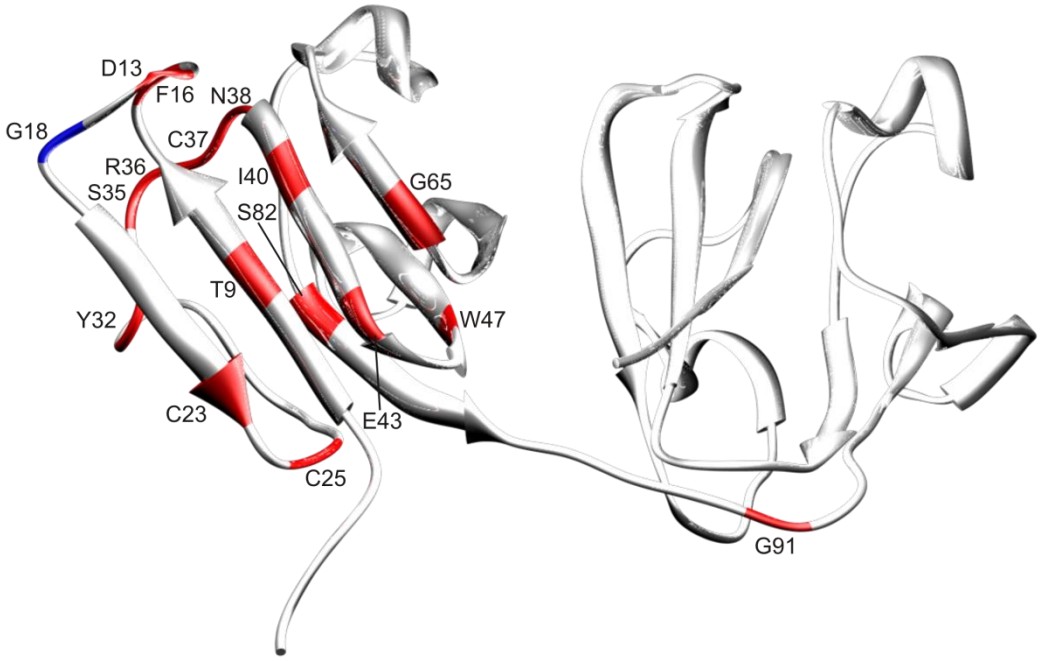

Fig.3.7: Wild-type structure of γS with G18 highlighted in blue. Signals of γS-G18V that experience complete loss of intensity upon binding of αB in solution NMR are highlighted in red. Perturbed residues cluster around the mutation site.

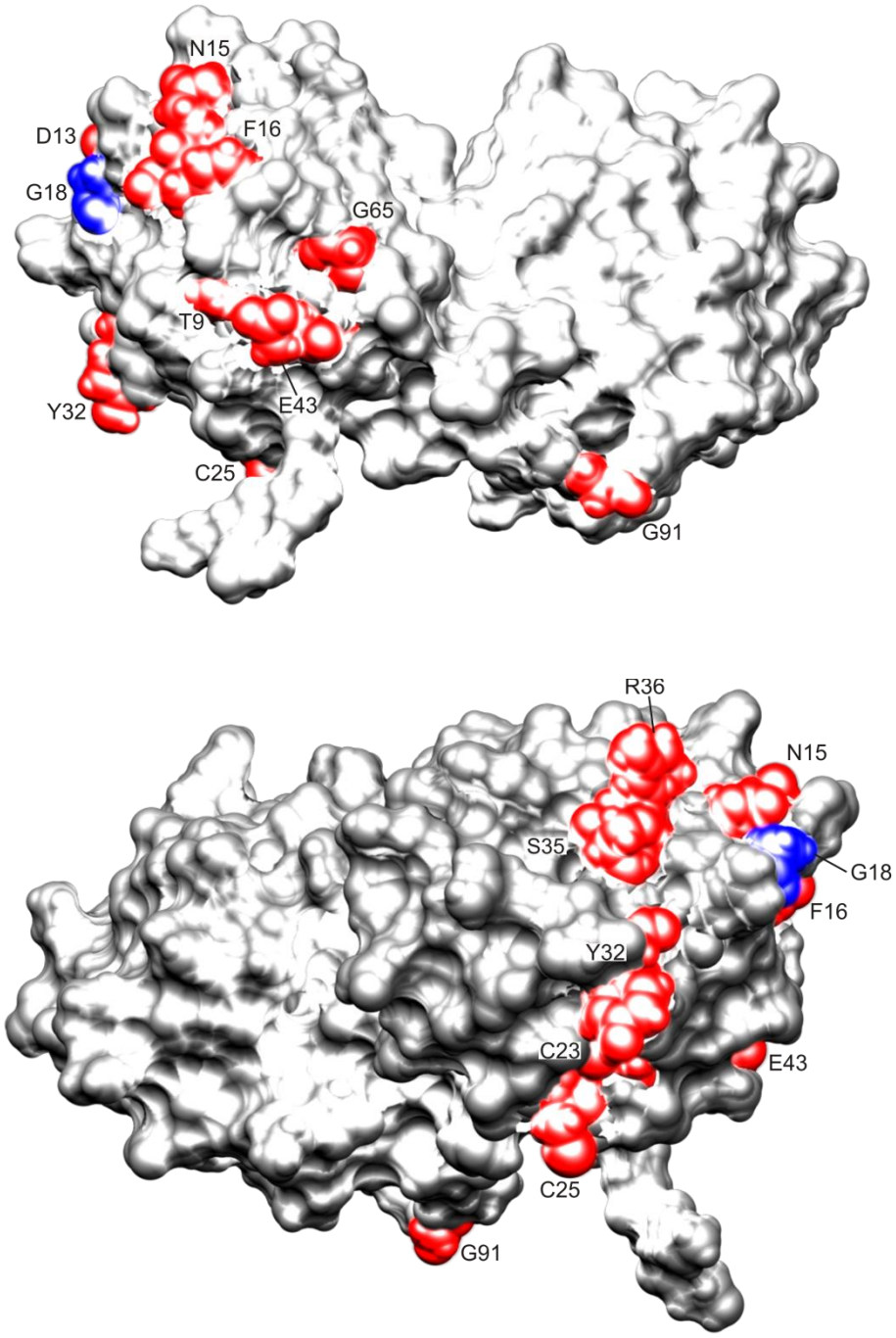

Fig.3.8: Wild-type structure of γS with G18 highlighted in blue. Signals of γS-G18V that experience complete loss of intensity upon binding of αB in solution NMR are highlighted in red. Perturbed residues cluster around the mutation site. Top: Surface representation. Bottom: Surface representation, horizontally rotated by 180°. Data from Carolyn Kingsley and Rachel Martin, UC Irvine (personal communication).

The structure of γS-G18V has not been published so far, however CD and fluorescence measurements show similar profiles as compared to the wild-type [Ma 09]. The mutation decreases the melting temperature from 75°C to 65°C, however

structural changes can be detected at even lower temperatures [Ma 09; Brubaker 11]. Aggregation of γS-G18V can be observed even at room temperature (Carolyn Kingsley, personal communication). Interestingly wild-type γS unfolds via two states in contrast to γS-G18V, which unfolds via an intermediate state [Ma 09]. The requirement of a client-protein intermediate to see binding to the chaperone was reported previously [Sathish 04; Evans 08]. However also intrinsically disordered proteins that lack tertiary structure, such as α-syn or Aβ, bind to αB and thereby are prevented from aggregation. An IR study of αA-crystallin in complex with wild-type γS showed a mild increase in substrate disorder from 5%, when natively folded, to 10%, when bound to the chaperone [Das 99]. An interaction study with destabilized γD-crystallin mutants states no protectivity by αB [Mishra 12]. It is still under debate whether and under which conditions a substrate is recognized by αB. It is noteworthy to differentiate that the study (from Mishra et al.) employing γD-crystallin checks for binding upon denaturation. In contrast, the γS-G18V study performed in this thesis (and in collaboration with Carolyn Kingsley & Rachel Martin) investigates the interaction of substrate protein that is folded, however aggregating when kept even below its T_m and therefore not denatured.

Although complexes of αB with γS and its mutant γS-G18V showed only indications of transient binding, all data point towards two independent binding sites (at least). The β7-β7 dimer interface groove serves as one point-symmetric substrate binding site, which is independent of the substrate binding site formed by the β4/8-groove with its bound IXI-motif.

Signals of residues located in the β4/8-groove and the IXI-motif are clearly perturbed upon complexation of the chaperone with α-syn, illustrating for the first time a binding site of full-length αB mapped at atomic resolution.

This thesis demonstrates the structural basis for the activity of αB by solid-state NMR complemented with other methods. αB oligomer formation, pH activation and substrate binding are inevitably linked with each other (Fig.3.9) and serve as major pillars for an understanding of chaperone function.

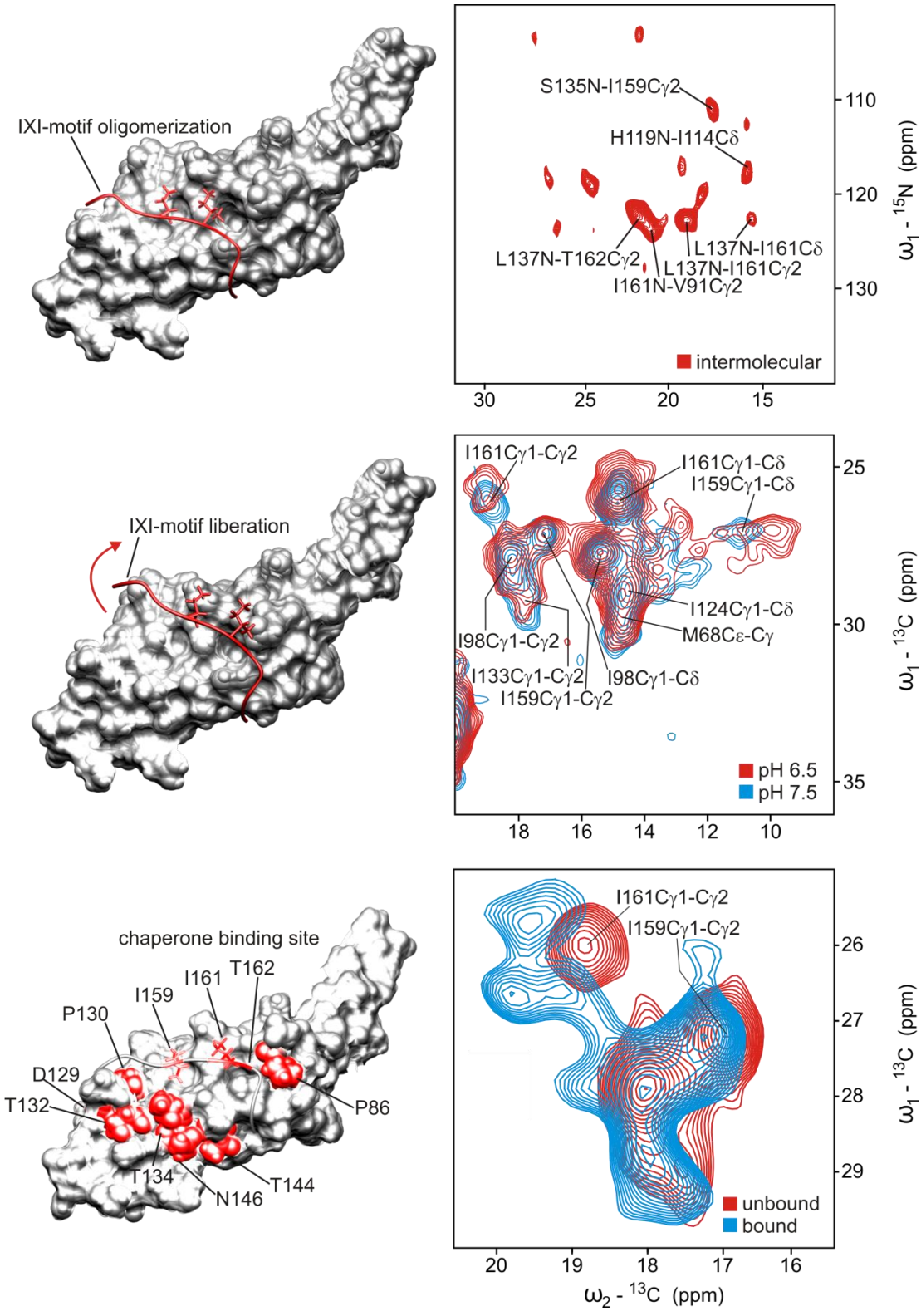

Fig.3.9: Oligomerization (top trace), activation (middle trace) and α-syn binding (bottom trace) of αB, as demonstrated by solid-state NMR in this thesis.

4. Material, Methods & Supplementary Information

Solid-state NMR spectra were recorded on Bruker 9.4/14.1/16.4/21.2 Tesla NMR spectrometers equipped with 3.2 or 4 mm triple resonance probes. Precipitates were recorded at 270K, solutions at 263K. Magnets were shimmed to an adamantane linewidth <5 Hz. Spectral temperature and shimming were carefully checked. **PDSD** spectra [Szeverneyi 82] were recorded at 10-12.5 kHz magic angle spinning with an initial ^{1}H-^{13}C CP [Pines 73] step with a 50%-100% amplitude ramp for 1.5 ms with spin locks of 60 kHz for ^{1}H and 47.5-50 kHz for ^{13}C. CP was followed by ~ 5 µs 90° carbon pulses. A total acquisition time of approx. 12 ms with 85 kHz spinal64 proton decoupling [Fung 00] in both dimensions was used. During **DARR** [Takegoshi 01] mixing, a proton spin lock field that matches the MAS frequency has been applied. The recycle delay was 3 s. In all carbon-detected spectra, all parameters used were identical unless noted.

Spectra of **mixed protomers** were recorded with 4-8k scans with 26-40 T1 increments. **TEDOR** spectra [Hing 92] from mixed protomers were recorded at 8 kHz magic angle spinning with an initial ^{1}H-^{13}C CP step with a 50%-100% amplitude ramp for 1.5 ms with spin locks of 60 kHz for ^{1}H and 52 kHz for ^{13}C. π pulses were 10 µs for ^{13}C and 14 µs for ^{15}N with a loop counter up to 40 corresponding to a mixing time of 10 ms. **PAIN** [Lewandowski 07] spectra from mixed protomers were recorded at 12.5 kHz magic angle spinning with an initial ^{1}H-^{15}N CP step with a 75%-100% amplitude ramp for 1.5 ms with spin locks of 60 kHz for ^{1}H and 47.5 kHz for ^{15}N. PAIN mixing was achieved by spin lock fields of 31 kHz for ^{13}C and ^{15}N and 32 kHz for ^{1}H for 4.25 ms.

NHHC [Etzkorn 04] spectra from mixed protomers were recorded at 10 kHz magic angle spinning with an initial ^{1}H-^{15}N CP step with a 75%-100% amplitude ramp for 1.5 ms with spin locks of 60 kHz for 1H and 50 kHz for ^{15}N. After T1 incrementation a CP followed from ^{15}N back to ^{1}H under the same condition with an 80%-100% ramp for 200-230 µs. Subsequent ^{1}H-^{1}H mixing was followed by a ^{1}H-^{13}C CP with spin locks of 60 kHz for ^{1}H and 50 kHz for ^{13}C with an 80%-100% ramp for 70-120 µs.

Proton-detected **CP-HSQC** [Chevelkov 06; Linser 11] spectra were recorded at 20 kHz MAS with 512-1024 scans and 80 increments. Pulselengths were similar to carbon-detected spectra unless noted. CP-based HSQCs had an initial 90° preparation pulse followed by ^{1}H-^{15}N CP for 500 µs with 75%-100% amplitude ramp using spin locks of 60 kHz for ^{1}H and 40 kHz for ^{15}N. Carbon decoulpling in F1 was

achieved by a π pulse, proton J-decoupling by a 2 kHz WALTZ scheme. After incrementation, nitrogen magnetization was stored in z for water suppression which was achieved by four proton pulses at 20 kHz for 20-50 ms each [Paulson 03]. Protons were acquired for 80 ms with 2 kHz ^{15}N WALTZ decoupling [Shaka 83]. The recycle delay was 500 µs for Cu(II)-doped samples.

INEPT-based HSQC spectra were recorded like CP-based HSQCs unless noted [Chevelkov 06; Linser 11]. Polarization transfer was achieved by INEPT steps with delays corresponding to a ^{1}H-^{15}N coupling constant of 90 Hz (1/(4J)=2.7ms). Water suppression was achieved by a 1 ms purgepulse at 80 kHz after antiphase magnetization in the first INEPT step is created.

Solution-NMR HSQC spectra were recorded with a standard pulse program delivered by Bruker with delays corresponding to an INEPT coupling constant of 90 Hz (1/(4J)=2.7ms). Spectra were recorded at 310K at a concentration of 1 mM with π proton/nitrogen/carbon pulselengths of 24/86/28 µs respectively.

αB protein expression and purification was performed by Kristina Rehbein, FMP-Berlin. αB-10.1 was donated by Andi Mainz, TU-München. α-synuclein was donated by Silvia Verzini, FMP-Berlin. γS-crystallin(-G18V) protein expression and purification was performed by Carolyn Kingsley and Will Brubaker, UC Irvine.

Samples of αB were in 20 mM phosphate **buffer** with 50 mM NaCl and 0.02% NaN_3 at pH 7.5 unless noted. In all experiments special care about the pH/pD was taken. Deuterated solution pD measurements were isotope-effect corrected [Covington 68]. Binding partner solutions were dialysed or diluted and re-concentrated to have identical buffers upon mixing. Solutions for interaction studies were mixed and incubated for 1 h at 55°C.

Samples were **precipitated** at 20 mg/ml with 150 µl 50% PEG-8000 (per ml protein) solution in a vapourization chamber for 2-3 days with a surrounding solution of 50% PEG. The precipitate was centrifuged into 3.2 mm or 4 mm rotors leaving a tip of PEG solution on top of the sediment.

FROSTY solution MAS samples were concentrated up to 250 mg/ml in optionally 20% glycerol for cryoprotection [Mainz 09; Gardinnet 12; Bertini 11]. Solution MAS samples for proton detection had 20% ^{1}H protonation on labile sites and all consequent solutions had the same protonation level [Akbey 10]. d8-glycerol was used and 60 mM Cu(II)EDTA for PRE-assisted shortening of T1 relaxation times [Linser 07]. Solutions for interaction studies were mixed and incubated at high

concentrations prior to addition of glycerol and Cu(II)EDTA.

Solution NMR measurements were carried out in 20 mM phosphate buffer with 50 mM NaCl and 0.02% NaN_3 at pH 7.5 with addition of 10% D_2O. Solution NMR studies of α-synuclein complexed with αB-10.1 were carried out with two independent samples, a control sample with ^{15}N-labelled α-synuclein alone and a second sample with ^{15}N-labelled α-synuclein in complex with αB-10.1. Therefore data analysis was not sensitive to loss of signal due to α-synuclein aggregation.

All NMR spectra were processed with Topspin and analysed in Sparky [Goddard] and CCPN [Stevens 11]. Protein structures were viewed in UCSF Chimera [Pettersen 04] and rendered in Cinema4D.

SAXS data were recorded at the EMBL Hamburg X33 beamline. Measurements were assisted by Weifeng Shang and Clement Blanchet. A freshly prepared bovine serum albumin solution was used to calibrate for concentration measurements. Preparations of αB were recorded in concentration series from 1 mg/ml up to 20 mg/ml depending on the sample. Subsequent scattering curves were merged. Buffer scattering curves were recorded before and after a protein measurement and consequently subtracted. The Atsas software package [Petoukhov 12] was used for SAXS data analysis, GNOM [Svergun 92] for determination of R_g and D_{max} values. Data was processed for a polydisperse system of solid spheres. Initial 20 data points were omitted. Around 1700 data points were analyzed for each measurement. For all other parameters standard settings were used.

HADDOCK-driven docking [Dominguez 03] of the C-terminal domain IXI-motif to the αB core domain structure was run on the WeNMR web-server. The C-terminal IXI-motif peptide ^{157}PERTIPITREEK^{166} was modelled in UCSF chimera using the “build-structure” application with randomized values for phi and psi angles. Docking was performed to the solid-state NMR structure of αB core domain. Docking restraints from measurements of intermolecular contacts were listed in a .tbl file. The docking process was run with the standard “expert” parameter set with 1000 structures of rigid body modelling, followed by 200 structures of semi-flexible refinement and 200 structures of explicit solvent refinement.

Throughout this thesis several isotopic labelling schemes have been applied. In the following, these are briefly discussed and benefits/drawbacks are pointed out.

Uniformly labelled samples are fully protonated and ^{13}C, ^{15}N labelled.

Glycerol labelling schemes [LeMaster 96; Castellani 02] have been extensively used in carbon-detected solid-state NMR spectroscopy. A minimal medium is used where ^{13}C-labelled glycerol is the only carbon source. Labelling glycerol with ^{13}C at either 2 or 1,3 positions gives complementary amino acid labelling patterns (Fig.5.1). Adjacent spins are not labelled having three major benefits: 1) less spectral crowding 2) suppression of carbon ^{1}J couplings 3) less assignment options.

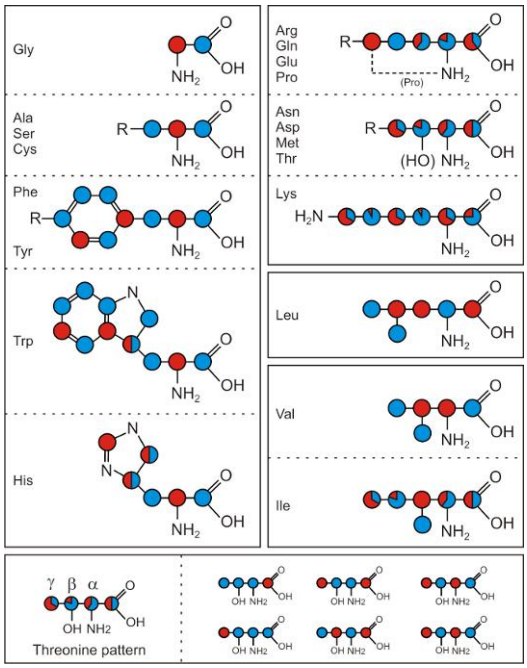

Fig.5.1: Incorporation of complementary ^{13}C labelling by the glycerol labelling scheme. Blue spins are ^{13}C labelled when glycerol is used that is ^{13}C labelled in its 1,3 positions, red spins are ^{13}C labelled when glycerol is used that is ^{13}C labelled in its 2 position. For some amino acids mixtures of different isotopomers are obtained (see threonine pattern). Plot contributed by Dr. Victoria Davies-Higman.

RIGAS $^{1}H^{13}C^{15}N$ labelled amino acids RIGAS were used and bacteria were grown in a deuterated, otherwise unlabelled background.

PFLS ^{2}H labelled amino acids PFLS were used and bacteria grown in a ^{2}H, ^{13}C, ^{15}N background. Therefore these specific amino acids were incorporated and depleted from the ^{15}N-^{1}H HSQC spectrum. Labile sites were back exchanged with 20% H_2O for proton detected experiments.

IVWY ^{2}H, ^{15}N labelled amino acids IWY and ^{2}H, ^{13}C, ^{15}N labelled V were used and

bacteria grown in a ^{2}H, ^{12}C, ^{14}N background. Therefore these specific amino acids were incorporated and detected in a ^{15}N-^{1}H HSQC spectrum. Labile sites were back exchanged with 20% H_2O for proton detected experiments.

4.1 Protein information UNIPROT

P02511[1-175], Alpha-crystallin B chain, Homo sapiens

```
MDIAIHHPWI RRPFFPFHSP 20
SRLFDQFFGE HLLESDLFPT 40
STSLSPFYLR PPSFLRAPSW 60
FDTGLSEMRL EKDRFSVNLD 80
VKHFSPEELK VKVLGDVIEV 100
HGKHEERQDE HGFISREFHR 120
KYRIPADVDP LTITSSLSSD 140
GVLTVNGPRK QVSGPERTIP 160
ITREEKPAVT AAPKK      175

Ala (A)   6      3.4%
Arg (R)  14      8.0%
Asn (N)   2      1.1%
Asp (D)  11      6.3%
Cys (C)   0      0.0%
Gln (Q)   3      1.7%
Glu (E)  14      8.0%
Gly (G)   8      4.6%
His (H)   9      5.1%
Ile (I)   9      5.1%
Leu (L)  15      8.6%
Lys (K)  10      5.7%
Met (M)   2      1.1%
Phe (F)  14      8.0%
Pro (P)  17      9.7%
Ser (S)  17      9.7%
Thr (T)   9      5.1%
Trp (W)   2      1.1%
Tyr (Y)   2      1.1%
Val (V)  11      6.3%
```

P37840[1-140], Alpha-synuclein, Homo sapiens

```
MDVFMKGLSK AKEGVVAAAE 20
KTKQGVAEAA GKTKEGVLYV 40
GSKTKEGVVH GVATVAEKTK 60
EQVTNVGGAV VTGVTAVAQK 80
TVEGAGSIAA ATGFVKKDQL 100
GKNEEGAPQE GILEDMPVDP 120
DNEAYEMPSE EGYQDYEPEA 140

Ala (A)  19     13.6%
Arg (R)   0      0.0%
Asn (N)   3      2.1%
Asp (D)   6      4.3%
Cys (C)   0      0.0%
Gln (Q)   6      4.3%
Glu (E)  18     12.9%
Gly (G)  18     12.9%
His (H)   1      0.7%
Ile (I)   2      1.4%
Leu (L)   4      2.9%
Lys (K)  15     10.7%
Met (M)   4      2.9%
Phe (F)   2      1.4%
Pro (P)   5      3.6%
Ser (S)   4      2.9%
Thr (T)  10      7.1%
Trp (W)   0      0.0%
Tyr (Y)   4      2.9%
Val (V)  19     13.6%
```

P22914[2-178], Beta-crystallin S, Homo sapiens

```
MSKTGTKITF YEDKNFQGRR 20
YDCDCDCADF HTYLSRCNSI 40
KVEGGTWAVY ERPNFAGYMY 60
ILPQGEYPEY QRWMGLNDRL 80
SSCRAVHLPS GGQYKIQIFE 100
KGDFSGQMYE TTEDCPSIME 120
QFHMREIHSC KVLEGVWIFY 140
ELPNYRGRQY LLDKKEYRKP 160
IDWGAASPAV QSFRRIVE   178

Ala (A)   7      3.9%
Arg (R)  13      7.3%
Asn (N)   5      2.8%
Asp (D)  10      5.6%
Cys (C)   7      3.9%
Gln (Q)   9      5.1%
Glu (E)  14      7.9%
Gly (G)  14      7.9%
His (H)   4      2.2%
Ile (I)  10      5.6%
Leu (L)   9      5.1%
Lys (K)  10      5.6%
Met (M)   6      3.4%
Phe (F)   9      5.1%
Pro (P)   8      4.5%
Ser (S)  11      6.2%
Thr (T)   7      3.9%
Trp (W)   4      2.2%
Tyr (Y)  14      7.9%
Val (V)   7      3.9%
```

5. Summary/Zusammenfassung

Summary

The chaperone alpha-B crystallin is a paradigm example of a major challenge for modern structural biology. Its intrinsic polydispersity, heterogeneity and oligomeric architecture have hampered high resolution structural studies by solution NMR spectroscopy or X-ray crystallography. Solid-state NMR is a technique that is particularly useful for studies of the structure and dynamics of systems that are insoluble, heterogenous or oligomeric. This thesis describes a structural link between alpha-B crystallin oligomerization, pH activation and substrate protein binding. The data suggest that oligomerization serves as a mechanism of chaperone autoinhibition. Oligomerization sites can be activated by pH and may serve as chaperone binding sites. To my knowledge, this study presents for the first time a chaperone binding site of full-length alpha-B crystallin (in complex with proteins involved in cataract formation and Parkinson's disease), mapped at atomic resolution.

Alpha-B crystallin oligomerization was studied by solid-state NMR with mixed oligomers of differential isotopic labelling. These measurements revealed intermolecular contacts such as the interaction between a conserved C-terminal IXI-motif with a groove formed by β-strands 4 and 8 from the core domain. Intermolecular constraints were used to generate a structure from the alpha-B crystallin core domain in complex with an IXI-motif peptide. Activation of the chaperone by pH drop modulates this interaction. Signals for I133, I159 and I161 were broadened and smeared in solid-state NMR PDSD spectra at pH 6.5 in comparison to spectra at pH 7.5. Solution NMR spectra of alpha-B crystallin at low pH showed increased dynamics in the C-terminus of the protein accompanied by an increase in oligomeric size, as shown by SAXS. This trigger points at an uncovering of the alpha-B crystallin core domain due to IXI-motif detachment. As a consequence, the core domain may be (more) receptive for substrate proteins.

The disease-related alpha-B crystallin mutant R120G leads to a doubling in oligomeric size, increased polydispersity and defective chaperoning behaviour [Bova 99]. However, comparison of solid-state NMR spectra of mutant and wild-type protein showed that the overall fold and heterogeneity of the monomer are essentially not

altered. Sensitivity for pH for the alpha-B crystallin β7-β7 dimer interface could only be observed in alpha-B crystallin R120G but not in the wild-type, as shown in PDSD spectra. This change may be explained by altered pH-dependent surface exposure or irregular homo-oligomerization. Additionally, pH drop SAXS data for the mutant showed a heavy increase in oligomeric size by another 50% which suggests chaperoning malfunction as a consequence of a distorted oligomerization equilibrium.
The substrate protein alpha-synuclein was used to map its binding site on isotopically labelled alpha-B crystallin. Cross peaks that belong to residues of β-strands 4, 8, 9 and the IXI-motif experienced signal perturbations in solid-state NMR PDSD spectra upon complex formation. A mechanistic model is proposed, in which the IXI-motif oligomerization site can be modulated and alternatively occupied by a substrate protein. Solution NMR experiments of a truncated alpha-B crystallin core domain dimer in complex with isotopically labelled alpha-synuclein showed an interaction in the intermediate-exchange regime. No prominent binding site could be identified which suggests the interaction to be unspecific in respect to alpha-synuclein.
Mapping of the binding sites of the substrate gamma-S crystallin and its mutant gamma-S crystallin G18V on isotopically labelled alpha-B crystallin was studied by solid-state NMR. Indications of transient binding for signals mainly from residues of β-strands 5 and 7, 8 and the IXI-motif were observed. These residues form two independent binding sites, either the β7/β7-groove or the β4/8-groove, which are located on opposite sides of the monomer structure. For this substrate interaction, novel existing solid-state NMR technologies, such as FROSTY solution MAS and proton detection have been applied to circumvent limitations from conventional techniques used so far.

In conclusion, it is demonstrated that alpha-B crystallin oligomerization, pH activation and substrate binding are inevitably linked with each other by a structural trigger (Fig.3.9).

Zusammenfassung

Das Chaperon alpha-B crystallin ist ein Paradebeispiel für eine Herausforderung für die heutige Strukturbiologie. Die Polydispersität, Heterogenität und oligomere Architektur des Proteins haben strukturelle Untersuchungen mittels Lösungs-NMR und Röntgenkristallographie erschwert. Festkörper-NMR hingegen eignet sich besonders für Struktur- und Dynamikuntersuchungen an Systemen die unlöslich und/oder heterogen sind oder grosse Oligomere bilden. Diese Arbeit beschreibt Mechanismen der alpha-B crystallin Oligomerisierung, pH Aktivierung und Interaktion mit Substratproteinen. Die dargestellten Daten weisen darauf hin, dass sich das Chaperon durch Oligomer-Bildung selbst inhibiert. Kontaktstellen der Oligomerisierung können durch eine Veränderung des pH Wertes moduliert und aktiviert werden. Die Kontaktstelle kann dann alternativ ein Substratprotein binden. Nach meinem Kenntnisstand beschreibt diese Arbeit zum ersten mal eine Bindetasche von alpha-B crystallin im Komplex mit Substraten, die potentielle Auslöser für Katarkate und die Parkinson's Krankheit darstellen, auf atomarer Auflösung.

Die Oligomerisierung alpha-B crystallins wurde mittels Festkörper-NMR an gemischten Proben mit unterschiedlicher Isotopenmarkierung untersucht. Diese Messungen ergaben intermolekulare Kontakte wie z.B. die Interaktion eines konservierten, C-terminalen IXI-Motivs mit einer Furche der Hauptdomäne, die von den β-Strängen 4 und 8 gebildet wird. Diese Kontakte wurden genutzt um eine Struktur der alpha-B crystallin Hauptdomäne in Komplex mit einem IXI-Motiv Peptid zu errechnen. Aktivierung des Chaperons durch Senkung des pH Wertes modulierte diese Interaktion. Eine Verschiebung der Signale für I133, I159 und I161 wurde in Festkörper-NMR PDSD Spektren bei pH 6.5 beobachtet, im Gegenatz zu Spektren bei pH 7.5. Messungen von alpha-B crystallin bei tiefem pH zeigten eine Zunahme der Dynamik im C-Terminus durch Lösungs-NMR und eine Vergrösserung des Oligomers durch Kleinwinkel-Röntgenstreuung. Dies deutet auf eine Freisetzung der alpha-B crystallin Hauptdomäne durch Loslösung des IXI-Motivs. Dadurch wird die Bindung von Substratproteinen an die alpha-B crystallin Hauptdomäne ermöglicht.
Die alpha-B crystallin Mutante R120G weist eine veroppelte Oligomergrösse, höhere Polydispersität und defekte Chaperonaktivität auf [Bova 99]. Jedoch lassen

Festkörper-NMR Spektren darauf schliessen, dass die Faltung und Heterogenität des Monomers der Mutante sich kaum von der Faltung und Heterogenität des Wildtyp Monomers unterscheiden. Senkung des pH Wertes erzielte eine strukturelle Auswirkung für die β7-β7 Dimer Kontaktstelle der Mutante, jedoch nicht für den Wildtyp, was durch PDSD Spektren gezeigt werden konnte. Diese Auswirkung kann durch eine veränderte Oberflächenstruktur des Oligomers oder durch zusätzliche Interaktion zu anderen Protomeren erklärt werden. Weiterhin zeigte die pH Aktivierung der Mutante eine starke Zunahme der Oligomergrösse um weitere 50% in Kleinwinkel-Röntgenstreuungsdaten. Dies deutet auf eine gestörte Chaperonaktivität aufgrund eines veränderten Oligomergleichgewichts.

Das Substrat alpha-synuclein wurde mit isotopenmarkiertem alpha-B crystallin komplexiert um die Chaperon Bindetasche mittels Festkörper-NMR PDSD Spektren aufzuzueigen. Kreuzsignale von Resten aus den β-Strängen 4, 8, 9 und des IXI-Motiv zeigten Veränderungen die durch Bindung hervorgerufen wurden.

Demnach kann ein Mechanismus vorgeschlagen werden, in dem die IXI-Motiv Oligomerisierungs-Kontaktstelle moduliert und alternativ duch ein Substratprotein besetzt werden kann. Lösungs-NMR Experimente eines verkürzten alpha-B crystallin Konstrukts in Komplex mit isotopenmarkiertem alpha-synuclein zeigten eine Veränderung der Singalintensität für alle Reste des Substrats. Dies deutet auf eine unspezifische Bindestelle des Chaperons auf alpha-synuclein.

Die Bindestellen der Substrate gamma-S crystallin und der Mutante gamma-S crystallin G18V zu isotopenmarkiertem alpha-B crystallin wurden mittels Festkörper-NMR untersucht. Transiente Bindung wurde für Reste der β-Stränge 5, 7, 8 und des IXI-Motivs aufgezeigt. Diese Reste gehören zwei unabhängigen Substrat-Bindetaschen an, zum einen die β7/β7-Furche, zum anderen die β4/8-Furche. Weiterhin wurden für diese Interaktionsstudie neuere (bereits existierende) Festkörper-NMR Techniken wie z.B. FROSTY Lösungs-MAS und Protonendetektion angewandt, um Interaktionseffekte in NMR Spektren zu erzielen, die sich leicht(er) interpretieren lassen.

Zusammenfassend wurde gezeigt dass alpha-B crystallin Oligomerisierung, pH Aktivierung und Substratbindung strukturell eng miteinander verknüpft sind (Fig.3.9).

6. Personal Information

Publications from this thesis:

1) Jehle, Stefan, Ponni Rajagopal, Benjamin Bardiaux**, Stefan Markovic**, Ronald,Kuhne, Joseph R. Stout, Victoria A. Higman, Rachel E. Klevit, Barth Jan van Rossum, and Hartmut Oschkinat.

"Solid-State Nmr and Saxs Studies Provide a Structural Basis for the Activation of [Alpha]B-Crystallin Oligomers." *Nat Struct Mol Biol* 17, no. 99 (2010): 1037-1042.

Other Publications:

2) Linser, Rasmus, Muralidhar Dasari, Matthias Hiller, Victoria Higman, Uwe Fink, Juan-Miguel Lopez del Amo, **Stefan Markovic**, Liselotte Handel, Brigitte Kessler, Peter Schmieder, Dieter Oesterhelt, Hartmut Oschkinat, and Bernd Reif.

"Proton-Detected Solid-State Nmr Spectroscopy of Fibrillar and Membrane Proteins." *Angewandte Chemie International Edition* 50, no. 19 (2011): 4508-4512.

3) Koo, Seong Joo, **Stefan Markovic**, Dmytro Puchkov, Carsten C. Mahrenholz, Figen Beceren-Braun, Tanja Maritzen, Jens Dernedde, Rudolf Volkmer, Hartmut Oschkinat, and Volker Haucke.

"Snare Motif-Mediated Sorting of Synaptobrevin by the Endocytic Adaptors Clathrin Assembly Lymphoid Myeloid Leukemia (Calm) and Ap180 at Synapses." *Proceedings of the National Academy of Sciences* 108, no. 33 (2011): 13540-13545.

4) Higman, Victoria, Jeremy Flinders, Matthias Hiller, Stefan Jehle, **Stefan Markovic**, Sebastian Fiedler, Barth-Jan van Rossum, and Hartmut Oschkinat.

"Assigning Large Proteins in the Solid State: A Mas Nmr Resonance Assignment Strategy Using Selectively and Extensively 13C-Labelled Proteins." *Journal of Biomolecular NMR* 44, no. 4 (2009): 245-260.

5) Zou, Chao, Sowmini Kumaran, **Stefan Markovic** , Reto Walser, and Oliver Zerbe.

"Studies of the Structure of the N-Terminal Domain from the Y4 Receptor—a G Protein-Coupled Receptor—and Its Interaction with Hormones from the Npy Family." *ChemBioChem* 9, no. 14 (2008): 2276-2284.

7. Acknowledgements

This thesis would have not been possible without the scientific and mental support from many people. I want to mention (in no particular order):

Barth-Jan, you have always given me technical advice, support and a bunch of cheer-up laughs. Thanks for your help.

Mônica, we had so many great discussions about science and life and I miss these times a lot. Hope to see you again from time to time. Obrigado.

Janet, I hope that you are happy with your home and job. Thanks for your support.

Robert, you always would listen to my endless stories, I'll keep those fun times in good memory.

Silvia, you were always supporting me and believing in me. Thanks for your support on the alpha-synuclein project.

Trent, you are the most impressive spectroscopist that I've seen. Thanks for helping me out many times.

Hias, thanks for the good times in the lab. I enjoyed working with you on the OmpG project and I'm very thankful for the support that you've given me in the beginning.

Marco, we shared the office together for many years. Sometimes you would be the only one to discuss spectroscopy with me and we would get almost philosophic about it. I miss these times.

Thanks to our collaborators Carolyn, Will and Rachel from the University of California in Irvine. I enjoy working with you and I hope that we can carry on with this interesting project.

I also want to mention my former bosses Roland and Oliver who have always believed in me. Oliver you taught me the essential basics of NMR which were very helpful throughout my entire PhD.

Thanks to my labmates for the nice atmosphere and tolerating my bad hair days: Andy N, Anne W, Anja, Arne, Anup, Benjamin, Daniela, Florian, Focko, Jörg, Joren, Matthias D, Sascha, Shakeel, Ümit, Vicky and not to forget lovely Alex and Heidi from upstairs.

I also enjoyed spending time with the people from the Reif lab. Andi, Rasmus, Sam, Tomas, Verena and Bernd.

Andi you've been one major pillar, not just for protein, assignments, pulse programs, expertise and discussions. I cherish your happy mood and dedication and I will never forget the good times we've had.

Rasmus, I love your jokes and your easy-going personality. I hope to see you from time to time while you are globetrotting.

Tomas, I enjoyed times with you, especially in Australia and Hong Kong.

Bernd, thanks a lot for your support and for refereeing this thesis.

Kristina, you've gone through the efforts to prepare many samples that I could use for this research. I am deeply thankful to you.

Chao, Silke and Maya. You people have taught me all the biochemistry essentials during my time as an undergraduate student. I miss you a lot.

Thanks to my friends for your support. Matt, Victor, Tu-My, Reto, Mike, Franziska, Flo.

I am deeply indebted to my family: Bastian, Bernhard, Emina, Jay, Maurice, Michael, Roberto.

Dear Hartmut, you have gone through a lot of efforts to make this project work. I could not have solved the problems I was facing without you. Thanks for your constant support and commitment. I am deeply grateful to you.

8. References

Acosta-Sampson, L. and J. King (2010). "Partially Folded Aggregation Intermediates of Human γD-, γC-, and γS-Crystallin Are Recognized and Bound by Human αB-Crystallin Chaperone." Journal of Molecular Biology **401**(1): 134-152.

Akbey, Ü., S. Lange, et al. (2010). "Optimum levels of exchangeable protons in perdeuterated proteins for proton detection in MAS solid-state NMR spectroscopy." Journal of Biomolecular NMR **46**(1): 67-73.

Aquilina, J. A., J. L. P. Benesch, et al. (2003). "Polydispersity of a mammalian chaperone: Mass spectrometry reveals the population of oligomers in αB-crystallin." Proceedings of the National Academy of Sciences **100**(19): 10611-10616.

Augusteyn, R. C. (2004). "α-crystallin: a review of its structure and function." Clinical and Experimental Optometry **87**(6): 356-366.

Bagnéris, C., O. A. Bateman, et al. (2009). "Crystal Structures of α-Crystallin Domain Dimers of αB-Crystallin and Hsp20." Journal of Molecular Biology **392**(5): 1242-1252.

Baldwin, A. J., G. R. Hilton, et al. (2011). "Quaternary Dynamics of αB-Crystallin as a Direct Consequence of Localised Tertiary Fluctuations in the C-Terminus." Journal of Molecular Biology **413**(2): 310-320.

Baldwin, Andrew J., H. Lioe, et al. (2011). "The Polydispersity of αB-Crystallin Is Rationalized by an Interconverting Polyhedral Architecture." Structure (London, England : 1993) **19**(12): 1855-1863.

Baldwin, A. J., H. Lioe, et al. (2011). "αB-Crystallin Polydispersity Is a Consequence of Unbiased Quaternary Dynamics." Journal of Molecular Biology **413**(2): 297-309.

Baldwin, A. J., P. Walsh, et al. (2012). "Probing dynamic conformations of the high molecular weight αB-crystallin heat shock protein ensemble by NMR spectroscopy." Journal of the American Chemical Society.

Bennardini, F., A. Wrzosek, et al. (1992). "Alpha B-crystallin in cardiac tissue. Association with actin and desmin filaments." Circulation Research **71**(2): 288-294.

Bernadó, P., C. W. Bertoncini, et al. (2005). "Defining Long-Range Order and Local Disorder in Native α-Synuclein Using Residual Dipolar Couplings." Journal of the American Chemical Society **127**(51): 17968-17969.

Bertini, I., C. Luchinat, et al. (2011). "Solid-state NMR of proteins sedimented by ultracentrifugation." Proceedings of the National Academy of Sciences **108**(26): 10396-10399.

Bertoncini, C. W., Y.-S. Jung, et al. (2005). "Release of long-range tertiary interactions potentiates aggregation of natively unstructured α-synuclein." Proceedings of the National Academy of Sciences of the United States of America **102**(5): 1430-1435.

Bhattacharyya, J., E. G. Padmanabha Udupa, et al. (2006). "Mini-αB-Crystallin: A Functional Element of αB-Crystallin with Chaperone-like Activity†." Biochemistry **45**(9): 3069-3076.

Bloemendal, H., W. de Jong, et al. (2004). "Ageing and vision: structure, stability and function of lens crystallins." Progress in Biophysics and Molecular Biology **86**(3): 407-485.

Bova, M. P., O. Yaron, et al. (1999). "Mutation R120G in αB-crystallin, which is linked to a desmin-related myopathy, results in an irregular structure and defective chaperone-like function." Proceedings of the National Academy of Sciences

96(11): 6137-6142.
Boyle, D. and L. Takemoto (1994). "Characterization of the α-γ and α-β Complex: Evidence for an In Vivo Functional Role of α-Crystallin as a Molecular Chaperone." Experimental Eye Research **58**(1): 9-16.
Braun, N., M. Zacharias, et al. (2011). "Multiple molecular architectures of the eye lens chaperone αB-crystallin elucidated by a triple hybrid approach." Proceedings of the National Academy of Sciences **108**(51): 20491-20496.
Brubaker, W. D., J. A. Freites, et al. (2011). "Separating Instability from Aggregation Propensity in γS-Crystallin Variants." Biophysical journal **100**(2): 498-506.
Bruinsma, I. B., K. A. Bruggink, et al. (2011). "Inhibition of α-synuclein aggregation by small heat shock proteins." Proteins: Structure, Function, and Bioinformatics **79**(10): 2956-2967.
Castellani, F., B. van Rossum, et al. (2002). "Structure of a protein determined by solid-state magic-angle-spinning NMR spectroscopy." Nature **420**(6911): 98-102.
Cavanagh, J., Fairbrother, W. J., et al. (2008). “Protein NMR Spectroscopy, Principles and Practice.” Academic Press.
Chen, J., M. J. Feige, et al. (2010). "Regions Outside the α-Crystallin Domain of the Small Heat Shock Protein Hsp26 Are Required for Its Dimerization." Journal of Molecular Biology **398**(1): 122-131.
Chevelkov, V., K. Rehbein, et al. (2006). "Ultrahigh Resolution in Proton Solid-State NMR Spectroscopy at High Levels of Deuteration." Angewandte Chemie International Edition **45**(23): 3878-3881.
Clark, A. R., C. E. Naylor, et al. (2011). "Crystal Structure of R120G Disease Mutant of Human αB-Crystallin Domain Dimer Shows Closure of a Groove." Journal of Molecular Biology **408**(1): 118-134.
Comellas, G., L. R. Lemkau, et al. (2011). "Structured Regions of α-Synuclein Fibrils Include the Early-Onset Parkinson's Disease Mutation Sites." Journal of Molecular Biology **411**(4): 881-895.
Cookson, M. R. and M. van der Brug (2008). "Cell systems and the toxic mechanism(s) of α-synuclein." Experimental Neurology **209**(1): 5-11.
Covington, A. K., M. Paabo, et al. (1968). "Use of the glass electrode in deuterium oxide and the relation between the standardized pD (paD) scale and the operational pH in heavy water." Analytical Chemistry **40**(4): 700-706.
Das, K. P., L.-P. i. Choo-Smith, et al. (1999). "Insight into the Secondary Structure of Non-native Proteins Bound to a Molecular Chaperone α-Crystallin." Journal of Biological Chemistry **274**(47): 33209-33212.
Der Perng, M., S. F. Wen, et al. (2004). "Desmin Aggregate Formation by R120G αB-Crystallin Is Caused by Altered Filament Interactions and Is Dependent upon Network Status in Cells." Molecular Biology of the Cell **15**(5): 2335-2346.
Dominguez, C., R. Boelens, et al. (2003). "HADDOCK: A Protein−Protein Docking Approach Based on Biochemical or Biophysical Information." Journal of the American Chemical Society **125**(7): 1731-1737.
Duer, M. J. (2002). “Solid-state NMR spectroscopy. Principles and applications.“ Blackwell Science, Oxford.
Ecroyd, H. and J. A. Carver (2008). "The effect of small molecules in modulating the chaperone activity of αB-crystallin against ordered and disordered protein aggregation." FEBS Journal **275**(5): 935-947.
El-Agnaf, O. M. A. and G. B. Irvine (2000). "Review: Formation and Properties of Amyloid-like Fibrils Derived from α-Synuclein and Related Proteins." Journal of Structural Biology **130**(2–3): 300-309.

Etzkorn, M., A. Böckmann, et al. (2004). "Probing Molecular Interfaces Using 2D Magic-Angle-Spinning NMR on Protein Mixtures with Different Uniform Labeling." Journal of the American Chemical Society **126**(45): 14746-14751.
Evans, P., C. Slingsby, et al. (2008). "Association of partially folded lens βB2-crystallins with the α-crystallin molecular chaperone." Biochem J **409**(3): 691-699.
Ferreon, A. C. M., Y. Gambin, et al. (2009). "Interplay of α-synuclein binding and conformational switching probed by single-molecule fluorescence." Proceedings of the National Academy of Sciences **106**(14): 5645-5650.
Franks, W. T., A. H. Linden, et al. (2012). "Solid-state magic-angle spinning NMR of membrane proteins and protein–ligand interactions." European Journal of Cell Biology **91**(4): 340-348.
Fulda, S., A. M. Gorman, et al. (2010). "Cellular Stress Responses: Cell Survival and Cell Death." International Journal of Cell Biology **2010**.
Fung, B. M., A. K. Khitrin, et al. (2000). "An Improved Broadband Decoupling Sequence for Liquid Crystals and Solids." Journal of Magnetic Resonance **142**(1): 97-101.
Gardiennet, C., A. K. Schütz, et al. (2012). "A Sedimented Sample of a 59 kDa Dodecameric Helicase Yields High-Resolution Solid-State NMR Spectra." Angewandte Chemie International Edition **51**(31): 7855-7858.
Gath, J., B. Habenstein, et al. (2012). "Solid-state NMR sequential assignments of α-synuclein." Biomolecular NMR Assignments **6**(1): 51-55.
Ghosh, J. G., M. R. Estrada, et al. (2005). "Interactive Domains for Chaperone Activity in the Small Heat Shock Protein, Human αB Crystallin†." Biochemistry **44**(45): 14854-14869.
Ghosh, J. G., S. A. Houck, et al. (2008). "Interactive sequences in the molecular chaperone, human αB crystallin modulate the fibrillation of amyloidogenic proteins." The International Journal of Biochemistry & Cell Biology **40**(5): 954-967.
Goddard, T. D., Kneller, D.G.. „Sparky 3“, University of California, San Francisco.
Gopalakrishnan, S., D. Boyle, et al. (1994). "Preferential interaction of alpha crystallin with denatured forms of gamma crystallin." Investigative Ophthalmology & Visual Science **35**(2): 382-387.
Haley, D. A., J. Horwitz, et al. (1998). "The small heat-shock protein, αb-crystallin, has a variable quaternary structure." Journal of Molecular Biology **277**(1): 27-35.
Haslbeck, M., T. Franzmann, et al. (2005). "Some like it hot: the structure and function of small heat-shock proteins." Nat Struct Mol Biol **12**(10): 842-846.
Heise, H., W. Hoyer, et al. (2005). "Molecular-level secondary structure, polymorphism, and dynamics of full-length α-synuclein fibrils studied by solid-state NMR." Proceedings of the National Academy of Sciences of the United States of America **102**(44): 15871-15876.
Hing, A. W., S. Vega, et al. (1992). "Transferred-echo double-resonance NMR." Journal of Magnetic Resonance (1969) **96**(1): 205-209.
Horwitz, J. (1992). "Alpha-crystallin can function as a molecular chaperone." Proceedings of the National Academy of Sciences **89**(21): 10449-10453.
Huang, B. and W. He (2010). "Molecular characteristics of inherited congenital cataracts." European Journal of Medical Genetics **53**(6): 347-357.
Hura, G. L., A. L. Menon, et al. (2009). "Robust, high-throughput solution structural analyses by small angle X-ray scattering (SAXS)." Nat Meth **6**(8): 606-612.
Jehle, S. (2008). “Solid-state NMR as a tool in structural biology” FU-Berlin Thesis

000000006446.
Jehle, S., P. Rajagopal, et al. (2010). "Solid-state NMR and SAXS studies provide a structural basis for the activation of [alpha]B-crystallin oligomers." Nat Struct Mol Biol **17**(99): 1037-1042.
Jehle, S., B. van Rossum, et al. (2009). "αB-Crystallin: A Hybrid Solid-State/Solution-State NMR Investigation Reveals Structural Aspects of the Heterogeneous Oligomer." Journal of Molecular Biology **385**(5): 1481-1497.
Jehle, S., B. S. Vollmar, et al. (2011). "N-terminal domain of αB-crystallin provides a conformational switch for multimerization and structural heterogeneity." Proceedings of the National Academy of Sciences **108**(16): 6409-6414.
Jellinger, K. A. (2000). "Cell death mechanisms in Parkinson's disease." Journal of Neural Transmission **107**(1): 1-29.
Kim, K. K., R. Kim, et al. (1998). "Crystal structure of a small heat-shock protein." Nature **394**(6693): 595-599.
Knight, M. J., A. L. Webber, et al. (2011). "Fast Resonance Assignment and Fold Determination of Human Superoxide Dismutase by High-Resolution Proton-Detected Solid-State MAS NMR Spectroscopy." Angewandte Chemie International Edition **50**(49): 11697-11701.
Koo, S. J., S. Markovic, et al. (2011). "SNARE motif-mediated sorting of synaptobrevin by the endocytic adaptors clathrin assembly lymphoid myeloid leukemia (CALM) and AP180 at synapses." Proceedings of the National Academy of Sciences **108**(33): 13540-13545.
Koteiche, H. A. and H. S. Mchaourab (2003). "Mechanism of Chaperone Function in Small Heat-shock Proteins." Journal of Biological Chemistry **278**(12): 10361-10367.
Laganowsky, A., J. L. P. Benesch, et al. (2010). "Crystal structures of truncated alphaA and alphaB crystallins reveal structural mechanisms of polydispersity important for eye lens function." Protein Science **19**(5): 1031-1043.
Lange, A., K. Giller, et al. (2006). "Toxin-induced conformational changes in a potassium channel revealed by solid-state NMR." Nature **440**(7086): 959-962.
LeMaster, D. M. (1990). "Deuterium labelling in NMR structural analysis of larger proteins." Quarterly Reviews of Biophysics **23**(02): 133-174.
LeMaster, D. M. and D. M. Kushlan (1996). "Dynamical Mapping of E. coli Thioredoxin via 13C NMR Relaxation Analysis." Journal of the American Chemical Society **118**(39): 9255-9264.
Levitt, M. H. (2001). “Spin dynamics: basics of nuclear magnetic resonance.” John Wiley & Sons, Chichester, UK.
Lewandowski, J. R., G. De Paëpe, et al. (2007). "Proton Assisted Insensitive Nuclei Cross Polarization." Journal of the American Chemical Society **129**(4): 728-729.
Linser, R., V. Chevelkov, et al. (2007). "Sensitivity enhancement using paramagnetic relaxation in MAS solid-state NMR of perdeuterated proteins." Journal of Magnetic Resonance **189**(2): 209-216.
Linser, R., M. Dasari, et al. (2011). "Proton-Detected Solid-State NMR Spectroscopy of Fibrillar and Membrane Proteins." Angewandte Chemie International Edition **50**(19): 4508-4512.
Lowe, J., M. Landon, et al. (1990). "Dementia with β-amyloid deposition: involvement of αB-crystallin supports two main diseases." The Lancet **336**(8713): 515-516.
Ma, Z., G. Piszczek, et al. (2009). "The G18V CRYGS Mutation Associated with Human Cataracts Increases γS-Crystallin Sensitivity to Thermal and Chemical Stress." Biochemistry **48**(30): 7334-7341.

Mainz, A., S. Jehle, et al. (2009). "Large Protein Complexes with Extreme Rotational Correlation Times Investigated in Solution by Magic-Angle-Spinning NMR Spectroscopy." Journal of the American Chemical Society **131**(44): 15968-15969.
Mainz, A., B. Bardiaux, et al. (2012). "Structural and Mechanistic Implications of Metal Binding in the Small Heat-shock Protein αB-crystallin." Journal of Biological Chemistry **287**(2): 1128-1138.
McDermott, A. E. (2004). "Structural and dynamic studies of proteins by solid-state NMR spectroscopy: rapid movement forward." Current Opinion in Structural Biology **14**(5): 554-561.
McIntosh, L. P. and F. W. Dahlquist (1990). "Biosynthetic Incorporation of 15N and 13C for Assignment and Interpretation of Nuclear Magnetic Resonance Spectra of Proteins." Quarterly Reviews of Biophysics **23**(01): 1-38.
Mertens, H. D. T. and D. I. Svergun (2010). "Structural characterization of proteins and complexes using small-angle X-ray solution scattering." Journal of Structural Biology **172**(1): 128-141.
Michael, R. and A. J. Bron (2011). "The ageing lens and cataract: a model of normal and pathological ageing." Philosophical Transactions of the Royal Society B: Biological Sciences **366**(1568): 1278-1292.
Mishra, S., R. A. Stein, et al. (2012). "Cataract-linked γD-crystallin mutants have weak affinity to lens chaperones α-crystallins." FEBS Letters **586**(4): 330-336.
Nielsen, A., K. Székely, et al. (2012). "Simultaneous acquisition of PAR and PAIN spectra." Journal of Biomolecular NMR **52**(4): 283-288.
Outeiro, T. F., J. Klucken, et al. (2006). "Small heat shock proteins protect against α-synuclein-induced toxicity and aggregation." Biochemical and Biophysical Research Communications **351**(3): 631-638.
Paulson, E. K., C. R. Morcombe, et al. (2003). "Sensitive High Resolution Inverse Detection NMR Spectroscopy of Proteins in the Solid State." Journal of the American Chemical Society **125**(51): 15831-15836.
Perry, R., McKeith, I., et al. (1999). “Dementia with Lewy Bodies: Clinical, Pathological and Treatment Issues.” Cambridge University Press.
Peschek, J., N. Braun, et al. (2009). "The eye lens chaperone α-crystallin forms defined globular assemblies." Proceedings of the National Academy of Sciences **106**(32): 13272-13277.
Petoukhov, M. V., D. Franke, et al. (2012). "New developments in the ATSAS program package for small-angle scattering data analysis." Journal of Applied Crystallography **45**(2): 342-350.
Pettersen, E. F., T. D. Goddard, et al. (2004). "UCSF Chimera—A visualization system for exploratory research and analysis." Journal of Computational Chemistry **25**(13): 1605-1612.
Pines, A., M. G. Gibby, et al. (1973). "Proton-enhanced NMR of dilute spins in solids." The Journal of Chemical Physics **59**(2): 569-590.
Putilina, T., F. Skouri-Panet, et al. (2003). "Subunit Exchange Demonstrates a Differential Chaperone Activity of Calf α-Crystallin toward βLOW- and Individual γ-Crystallins." Journal of Biological Chemistry **278**(16): 13747-13756.
Raman, B., T. Ramakrishna, et al. (1995). "Rapid Refolding Studies on the Chaperone-like -Crystallin." Journal of Biological Chemistry **270**(34): 19888-19892.
Rekas, A., C. G. Adda, et al. (2004). "Interaction of the Molecular Chaperone αB-Crystallin with α-Synuclein: Effects on Amyloid Fibril Formation and

Chaperone Activity." Journal of Molecular Biology **340**(5): 1167-1183.
Renkawek, K., G. J. J. Stege, et al. (1999). "Dementia, gliosis and expression of the small heat shock proteins hsp27 and [alpha]B-crystallin in Parkinson's disease." NeuroReport **10**(11): 2273-2276.
Reynolds, N. P., A. Soragni, et al. (2011). "Mechanism of Membrane Interaction and Disruption by α-Synuclein." Journal of the American Chemical Society **133**(48): 19366-19375.
Sathish, H. A., H. A. Koteiche, et al. (2004). "Binding of Destabilized βB2-Crystallin Mutants to α-Crystallin." Journal of Biological Chemistry **279**(16): 16425-16432.
Schütz, A. K., A. Soragni, et al. (2011). "The Amyloid–Congo Red Interface at Atomic Resolution." Angewandte Chemie International Edition **50**(26): 5956-5960.
Shaka, A. J., J. Keeler, et al. (1983). "Evaluation of a new broadband decoupling sequence: WALTZ-16." Journal of Magnetic Resonance (1969) **53**(2): 313-340.
Shammas, Sarah L., Christopher A. Waudby, et al. (2011). "Binding of the Molecular Chaperone αB-Crystallin to Aβ Amyloid Fibrils Inhibits Fibril Elongation." Biophysical journal **101**(7): 1681-1689.
Shults, C. W. (2006). "Lewy bodies." Proceedings of the National Academy of Sciences of the United States of America **103**(6): 1661-1668.
Stevens, A. and R. C. Augusteyn (1993). "Acid-induced dissociation of alpha A- and alpha B-crystallin homopolymers." Biophysical journal **65**(4): 1648-1655.
Stevens, T., R. Fogh, et al. (2011). "A software framework for analysing solid-state MAS NMR data." Journal of Biomolecular NMR **51**(4): 437-447.
Sun, H., Z. Ma, et al. (2005). "Gamma-S crystallin gene (CRYGS) mutation causes dominant progressive cortical cataract in humans." Journal of Medical Genetics **42**(9): 706-710.
Sun, S., A. Siglin, et al. (2009). "Solid-State and Solution NMR Studies of the CAP-Gly Domain of Mammalian Dynactin and Its Interaction with Microtubules." Journal of the American Chemical Society **131**(29): 10113-10126.
Sun, Y. and T. H. MacRae (2005). "The small heat shock proteins and their role in human disease." FEBS Journal **272**(11): 2613-2627.
Svergun, D. (1992). "Determination of the regularization parameter in indirect-transform methods using perceptual criteria." Journal of Applied Crystallography **25**(4): 495-503.
Szeverenyi, N. M., M. J. Sullivan, et al. (1982). "Observation of spin exchange by two-dimensional fourier transform 13C cross polarization-magic-angle spinning." Journal of Magnetic Resonance (1969) **47**(3): 462-475.
Takegoshi, K., S. Nakamura, et al. (2001). "13C–1H dipolar-assisted rotational resonance in magic-angle spinning NMR." Chemical Physics Letters **344**(5–6): 631-637.
Takemoto, L. and D. Boyle (1994). "Binding of Denatured Protein Decreases the Chaperone Properties of α Crystallin." Archives of Biochemistry and Biophysics **315**(1): 133-136.
Takemoto, L., A. Ponce, et al. (2008). "Age-dependent association of γ-crystallins with aged α-crystallins from old bovine lens." Molecular Vision **14**: 970-974.
Treweek, T. M., A. Rekas, et al. (2005). "R120G αB-crystallin promotes the unfolding of reduced α-lactalbumin and is inherently unstable." FEBS Journal **272**(3): 711-724.
Treweek, T. M., A. Rekas, et al. (2010). "A quantitative NMR spectroscopic examination of the flexibility of the C-terminal extensions of the molecular

chaperones, αA- and αB-crystallin." Experimental Eye Research **91**(5): 691-699.
Trojanowski Jq, L. V. Y. (1998). "Aggregation of neurofilament and α-synuclein proteins in lewy bodies: Implications for the pathogenesis of parkinson disease and lewy body dementia." Archives of Neurology **55**(2): 151-152.
Ulmer, T. S., A. Bax, et al. (2005). "Structure and Dynamics of Micelle-bound Human α-Synuclein." Journal of Biological Chemistry **280**(10): 9595-9603.
van Montfort, R. L. M., E. Basha, et al. (2001). "Crystal structure and assembly of a eukaryotic small heat shock protein." Nat Struct Mol Biol **8**(12): 1025-1030.
van Rossum, B. J., E. A. M. Schulten, et al. (2002). "A 3-D Structural Model of Solid Self-Assembled Chlorophyll a/H2O from Multispin Labeling and MAS NMR 2-D Dipolar Correlation Spectroscopy in High Magnetic Field." Journal of Magnetic Resonance **155**(1): 1-14.
Vicart, P., A. Caron, et al. (1998). "A missense mutation in the [agr]B-crystallin chaperone gene causes a desmin-related myopathy." Nat Genet **20**(1): 92-95.
Vilar, M., H.-T. Chou, et al. (2008). "The fold of α-synuclein fibrils." Proceedings of the National Academy of Sciences **105**(25): 8637-8642.
Wang, J., E. Martin, et al. (2008). "Differential regulation of small heat shock proteins in transgenic mouse models of neurodegenerative diseases." Neurobiology of aging **29**(4): 586-597.
Wang, K. and A. Spector (1994). "The chaperone activity of bovine alpha crystallin. Interaction with other lens crystallins in native and denatured states." Journal of Biological Chemistry **269**(18): 13601-13608.
Wang, X., H. Osinska, et al. (2001). "Expression of R120G–αB-Crystallin Causes Aberrant Desmin and αB-Crystallin Aggregation and Cardiomyopathy in Mice." Circulation Research **89**(1): 84-91.
Waudby, C. A., T. P. J. Knowles, et al. (2010). "The Interaction of αB-Crystallin with Mature ±-Synuclein Amyloid Fibrils Inhibits Their Elongation." Biophysical journal **98**(5): 843-851.
Waudby, C. A., T. P. J. Knowles, et al. (2010). "The Interaction of αB-Crystallin with Mature ±-Synuclein Amyloid Fibrils Inhibits Their Elongation." Biophysical journal **98**(5): 843-851.
Waxman, E. A. and B. I. Giasson (2009). "Molecular mechanisms of α-synuclein neurodegeneration." Biochimica et Biophysica Acta (BBA) - Molecular Basis of Disease **1792**(7): 616-624.
Weinreb, O., A. F. van Rijk, et al. (2000). "In Vitro Filament-like Formation upon Interaction between Lens α-Crystallin and βL-Crystallin Promoted by Stress." Investigative Ophthalmology & Visual Science **41**(12): 3893-3897.
Wu, Z., F. Delaglio, et al. (2005). "Solution structure of γS-crystallin by molecular fragment replacement NMR." Protein Science **14**(12): 3101-3114.
Xi, J.-h., F. Bai, et al. (2006). "Alpha-crystallin expression affects microtubule assembly and prevents their aggregation." The FASEB Journal **20**(7): 846-857.
Zapke, J. (2011). „Untersuchungen zur Wechselwirkung von Mikrotubuli mit Kinesinen und Colchicin-Derivaten“ FU-Berlin Thesis 000000024907.
Zhou, D. H., G. Shah, et al. (2007). "Proton-Detected Solid-State NMR Spectroscopy of Fully Protonated Proteins at 40 kHz Magic-Angle Spinning." Journal of the American Chemical Society **129**(38): 11791-11801.